Synthesis, Characterization and Optical Properties of Rare Earth Based Non-toxic Inorganic Pigments

Thesis submitted to
Cochin University of Science and Technology (CUSAT)
in partial fulfillment of the requirements for the award of the degree of

DOCTOR OF PHILOSOPHY

in Chemistry
Under the Faculty of Science

By

GIABLE GEORGE

Under the supervision of
Dr. M. L. P. Reddy

Chemical Sciences and Technology Division
National Institute for Interdisciplinary Science and Technology
(*Formerly*, Regional Research Laboratory), CSIR
Thiruvananthapuram-695 019, KERALA

November 2010

DECLARATION

I hereby declare that the matter embodied in the thesis entitled ***"Synthesis, Characterization and Optical Properties of Rare Earth based Non-toxic Inorganic Pigments"*** is the result of investigations carried out by me at Chemical Sciences and Technology Division of the National Institute for Interdisciplinary Science and Technology (*formerly*, Regional Research Laboratory), CSIR, Thiruvananthapuram, under the supervision of Dr. M. L. P. Reddy, Scientist and the same has not been submitted elsewhere for any other degree.

In keeping with the general practice of reporting scientific observations, due acknowledgement has been made wherever the work described is based on the findings of other investigators.

Thiruvananthapuram

November 2010

Giable George

National Institute for Interdisciplinary Science and Technology (NIIST)

(Formerly Regional Research Laboratory)

Council of Scientific & Industrial Research (CSIR)
Industrial Estate P.O., Thiruvananthapuram - 695 019
Kerala, INDIA

Dr. M.L.P. Reddy
Scientist
Chemical Sciences and Technology Division

Tel: 91-471-2515 360
Fax: +91-471-2491 712
E-mail: mlpreddy55@gmail.com

23rd November 2010

CERTIFICATE

This is to certify that the work embodied in the thesis entitled ***"Synthesis, Characterization and Optical Properties of Rare Earth based Non-toxic Inorganic Pigments"*** has been carried out by Ms. Giable George under my supervision at Chemical Sciences and Technology Division of the National Institute for Interdisciplinary Science and Technology (NIIST), CSIR, Thiruvananthapuram and the same has not been submitted elsewhere for a degree.

Dr. M.L.P. Reddy
(Thesis Supervisor)

Acknowledgements

It is with immense pleasure that I express my wholehearted and sincere gratitude to my research supervisor Dr. M. L. P. Reddy, for suggesting the research topic and for his guidance, support and encouragement, leading to the successful completion of this work.

I wish to thank Dr. Suresh Das, Director and Professor T. K. Chandrashekar and Dr. B. C. Pai, former directors of the National Institute for Interdisciplinary Science and Technology (NIIST) for providing the necessary facilities for carrying out the work.

My sincere thanks are also due to,

- *Dr. P. Prabhakar Rao, Scientist, Materials and Minerals Division, NIIST, Trivandrum for guiding me during my NMLTI project period.*
- *Dr. Sreeram,CLRI, Chennai for helping me in doing surface coating studies.*
- *Dr. A. Ananthakumar, Scientist, Materials and Minerals Division, NIIST, Trivandrum for his help during my research.*
- *Dr. T. P. D Rajan, Scientist, Materials and Minerals Division, NIIST, Trivandrum for his help during my research.*
- *Mr. Guruswami, for XRD analysis.*
- *Mr. Chandran, for SEM analysis.*
- *My colleagues and friends.*
- *Council of Scientific and Industrial Research (CSIR) for research fellowship and for the financial assistance.*

I would like to extend my wholehearted and sincere gratitude to my parents and family members for their love, support and motivation. Words are insufficient to express my heartfelt thanks to my husband Abilash Mathew and my daughter for their support and understanding.

Finally, I would also like to extend my whole-hearted thanks to all my teachers for their encouragement and blessings.

Above all I thank God Almighty for giving me the courage to move on.

Giable George

Dedicated to my daughter

Ivana Mary Abilash

List of publications from the thesis

1. Synthesis and characterization of environmentally benign nontoxic pigments: $RE_2Mo_2O_9$ (RE = La or Pr), **Giable George**, Gisha George, P. Prabhakar Rao and M. L. P. Reddy, *Chem*istry *Letters*, 34, **2005**, 1702.
2. Synthesis and characterization of CeO_2–TiO_2–Pr_6O_{11} solid solutions for environmentally benign nontoxic red pigments, **Giable George**, P. Prabhakar Rao, and M. L. P. Reddy, *Chem*istry *Letters*, 12, **2006**, 1412.
3. Synthesis and characterization of environmentally benign calcium-doped $Pr_2Mo_2O_9$ pigments: Applications in coloring of plastics, **Giable George**, L. Sandhya Kumari, V. S. Vishnu, S. Ananthakumar, M. L. P. Reddy, *Journal of Solid State Chemistry,*181, **2008**, 487.
4. Synthesis, characterization and optical properties of silicon and praseodymium doped Y_6MoO_{12} compounds: Environmentally benign inorganic pigments with high NIR reflectance, **Giable George**, V. S. Vishnu, and M. L. P. Reddy, *Dyes and Pigments,* 88, **2011**, 109.

Out of the thesis

1. Synthesis and characterization of environmentally benign praseodymium-doped $TiCeO_4$ pigments, Sandhya Kumari L, **Giable George,** P. Prabhakar Rao, and M. L. P. Reddy, *Dyes and Pigments,*77, **2008**, 427.
2. Synthesis and characterization of new environmentally benign tantalum-doped $Ce_{0.8}Zr_{0.2}O_2$ yellow pigments: Applications in coloring of plastics, V.S. Vishnu, **Giable George**, V. Divya, M. L. P. Reddy, *Dyes and Pigments,* 82, **2009**, 53.
3. Effect of molybdenum and praseodymium dopants on the optical properties of $Sm_2Ce_2O_7$: Tuning of band gaps to realize various color hues, V.S. Vishnu, **Giable George**, M. L. P. Reddy, *Dyes and Pigments,* 85, **2010**, 117.

CONTENTS

PREFACE

The thesis entitled **"Synthesis, Characterization and Optical Properties of Rare Earth based Non-toxic Inorganic Pigments"** embodies the results of the investigations carried out on the synthesis, characterization and optical properties of a series of rare earth based inorganic pigments and their surface coating applications. Inorganic pigments are widely used in various applications such as paints, inks, plastics, rubbers, ceramics, enamels and glasses. Unfortunately, many of the inorganic pigments which are today actually employed on an industrial scale generally comprise toxic metal ions like cadmium, lead, chromium and cobalt. The use of these metal ions is becoming increasingly strictly controlled, indeed banned, by legislation in many countries because of their allegedly very high toxicity. Hence there is a strong incentive to develop new colored inorganic materials to substitute for industrial pigments that are based on heavy elements hazardous to health and the environment. Thus, the primary objective of the present work is to design and develop novel environmentally benign rare earth based inorganic pigments for surface coating applications.

The thesis has been divided into four chapters, of which the first chapter highlights the need for the development of new class of rare earth based inorganic pigments as alternatives to the existing toxic pigments. A general introduction to the inorganic pigments on the history, classification, uses and the theory behind the color properties has been reported in this chapter. Further, a detailed overview on the recent developments on the rare earth based pigments has also been incorporated towards the end of this chapter.

The second chapter describes the results on the synthesis, characterization and optical properties of Si^{4+} and Pr^{4+} doped Y_6MoO_{12} compounds. The designed products were characterized by X-ray powder diffraction, UV–vis diffuse reflectance spectroscopy and CIE-*L*a*b** 1976 color scales. The doping of Si^{4+} for Y^{3+} in Y_6MoO_{12} compound changes

the color hue from light-yellow to dark-yellow and the band gap gently decreases from 2.60 to 2.45 eV due to O_{2p}-Mo_{4d} charge transfer transitions. In contrast, replacing Pr^{4+} for Y^{3+} changed the color hue from light-yellow to dark-brown and the band gap shifted from 2.60 to 1.90 eV. The coloring mechanism is based on the introduction of an additional $4f^1$ electron energy level of Pr^{4+} between the valence and conduction bands. The NIR reflectance of the designed pigments has also been evaluated after coating on a roofing material like asbestos cement sheet for possible use as "cool pigment" (These results were published in ***Dyes and Pigments* 88, 2011, 109**).

The third chapter of the thesis deals with the synthesis, characterization and optical properties of environmentally benign inorganic pigments based on CeO_2–TiO_2–Pr_6O_{11} solid solutions, displaying colors ranging from brick-red to dark-brown. The coloring mechanism is based on the introduction of additional electronic level of energy in the cerianite forbidden band from the unpaired 4f electron of lanthanide ion. The utility value of the designed colorants in surface coating applications has been evaluated and the results are also given in this chapter. The typical designed pigment samples have been examined for their mass tone/hiding power, tinting strengths and weather resistance by coating on an opacity chart. The results demonstrated that the dark-brown pigment designed in the present study has been found to be interesting alternative to the existing classical toxic inorganic red pigments for surface coating applications (These results were published in ***Chemistry Letters* 35, 2006, 1412**).

A new class of inorganic pigments based on praseodymium molybdate having the general formula $Pr_{2-x}A_xMo_2O_{9-\delta}$ (where A = Ca^{2+}, Sr^{2+} and Ba^{2+} and x ranges from 0 to 1.0), displaying colors ranging from green to greenish-yellow were synthesized by traditional solid-state route, as alternatives to lead, cadmium and chromium colorants. These results have been summarized in chapter 4. The coloring mechanism is based on the strong absorptions of the pigments in the blue and red regions due to electronic transitions

between $4f^2 \rightarrow 4f^1 5d^1$ states of Pr^{3+}. The designed pigments consist of non-toxic elements and further found to be thermally and chemically stable. The greenish-yellow pigments were found to be interesting alternatives to existing toxic pigments for coloration of plastics (These results were published in ***Chemistry Letters*** **34, 2005, 1702;** ***Journal of Solid State Chemistry*** **181, 2008, 487**).

The relevant references used in this work have been cited towards the end of the thesis.

Chapter 1

Introduction

1.1. History, Classification and uses of Inorganic pigments

The word '**Pigment**' is of Latin origin (Pigmentum) and originally denoted a color in the sense of a coloring matter, but was later extended to indicate colored decoration. The modern meaning associated with the word pigment originated in the 20th century. According to accepted standards, the word pigment means a substance consisting of small particles that is practically insoluble in the applied medium and is used on account of its coloring, protective or magnetic properties. Pigments can be characterized by their chemical composition, and by their optical or technical properties.

Natural inorganic pigments have been known since prehistoric times, for example the drawings in the Pech-Merle caves (Fig.1) in the south of France, Northern Spain, and Northern Africa were made with charcoal, ocher, manganese brown and clays [Bittler and Ostertag 1980; Barnett *et al.* 2006].

Fig. 1. a) Detail from a cave drawing in Pech-Merle (France). b) Antique Grecian vase, from the 5th century BC.

About 2000 BC, natural ocher was burnt, sometimes in mixtures with manganese ores, to produce red, violet, and black pigments for pottery [Buxbaum and Pfaff 2005]. Arsenic sulfide and Naples yellow (a lead antimonate) were the first clear yellow pigments. Ultramarine (Fig. 2) and artificial lapis lazuli (Egyptian blue and cobalt aluminum spinel) were the first blue pigments [Berke 2006]. The development of the first known synthetic

blue pigment, Egyptian blue ($CaCuSi_4O_{10}$), is believed to have been patronized by the Egyptian pharaohs, who promoted the advancement of pigment technologies for use in the arts. The subsequent quest for blue pigments has a rich history linked with powerful civilizations, such as the Han Chinese [Han blue ($BaCuSi_4O_{10}$)] and the Maya blue [Maya blue (indigo intercalated in magnesium aluminosilicate clays)] [Berke 2006].

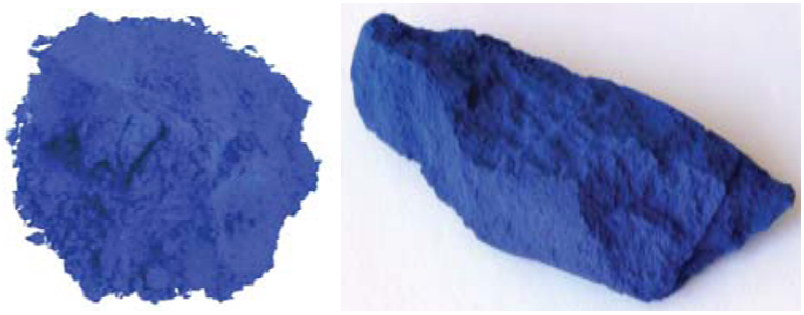

Fig. 2. An industrially produced Han Blue ($BaCuSi_4O_{10}$) and Ultramarine Blue.

Terra verte, malachite, and a synthetically prepared copper hydroxychloride were the first green pigments. Colored glazes for bricks (i.e., ceramic pigments) were widely used by the Chaldeans. Calcite, some phases of calcium sulfate, and kaolinite were the white pigments used at that time. Antimony sulfide and lead sulfide were commonly used as black pigments, and cinnabar (Fig. 3) as a red pigment [Barnett *et al.* 2006].

Fig. 3. Cinnabar

From the age of migration of the peoples to the end of the late Middle Ages, there were no notable additions to the range of coloring materials. New developments in the field of pigments first occurred during the early Renaissance. Carmine was introduced from Mexico by the Spanish. Smalt, safflore, and cobalt-containing blue glasses were developed in Europe. The pigment industry started in the 18th century with products such as Berlin blue (1704), cobalt blue (1777), Scheele's green, and chrome yellow (1778). In the 19th century, ultramarine, Guignet's green, cobalt pigments, iron oxide pigments were developed in quick succession. In the 20th century, pigments increasingly became the subject of scientific investigation. In the past few decades, the synthetic colored pigments cadmium red (Fig. 4), manganese blue, molybdenum red, and mixed oxides with bismuth came onto the market. Titanium dioxide with anatase or rutile structures was introduced as new synthetic white pigment.

Fig. 4. Cadmium Red Pigment

Inorganic pigments can be classified from various points of view. The classification given in Table 1 follows a system recommended by International Organization for Standardization (ISO) and the German Institute for Standardization, "Deutsches Institut für Normung (DIN)".

Table 1. Classification of inorganic pigments.

Term	Definition
White pigments	the optical effect is caused by nonselective light scattering (examples: titanium dioxide and zinc sulfide pigments)
Colored pigments	the optical effect is caused by selective light absorption and also to a large extent by selective light scattering (examples: iron oxide red and yellow, cadmium pigments, ultramarine pigments, chrome yellow, cobalt blue)
Black pigments	the optical effect is caused by nonselective light absorption (examples: carbon black, iron oxide black)
Effect pigments	the optical effect is caused by regular reflection or interference
Pearl luster pigments	regular reflection takes place on highly refractive parallel pigment platelets (examples: titanium dioxide on mica)
Metal effect pigments	regular reflection takes place on mainly flat and parallel metallic pigment particles (examples: aluminum flakes)
Interference pigments	the optical effect of colored luster pigments is caused mainly due to interference (examples: iron oxide on mica)
Luminescent pigments	the optical effect is caused by the capacity to absorb radiation and to emit it as light of a longer wavelength
Fluorescent pigments	the light of longer wavelength is emitted after excitation without a delay (examples: silver-doped zinc sulfide)
Phosphorescent pigments	the light of longer wavelength is emitted within several hours after excitation (examples: copper-doped zinc sulfide)

The most important areas of use of inorganic pigments are paints, plastics, printing inks for paper and textiles, leather decoration, building materials, floor coverings, rubber, cosmetics, ceramic glazes and enamels. The paint industry uses high-quality pigments and an optimal, uniform particle size are important because it influences gloss, hiding power, tinting strength, and lightening power. When choosing a pigment for a particular application, several points normally have to be considered. The coloring properties are

important in determining the application efficiency and hence economics. The following properties are also important:

1. *General chemical and physical properties*: Chemical composition, moisture and salt content, content of water soluble and acid soluble matter, particle size, density and hardness.
2. *Stability properties*: Resistance towards light, weather, heat and chemicals, anti-corrosive properties and retention of gloss.
3. *Behavior in binders*: Interaction with the binder properties, dispersibility, compatibility and solidifying effect.

1.2. Color properties

All color phenomena that we can observe in coatings have their origin in the interaction between the coating material and visible light, ie, the electromagnetic radiation in the wavelength range of 400 to 700 nm. When a photon enters a pigmented film one of three events may occur:

1. It may be absorbed by a pigment particle
2. It may be scattered by a pigment particle
3. It may simply pass through the film

The important physical-optical properties of pigments are therefore their light-absorption and light-scattering properties. If absorption is very small compared with scattering, the pigment is a white pigment. The absorption is much higher than scattering over the entire visible region, and then the pigment is a black pigment. In a colored pigment, absorption is selective.

The pigments and coatings may be unambiguously characterized by their spectral reflectance curves $\rho(\lambda)$ or spectral reflectance factor curves $R(\lambda)$. But the human eye cannot see reflection spectra; and it merely communicates color stimuli to the brain. The missing link in the chain is the conversion of reflection spectra to color stimuli; this is

accomplished by colorimetry. The reflectance spectrum ρ(λ) or R(λ) and hence the color properties can be almost completely derived from physical quantities (Fig.5):

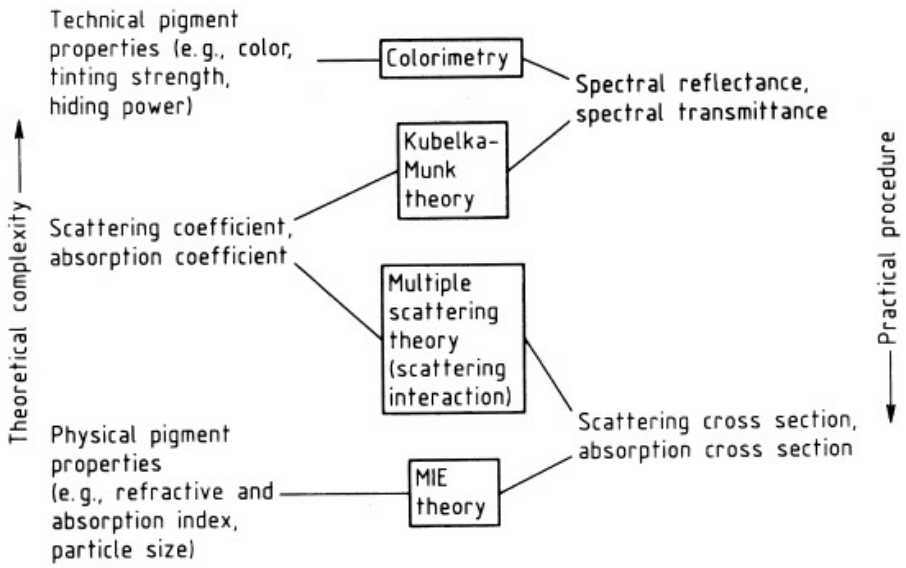

Fig. 5. Schematic diagram showing relationships between color properties and theoretical fundamentals.

(i) Colorimetry relates the perceived color quality to the color stimulus, which in turn is based on the reflectance spectrum ρ(λ). The principles of colorimetry are based on the fact that all color stimuli can be simulated by additively mixing only three selected color stimuli (trichromatic principle). A color stimulus can, however, also be produced by mixing the spectral colors. Thus, it has a spectral distribution, which in the case of nonluminous, perceived colors is called the spectral reflectance ρ(λ). After defining three reference stimuli, the trichromatic principle allows a three-dimensional color space to be built up in which the color coordinates (tristimulus values) can be interpreted as components of a vector (CIE system; for standards, "Colorimetry"; CIE = Commission Internationale de l'Éclairage). The three CIE tristimulus values depend on the spectral reflectance ρ(λ) and the spectrum of the illuminant $S(\lambda)$ as follows:

$$X = \int_{700}^{400} \bar{x}(\lambda)\, \rho(\lambda)\, S(\lambda) d\lambda$$

$$Y = \int_{700}^{400} \bar{y}(\lambda)\, \rho(\lambda)\, S(\lambda) d\lambda$$

$$Z = \int_{700}^{400} \bar{z}(\lambda)\, \rho(\lambda)\, S(\lambda) d\lambda$$

Where $\bar{x}(\lambda)$, $\bar{y}(\lambda)$, and $\bar{z}(\lambda)$ are the CIE tristimulus values of the spectral colors and are called the CIE spectral tristimulus values (color matching function). The CIE chromaticity coordinates (x, y and z) are given by

$$x = X/X + Y + Z$$

$$y = Y/X + Y + Z$$

$$z = 1 - x - y$$

They are represented as coordinates in a color plane. The chromaticity coordinates x and y are used to specify the saturation and hue of any color in the CIE chromaticity diagram (Fig. 6). The CIE spectral tristimulus value $y(\lambda)$ corresponds to the lightness sensitivity curve of the human eye. Therefore, a third color variable is specified in addition to x and y, namely the CIE tristimulus value Y, which is a measure of lightness.

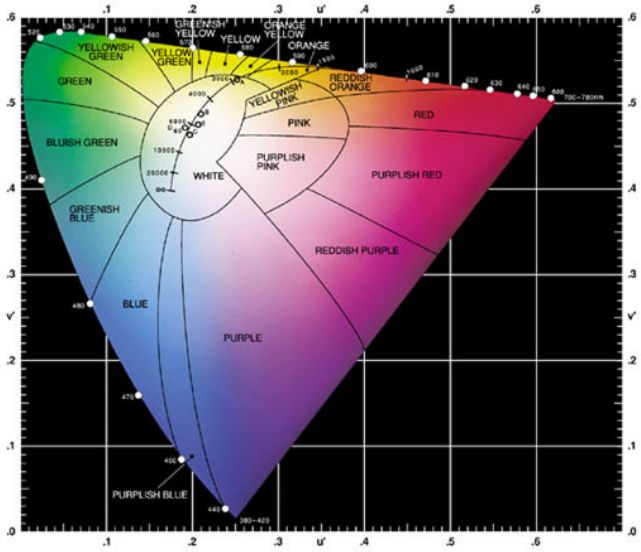

Fig. 6. CIE 1976 – Chromaticity diagram.

This system allows exact measurement of color with worldwide agreement. For pigment testing, however, this is not sufficient because small color differences usually have to be determined and evaluated (e.g., between test and reference pigment). Using the CIE system, it is certainly possible to say which spectral distributions are visually identical, but this is not suitable for determining color differences. To establish color differences an "absolute color space" must be used. Here, colors are arranged three-dimensionally such that the distance between two colors in any direction in space corresponds to the perceived difference. Such a type of color space can be based on the color qualities lightness, hue, and saturation. Several such systems exist. The most widespread color system is probably the Munsell system, which is available in the form of an atlas.

For the quantitative determination of color differences, the transformation relationships between the CIE system (which has to be used for color measurement) and the physiologically equidistant color system must be established. Color differences can then be calculated in the latter system. A large number of color difference systems have been developed, mainly as needed for industrial color testing. The Adams–Nickerson (AN) system, well known for many decades and derived from the Munsell system, was recommended for pigment testing by DIN (German Standards Institute) and later worldwide by the CIE 1976 $L^*a^*b^*$ ("CIELAB"; for standards, "Color differences"). The three coordinates are denoted by a^* (the red–green axis), b^* (the yellow–blue axis), and L^* (the lightness axis) (Fig. 7).

To calculate the CIELAB coordinates, X, Y, and Z are first converted into the functions X^*, Y^*, and Z^* by using a relationship that approximately takes account of the physiologically equidistant lightness steps:

$$X^* = \sqrt[3]{X / X_n}$$

$$Y^* = \sqrt[3]{Y / Y_n}$$

$$Z^* = \sqrt[3]{Z / Z_n}$$

where X_n, Y_n, and Z_n are the CIE tristimulus values of the illuminant, especially a standard illuminant. For radicands ≤ 0.008856, these equations become:

$$X^* = (7.787\ X / X_n) + 0.138$$

$$Y^* = (7.787\ Y / Y_n) + 0.138$$

$$Z^* = (7.787\ Z / Z_n) + 0.138$$

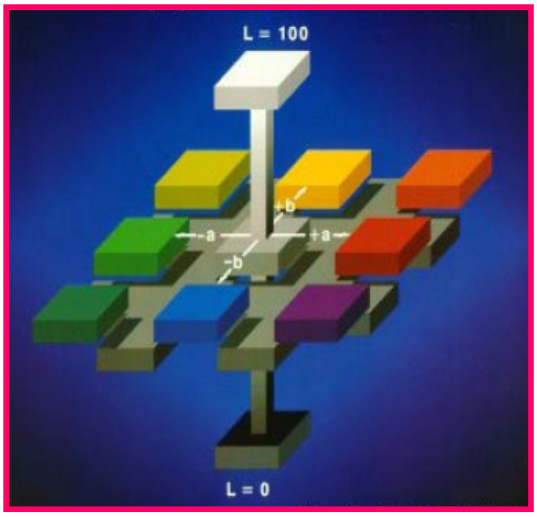

Fig. 7. Representation of the CIELAB system.

Values of a^*, b^*, and L^* are obtained from the values of X^*, Y^*, and Z^*:

$$a^* = 500\ (X^* - Y^*)$$

$$b^* = 200\ (Y^* - Z^*)$$

$$L^* = 116\ Y^* - 16$$

The components of the color difference are obtained as differences between the test sample (T) and the reference pigment (R):

$$\Delta a^* = a_T^* - a_R^*$$

$$\Delta b^* = b_T^* - b_R^*$$

$$\Delta L^* = L_T^* - L_R^*$$

The color difference is finally calculated as the geometrical distance between the two positions in the CIELAB color space:

$$\Delta E_{ab}^* = \sqrt{(\Delta a^*)^2 + (\Delta b^*)^2 + (\Delta L^*)^2}$$

An important advantage of the CIELAB system is that the resulting color difference can be split into component contributions, namely lightness, saturation, and hue, corresponding to the arrangement of the color space:

Lightness difference: $\Delta L^* = L_T^* - L_R^*$

Chroma difference (saturation difference): $\Delta C_{ab}^* = \sqrt{(a_T^*)^2 + (b_T^*)^2} - \sqrt{(a_R^*)^2 + (b_R^*)^2}$

Hue difference: $\Delta H_{ab}^* = \sqrt{(\Delta E_{ab}^*)^2 - (\Delta L^*)^2 - (\Delta C_{ab}^*)^2}$

(ii) The Kubelka-Munk theory is based on the fact that the optical properties of a film which absorbs and scatters light may be described by two constants: the absorption coefficient *K* and the scattering coefficient *S*. In a simplification, the flux of the diffuse incident light is represented by a single beam L+, and the flux of the light scattered in the opposite direction by a beam L–. Each beam is attenuated by absorption and scattering losses, but is reinforced by the scattering losses of the respectively opposite beam. The absorption and scattering losses are determined quantitatively by the two coefficients *K* and *S*. A simple system of two linked differential equations can be written. These can be integrated for the valid boundary conditions at the incident light side, and at the opposite side. Solutions for the transmittance τ and the reflectance ρ are obtained from these integrals as a function of the absorption coefficient *K*, the scattering coefficient *S*, the film thickness *h*, and in special cases of the reflectance ρ_o of a given substrate.

The most important and widely used quantity derived from the Kubelka–Munk theory is the reflectance of an opaque (infinitely thick) film that is described by a very simple eqn:

$$K/S = (1 - \rho_\infty)^2 / (2\rho_\infty)$$

From this expression (Kubelka–Munk function) it follows that, within the range of validity of the theory, ρ_∞ depends only on the ratio of the absorption coefficient to the scattering coefficient, and not on their individual values. The equation has been most useful where

reflectance measurements are used to obtain information about absorption and scattering (e.g., in textile dyeing, thin layer chromatography and IR spectroscopy).

This theory is especially useful for computer color matching of pigmented systems: absorption and scattering coefficients are combined additively using the specific coefficients of the components multiplied by their concentrations.

(iii) Multiple Scattering: The absorption coefficient K obeys Beer's law, even at high pigment volume concentrations σ, and is therefore proportional to σ. The relationship between the scattering coefficient S and the concentration gives rise to problems, however. The distance between the pigment particles decreases with increasing concentration; consequently there is interaction and hindrance between the light scattered by individual particles, and their scattering power usually falls. The scattering coefficient S is therefore linearly related to concentration only at low concentrations (the Beer's law region), at higher concentrations it remains below the linear value. The concentration dependence of the scattering coefficient can be quantitatively represented by using empirical formulae, e.g., there is a linear relationship between S/σ and $\sigma^{2/3}$.

***(iv) Mie's Theory*:** Mie applied the Maxwell equations to a model in which a plane wave front meets an optically isotropic sphere with refractive index n and absorption index κ. Integration gives the values of the absorption cross section Q_A and the scattering cross section Q_S; these dimensionless numbers relate the proportion of absorption and scattering to the geometric diameter of the particle. The theory has provided useful insights into the effect of particle size on the color properties of pigments.

Scattering is considered first. Here, the crucial parameter α in the Q_A and Q_S formulae is a relative measure of particle size because it is proportional to the particle diameter D and is inversely proportional to the wavelength λ. At a constant wavelength λ and for various relative refractive indices n (i.e., relative to the binder, $n = n_p / n_B$ where n_p and n_B

are the refractive indices of the particle and binder, respectively), it gives the relationship between scattering and particle size. If, on the other hand, the particle size D is kept constant, α denotes the relationship between the scattering and the wavelength (1/ λ replaces D on the abscissa). The well-marked maxima are typical, and their existence signifies

1. That an optimum particle size must exist with respect to lightening power
2. That for a given particle size, there must be a particular wavelength for maximum light scattering.

The first relationship can be used to predict the optimum particle size of white pigments. The second relationship explains, for example, how white pigments in gray color mixtures can produce colored undertones as a result of selective light scattering.

The consequences of Mie's theory for *absorption* (i.e., for tinting strength) are now considered. Calculations from Mie's theory, using the relative refractive index n and the absorption index κ, are given in Fig. 8.

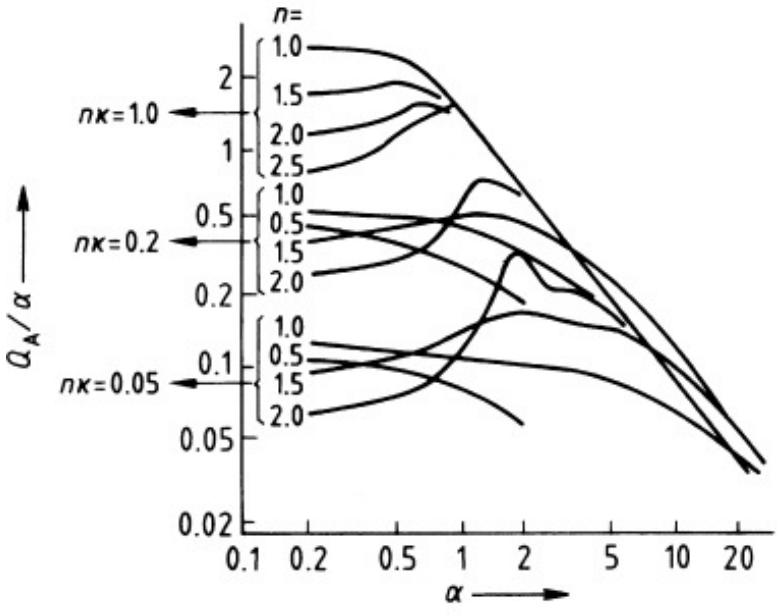

Fig. 8. Absorption as a function of particle size.

The parameter α on the abscissa can once more be taken as a relative measure of the particle size. The following conclusions may be drawn:

1. For very small particles, the absorption is independent of the particle size, and hence any further reduction in particle size does not produce additional absorption.
2. With increasing absorption index κ, the absorption of very small particles increases.
3. Absorption values for large particles are approximately equal for all relative refractive indices n and absorption indices κ, and decrease hyperbolically.
4. The top curve in Fig. 8 applies to pigments with a high absorption index κ and low refractive index n (e.g., carbon black) and shows that the optimal particle size lies below a given limit.
5. The lowest curve applies to pigments with a small absorption index κ and high relative refractive index n, as is usually the case with inorganic pigments (e.g., red iron oxide). Here, there is a distinct maximum.

The above relationships (Fig. 8) show that the optical pigment properties depend on the particle size D and the complex refractive index $n^* = n\ (1 - i\kappa)$, which incorporates the real refractive index n and the absorption index κ. As a result, the reflectance spectrum, and hence the color properties, of a pigment can be calculated if its complex refractive index, concentration, and particle size distribution are known.

1.3. Objectives of the present investigation

Inorganic pigments/colorants are currently widely used in numerous industries, especially in those of paints, plastics and ceramics. For such applications their properties, inter alia, of thermal and/or chemical stability, dispersibility, chromaticity, tinting strength and covering or masking power are particularly important criteria to be taken into consideration in the selection of a suitable inorganic pigment. Unfortunately, many of the inorganic pigments which are suitable for applications such as those indicated above and which are today actually employed on an industrial scale generally comprise toxic metal ions like cadmium, lead, chromium and cobalt. The use of these metal ions is becoming increasingly strictly controlled, indeed banned, by legislation in many countries because of their allegedly very high toxicity. This is the case as regards red pigments based on cadmium sulfoselenide encapsulated in zircon matrix and lead oxide in tin oxide matrix and yellow pigments such as $Pb_2Sb_2O_7$, $PbCrO_4$ and CdS. Similarly, green pigments based on chromium oxide. Thus, serious economic and industrial need continues to exist for substitute inorganic pigments devoid of the above disadvantages and drawbacks.

Recently, pigment colorant researchers are also developing new complex inorganic pigments that exhibit dark color in the visible spectrum and high reflectance in the near infrared portion of the electromagnetic spectrum. This class of pigments increases the near infrared reflectance of exterior finishes and paints, there by dropping the surface temperatures of roofs and walls, which, in turn, reduces the cooling-energy demand of the building. The inorganic NIR reflective pigments are mainly metal oxides and are primarily useful in two major applications: (i) visual camouflage and (ii) reducing heat build up. However, many of these pigments currently employed are toxic and there is a need to develop novel colored, NIR reflecting inorganic pigments that are less hazardous to the environment.

Rare earth elements offer a vast opportunity for development of environmentally secure alternatives for many of the eco-constrained colorants. India is rich in rare earth resources and occupies the third place in the world in terms of rare earth deposits. Industrial utilization of rare earths is growing very rapidly because of their known low toxicity [Garcia *et al.* 2001]. The main industrial application in the field of rare earths is the ceramic industry, which consumes up to 31% world production of rare earth compounds. CeO_2 promotes opacity in ceramic glazes and the so called yellow of praseodymium-zircon color is the best ceramic pigment. Similarly, cerium sulfide has substituted the orange and red colors based on the cadmium sulfoselenide pigment used in the ceramic and painting industries. Electronic configuration of the valence layer of the trivalent rare earth ions, $[Xe]4f^n$, involves the activity of internal f electrons, strongly protected by 5s and 5p electrons. Therefore, the resulting crystalline field caused by their interaction with neighboring ions is very low and usually optical spectra of lanthanide compounds present weak and profuse bands.

Thus, the objectives of the present work are as follows:

1. To develop environmentally benign rare earth based inorganic pigments displaying colors of red and yellow as viable alternatives to the existing toxic inorganic pigments.
2. To convert the developed inorganic pigment formulations suited for various surface coating applications.
3. To develop non-toxic NIR reflective colored inorganic pigments based on rare earth elements and their application towards building roofing materials.

1.4. Recent advances on the design and development of rare earth based inorganic pigments

***1.4.1. Rare earth based blue inorganic pigments*:** Currently used blue inorganic pigments are cobalt blue ($CoAl_2O_4$), ultramarine ($Na_7Al_6Si_6O_{24}S_3$), Prussian blue ($Fe_4[Fe(CN)_6]_3$) (Fig. 9), and azurite [$Cu_3(CO_3)_2(OH)_2$]. All suffer from environmental and/or durability issues: Cobalt is considered to be highly toxic. Ultramarine and azurite are not stable with respect to heat and acidic conditions. Prussian blue liberates HCN under mild acidic conditions. In addition, the manufacture of ultramarine involves a large amount of SO_2 emission. Hence, the identification of intense blue inorganic pigments that are environmentally benign, earth-abundant, and durable is important but remains a challenge today.

Fig. 9. Prussian blue ($Fe_4[Fe(CN)_6]_3$)

Recently, environmentally benign intense bright blue color pigments have been obtained by substituting Mn^{3+} for indium in hexagonal $YInO_3$ (Fig. 10), in spite of the fact that $YInO_3$ and $YMnO_3$ are white and black, respectively [Smith *et al.* 2009]. It has been concluded that the blue color is a consequence of both the crystal field splitting is associated with the trigonal-bipyramidal coordination and the short Mn−O bonds.

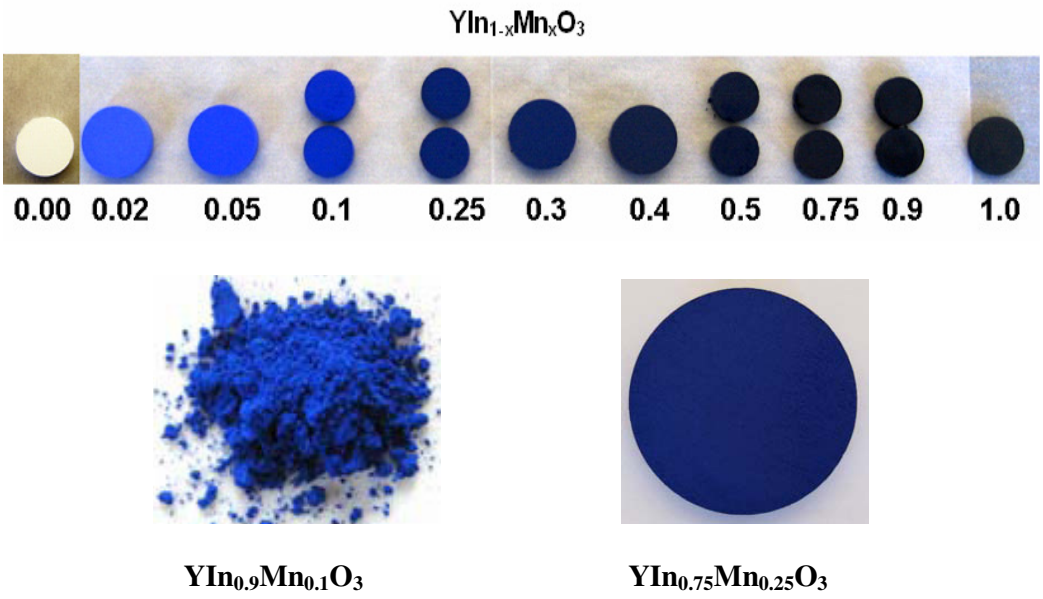

Fig. 10. The intense blue color appears at lowest concentration of Mn doping in $YMnO_3$. With increasing Mn composition, the color darkens until $YMnO_3$ is found to be black.

1.4.2. Rare earth based green pigments: In the industrial ceramic production, green coloration can be obtained by using several pigments: eskolaite (Cr_2O_3) (Fig. 11), uvarovite $Ca_3Cr_2[SiO_4]_3$, spinel $(Co,Zn)(Cr,Al)_2O_4$, and zircon $(Zr,Pr)SiO_4$ + $(Zr,V)SiO_4$. However, many of these conventional pigments consist of heavy metal ions and thus classified them as toxic inorganic pigments, which are hazardous to human health and environment.

Fig. 11. Chromium oxide (Cr_2O_3) green pigment.

Therefore, discovery and development of new inorganic pigments have been designed in order to replace that existing toxic pigments. In this context, new pigments based on

cerium orthophosphate doped with alkaline-earth metals have been synthesized and their color properties have been investigated from the view point of possible ecological inorganic pigments [Imanaka *et al.* 2003; Masui *et al.* 2004; Sivakumar and Varadaraju 2005]. The origin of the yellow-green coloration of these pigments were attributed to the appearance of the principle broad absorption band corresponding to the 4f-5d electronic transition of Ce^{3+} and the additional O_{2p} - Ce_{4f} charge transfer transition of Ce^{4+} by the doping of alkaline-earth metal into $CePO_4$ lattice.

Compounds based on $YCrO_3$, perovskite structure, doped with Al, Ti were designed aiming at assessing their potential as green ceramic pigments [Ardit *et al.* 2009]. It has been reported that the doping of Al, Ti and Ca affected the phase composition and induced a series of structural rearrangements in perovskite and their optical properties. Further more these authors noted that the oxidation of Cr^{3+} to Cr^{4+} had a deleterious effect on its green color, tuning to grey-brown color.

Thermally/chemically stable and nontoxic inorganic pigments/colorants, characteristically green and well suited for the coloration of a wide variety of materials and substrates, for example, plastics, ceramics, etc. comprising at least one mixed oxide of the formula: Y_2BaCuO_5, Sm_2BaCuO_5 and Yb_2BaCuO_5 has been reported in the U.S. Patent No. 6,284,03 [Chopin and Macaudiere 2001].

The structural characterization and optical properties of Ca-doped Nd_2S_3 pigments have been investigated and found that the introduction of CaS into the α-Nd_2S_3 matrix induces a change in color from dark red to green color [Garrotte *et al.* 2006].

1.4.3. Rare earth based red pigments: To date the pigment industry has typically used three types of red pigments: Fe_2O_3 in zircon matrixes, Pb_3O_4 in tin oxide matrixes, and $CdS_{1-x}Se_x$ encapsulated in a zircon matrix [Smith 2002]. The first two yield pink and red colors. The third yields a red color, and is unstable at temperatures exceeding 900°C.

However, the second and third class of pigments are toxic. These materials can be replaced by rare-earth oxides, which provide new stable red colors; moreover, rare-earth metal ions generally have a low toxicity rating [Haley 1965; Arvela 1979].

Praseodymium-doped ceria has been successfully examined by many investigators as an inorganic pigment in the ceramic industry to obtain colors ranging from pink-orange to red-brown [Bondioli *et al.* 2000; Bondioli *et al.* 2001; Garcia *et al.* 2001; Wang *et al.* 2002; Maso *et al.* 2003; [b]Sulcova *et al.* 1998]. It has been noted that the color hue of the pigments depends on the quantity of praseodymium present, synthesis conditions and calcination temperatures. Jorgensen and Rittershaus explained the color of the praseodymium-doped ceria by assigning the absorption band appearing at $\lambda <$ 600 nm is due to electron transfer from the ligands to the chromophore ion [Jorgensen and Rittershaus 1967]. According to the band structure model proposed by Koelling for CeO_2 and PrO_2, the electronic spectra arise due to the electron transfer from the ligand orbitals to the localized $4f^1$ level of the Pr^{4+} cation [Koelling *et al.* 1983].

Nano-crystalline praseodymium-doped ceria powders were prepared by the first time by a microwave-assisted hydrothermal route [Bondioli *et al.* 2005]. The effect of the microwave treatment in relation to the conventional hydrothermal technique was evaluated.

Praseodymium-doped ceria red pigments, $Ce_{1-x}Pr_xO_{2-\delta}$ (x = 0–0.5) have also been prepared by the thermal decomposition of the redox compound $Ce_{1-x}Pr_x(N_2H_3COO)_3.3H_2O$ as well as by the combustion of aqueous solutions containing cerous nitrate, praseodymium nitrate and oxalyl dihydrazide/ammonium acetate. Formation of the pigment has been confirmed by its characteristic red color and reflectance spectrum which shows the reflection edge ~ 690 nm corresponding to charge transfer from the ligand orbitals to the localized $4f^1$ of Pr^{4+} [Aruna *et al.* 2001].

In our laboratory, novel environmentally secure inorganic pigments by doping praseodymium into CeO_2 matrix of $TiCeO_4$ with colors ranging from white to brick-red have been obtained (Fig. 12), as viable alternatives to the existing toxic red pigments [Kumari *et al.* 2008]. The color mechanism has been explained on the basis of shift of the charge transfer band of CeO_2 to higher wavelengths and the band gap of the pigment reduces from 2.96 to 1.84 eV with increasing the dopant concentration.

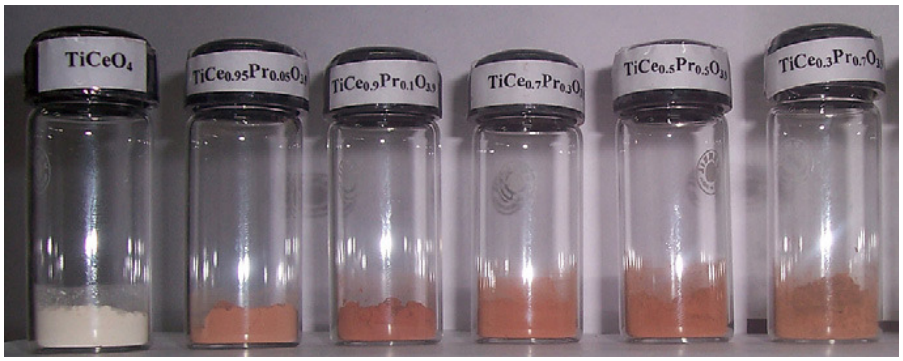

Fig. 12. Photographs of $TiCe_{1-x}Pr_xO_{4-\delta}$ pigments.

In the later studies [Vishnu *et al.* 2010], the effect of praseodymium doping on the optical properties of $Sm_2Ce_2O_7$ has also been systematically investigated and found that the color of the resultant pigments vary from cream through brick-red to dark-brown (Fig. 13). The influence of various mineralizers on the calcination temperatures and the optical properties of the pigments have also been evaluated and reported that the calcination temperature can be lowered by employing an appropriate mineralizer along with the precursor oxides.

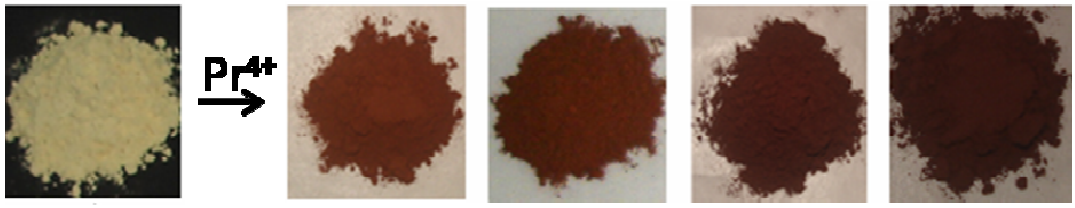

Fig. 13. Photographs of $Sm_2Ce_{2-x}Pr_xO_{7+\delta}$ (x = 0 to 0.4) pigments.

New inorganic pigments based on fluorite solid solutions, $Ce_{0.95}M_xPr_{0.05-x}O_2$ (M = Zr and Sn; *x* ranges from 0 to 0.05) displaying colors from brick-red to dark-brown have been reported [Kumari *et al.* 2010]. The substitution of zirconium or tin in $Ce_{0.95}Pr_{0.05}O_2$ system changes the optical band gap from 1.88 to 3.06 eV.

Fe_2O_3 doped rare earth pigments aiming at producing ceramic pigments with hues that vary from orange to brown (Fig. 14) have been successfully synthesized by both solid-state route and sol-gel methods [Melo et al. 2007; Dohnalova *et al.* 2008; Nunes *et al.* 2008]. In the case of calcinations route, the color of the pigment changes as the calcination temperature increases from 900 to 1000°C. On the other hand, in sol-gel route, bright red pigments are obtained after heat treatment at 800°C for 2 h in the presence of low concentrations of praseodymium.

Fig. 14. 20% α-Fe_2O_3.80% CeO_2 heat treated at 800°C for 2 h in air atmosphere.

The US Patent No. 5,401,309 discloses a process for the synthesis of Ce_2S_3 based pigments having colors varying from brown to red according to the conditions for the preparation thereof, in particular the calcination temperature [Chopin and Dupuis 1995]. These pigments are brown or blood-red depending on whether they have the orthorhombic β-Ce_2S_3 phase or the cubic γ- Ce_2S_3 phase.

Recently, a novel erbium titanate pink pigment synthesized by sol-gel methodology has been reported [Martos *et al.* 2008]. The success on the development of color is

completely related to the sol-gel preparation method, underlying its higher reactivity compared to classical solid-state synthesis. Erbium ions possess a constricted environment and the Er-O bond covalence is higher than in a regular cubic pyrochlore structure. The higher covalent character reduces the interaction between the electrons, since they spread out over wider orbitals, and electron transitions require lower energy, leading to the shift of absorption bands to higher wavelengths. Thus, the change in the Er-O bond covalence from fluorite to pyrochlore structure would be responsible for the color evolution. The above study also revealed that $Er_2Ti_2O_7$ exhibits a pink color only in its defect fluorite-type structure. Further it demonstrated that the intense coloration depends on the presence of fluorite structure, which transforms to pyrochlore at temperature over 700°C causing loss of intensity. In the later studies, these authors have improved the intense pink coloration through the substitution of Ti^{4+} with larger Zr^{4+} ions in $Er_2Ti_2O_7$ [Marthos *et al.* 2009] (Fig. 15).

Fig. 15. Picture of the $Er_2Ti_{0.6}Zr_{1.4}O_7$ powders fired at different temperatures.

1.4.4. Rare earth based yellow pigments: The most known yellow inorganic pigments are praseodymium-zircon yellow, vanadium–zirconia yellow, tin–vanadium yellow, chromates of alkaline earth metal ions, and lead antimonate, cadmium yellow, iron oxide yellow, and nickel–antimony doped rutile phase TiO_2. Among these inorganic yellow pigments, the application of iron oxide yellow gets constrained due to thermal stability only up to 220°C [Cornell and Schwertmann 1996], while the toxicity [Badenes *et al.* 2002] of chromium(VI), cadmium and lead based yellow pigments restricts their commercial usage; and praseodymium-zircon yellow, vanadium–zirconia yellow which

are even if most popular in the market of yellow inorganic pigments, they have some limitations in bulk coloration porcelain stoneware at high temperature [Sorly *et al.* 2004; Biswas *et al.* 2008].

The use of praseodymium doped zirconium silicate crystals as a pigment for use in ceramic glazes was first reported by Seabright [U.S. Patent No. 2,992,123; 1961]. Since that time, there have been numerous patents issued for praseodymium doped zircons for ceramic applications and now it is manufactured worldwide [Blonski 1994; Linke *et al.* 1994; Huguenin *et al.* 1996]. Although praseodymium yellow pigments are used in the industry for many years, a quantitative description of the effects of the processing parameters does not exist in the open literature. Hence, many attempts have been made to investigate the effect of various process parameters on the synthesis of praseodymium-zircon yellow pigments [Hill *et al.* 2000; Badenes *et al.* 2002; Del Nero *et al.* 2004; Kar *et al.* 2004; Kar *et al.* 2007]. These studies clearly highlight that the color formation correlates strongly with the processing temperature, mineralizer content and to a lesser extent, particle size of the zirconia raw material. Further, the results demonstrate that the formation of Pr-$ZrSiO_4$ yellow pigment has been explained by two simultaneous mechanisms: formation of a solid solution of praseodymium in a $ZrSiO_4$ network and occlusion mechanism [Badenes *et al.* 2002]. When praseodymium oxide is incorporated into the zircon host lattice, Pr^{3+} replaces the Zr^{4+} and going to the interaction of the surrounding f-electrons with the host lattice, the f-orbitals split into two groups, of which one has a higher energy and the other has a lower energy. Hence, splitting of the energy level depends on the interaction of the surrounding f-electrons with the host lattice. Since the transition of energy from higher energy level to a lower energy falls in the yellow region of the visible spectrum, a yellow color is observed. Addition of cerium oxide to praseodymium oxide in zircon host lattice shifts the color towards the orange region of the spectrum because of the change in the splitting of the energy level owing to the change in

the interaction of the f-electrons with the surrounding electrons of the host lattice, thereby inducing the color change [Kar *et al.* 2007]. It is also been reported elsewhere that the incorporation of terbium oxide into the zircon host lattice in the presence of different types of mineralizes creates various shades of yellow which are different from the praseodymium-zircon yellow [Kar *et al.* 2004].

As yellow pigments to substitute for CdS, $PbCrO_4$ and $PbMoO_4$, sulfides of Ce^{3+} ions are also appropriate if their Ce^{3+} $4f^1 \rightarrow 5d^0$ transition starts at ~2.5 eV (Fig. 16). This can be achieved by increasing the net positive charge on the Ce atoms, i.e., by increasing the ionicity of the Ce–S bonds [Gauther *et al.* 2003]. According to the inductive effect, one can increase the ionicity of a Ce–S bond by forming a Ce–S–M bond linkage with third element M that makes a strong covalent bond with S. An increase in the net positive charge on a cation lowers the energies of its orbitals. In a Ce–S–M compound, one might expect that this energy lowering effect is larger for the 4f than for the 5d orbitals of Ce, thereby increasing the Ce^{3+} $4f^1 \rightarrow 5d^0$ gap, because the Ce 4f orbitals are much more localized on the Ce atom than the Ce 5d orbitals. Based on the above phenomenon, yellow colors are found for cerium thiosilicates (Ce_2SiS_5, $Ce_6Si_4S_{17}$ and $Ce_4Si_3S_{12}$) and cerium thiophosphates ($CePS_4$). $Ce_4Si_3S_{12}$ and $Ce_6Si_4S_{17}$ possess chromatic properties similar to those found for industrially used pigments such as CdS, $PbCrO_4$ and $PbMoO_4$, and show thermal and chemical stabilities.

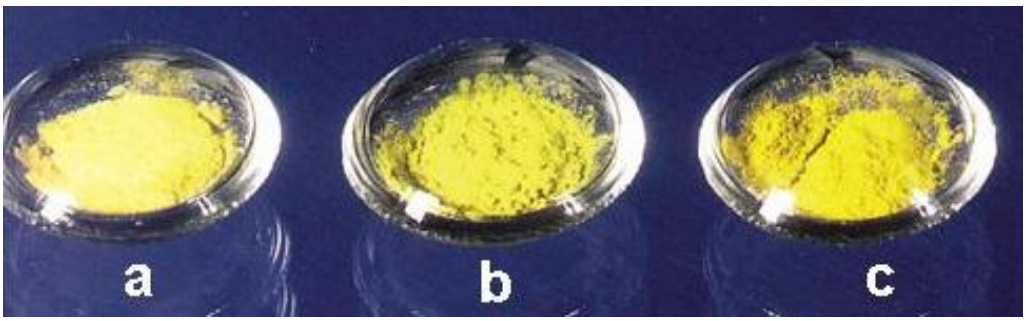

Fig. 16. Colors of (a) $CePS_4$, (b) $Ce_6Si_4S_{17}$, and (c) $Ce_4Si_3S_{12}$.

Crystalline cerium molybdenum oxides have been reported as novel yellow pigments as alternatives to lead, cadmium and chromium based toxic pigments [Sreeram *et al.* 2007; Marc *et al.* 1993]. The reflectance spectrum of the cerium double molybdates indicates strong absorption in both visible and ultraviolet regions, which could originate from the O_{2p}–Ce_{4f} and the O_{2p}–Mo_{3d} double charge transitions and as a result the pigments show yellow color. Amorphous cerium tungstate, $Ce_{1-x}M_xW_2O_8$ (M = Zr or Ti, $0 \leq x \leq 0.6$) has been reported as a possible ecological inorganic yellow pigment [Masui *et al.* 2005; Furukawa *et al.* 2006]. This pigment exhibits brilliant yellow color due the effective absorptions in the visible and ultraviolet regions (under 500 nm efficiently), which is originated from the O_{2p}–Ce_{4f} and the O_{2p}–W_{5d} double charge transitions (Fig. 17).

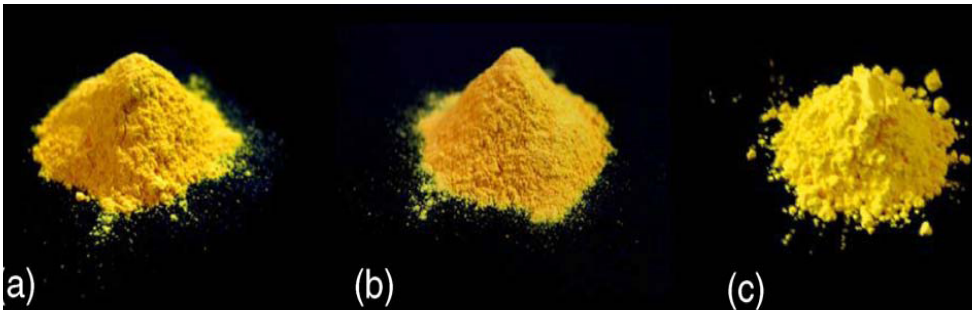

Fig. 17. Representative photographs of the samples: (a) amorphous $Ce_{0.8}Zr_{0.2}W_2O_8$, (b) amorphous $Ce_{0.8}Ti_{0.2}W_2O_8$, and (c) commercial praseodymium yellow.

$Ce_{1-x-y}Zr_xBi_yO_{2-y/2}$ solid solutions have been reported as new inorganic yellow pigments [Masui *et al.* 2006; Furukawa *et al.* 2008]. The doping of Bi^{3+} ions into the CeO_2 lattice results in enhancement of visible light absorptions due to the transition from a new valence band, made up of a hybrid orbital of Bi_{6p} and O_{2p}, to the Ce_{4f} conduction band.

Yellow inorganic pigments also have been obtained by suitably doping of tantalum in ZrO_2 matrix in $Ce_{0.8}Zr_{0.2}O_2$ compound [Vishnu *et al.* 2009]. The coloring mechanism has been explained on the basis of strong absorptions of the pigments in the visible region under 500 nm, which could originate from the additional energy level between O_{2p} valence and the Ce_{4f} conduction bands by forming a hybrid orbital of Ta_{5d} and O_{2p} (Fig. 18).

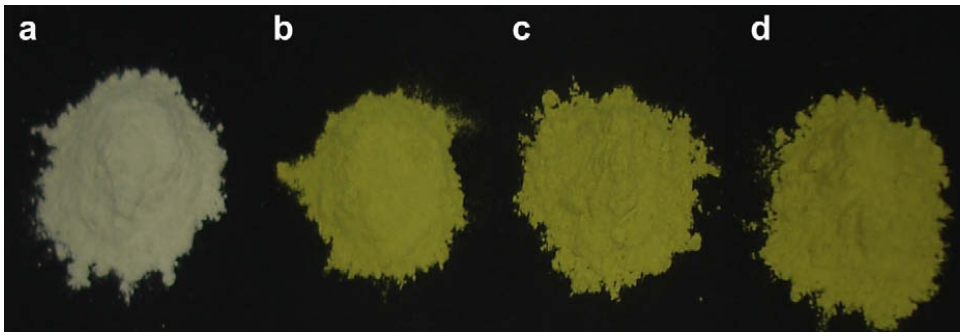

Fig. 18. Photographs of (a) $Ce_{0.8}Zr_{0.20}O_2$ (b) $Ce_{0.8}Zr_{0.19}Ta_{0.01}O_{2+\delta}$ (c) $Ce_{0.8}Zr_{0.17}Ta_{0.03}O_{2+\delta}$ (d) $Ce_{0.8}Zr_{0.15}Ta_{0.05}O_{2+\delta}$ pigments.

Earlier investigations reveal that the classical toxic inorganic pigments can be replaced by solid solutions of perovskites $CaTaO_2N$ and $LaTaON_2$, which gives colors ranging from yellow to deep red [Jansen and Letschert 1997; Jansen and Letschert 2000]. Although these pigments are non-toxic and show excellent color hue, it is necessary to heat the starting materials in a flow of toxic and inflammable ammonia gas for a long time (20–60 h) to synthesize them. Therefore, research needs to be performed in developing novel yellow inorganic pigments with various advantages over traditional toxic pigment formulations.

U.S. Pat. No. 6,419,735 [Busnot and Macaudiere 2002], discloses a process for the preparation of samarium sesquisulfide pigment. The process consist of reacting samarium, trivalent rare earth metal, and alkali metal or alkaline earth metal compounds with a gaseous mixture of hydrogen sulfide and carbon disulfide. The compositions of the invention exhibit a strong yellow color.

Recently, a series of non-toxic inorganic pigments having the general formula $Sm_2Ce_{2-x}Mo_xO_{7+\delta}$ (x = 0 to 0.4) displaying wide range of colors from cream to yellow have been designed by a simple calcination route [Vishnu *et al.* 2010]. The band gap of the resulted pigments decreases from 2.76 to 2.52 eV due to the O_{2p}–Mo_{4d} charge transfer transition (Fig. 19).

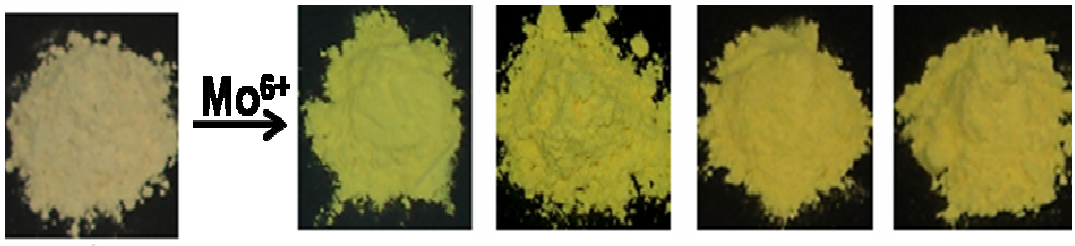

Fig. 19. Photographs of $Sm_2Ce_{2-x}Mo_xO_{7+\delta}$ (x = 0 to 0.4) pigments.

1.4.5. Infrared Reflective Rare earth based Inorganic Pigments: Recently, a few rare earths based NIR-reflective pigments have been proposed as alternatives to traditional toxic NIR pigments, in view of their low toxicity. The U S Patent 6,541,112 [Swiler and Axtell 2003] describes a process for the synthesis of a series of rare earth manganese oxides, $(RE_xMn)O_y$ (RE = Y, La, Ce, Pr, Nd, and Sm) with good IR reflectivity. In an another invention, Swiler *et al* have developed a coating system with high infrared reflectivity based on rare earth transition metal oxide systems [Swiler *et al.* 2002].

Chapter 2

The synthesis, characterization and optical properties of Si^{4+} and Pr^{4+} doped Y_6MoO_{12} compounds: Environmentally benign inorganic pigments with high NIR reflectance

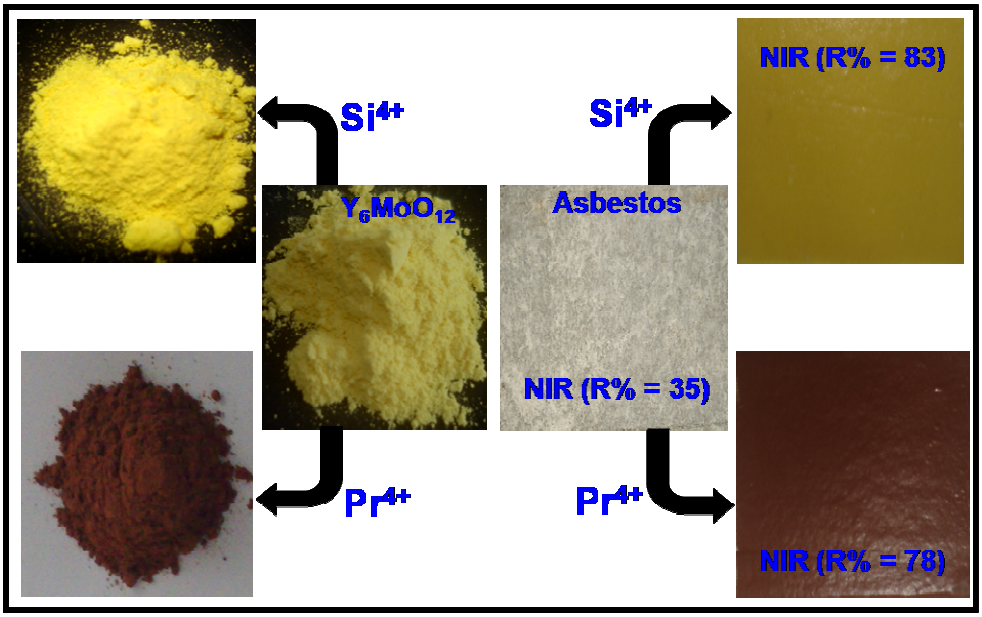

Summary

A novel class of environmentally benign near-infrared (NIR) reflective inorganic pigments based on yttrium molybdate (Y_6MoO_{12}) through appropriate doping of metal ions such as Si^{4+} or Pr^{4+}, exhibiting colors ranging from light-yellow to dark-yellow and brick-red to dark-brown have been synthesized. The doping of Si^{4+} for Y^{3+} in Y_6MoO_{12} changes the color hue from light-yellow to dark-yellow and the band gap gently decreases from 2.60 to 2.45 eV due to O_{2p}-Mo_{4d} charge transfer transitions. In contrast, replacing Pr^{4+} for Y^{3+} changed the color hue from light-yellow to dark-brown and the band gap shifted from 2.60 to 1.90 eV. The coloring mechanism is based on the introduction of an additional $4f^1$ electron energy level of Pr^{4+} between the valence and conduction bands. The NIR reflectance of the designed pigments has also been evaluated after coating on a roofing material like asbestos cement sheet for possible use as "cool pigment".

Dyes and Pigments *88* (2011) 109-115

2.1. Introduction

The world is facing disruptive global climate change from green-house gas emissions and increasingly expensive and scarce energy supplies. Energy efficiency reduces those emissions and mitigates the rising cost of energy. Cool-color roofing – a new technology that uses solar reflective pigments to reduce a home's energy and peak demand – promises a significant leap in energy efficiency. Coatings colored with conventional inorganic pigments tend to absorb the invisible near-infrared (NIR) radiation that bears more than half of the power in sunlight. The sun's energy that reaches the earth's surface is divided in to three main parts (Fig. 1): Ultraviolet Region (300-400 nm): UV accounts for about 5% of the sun's energy that reaches the earth's surface; Visible Region (400-700 nm): Around 43% of the sun's energy occurs in the visible region of the electromagnetic spectrum; Infrared Region (700-2500 nm): 52% of the total solar energy is in the non-visible infrared region. The heat producing region of the infrared radiations ranges from 700 to 1100 nm. These radiations on absorption result in heating up of the surfaces [Levinson *et al.* 2007; Bendiganavale and Malshe 2008].

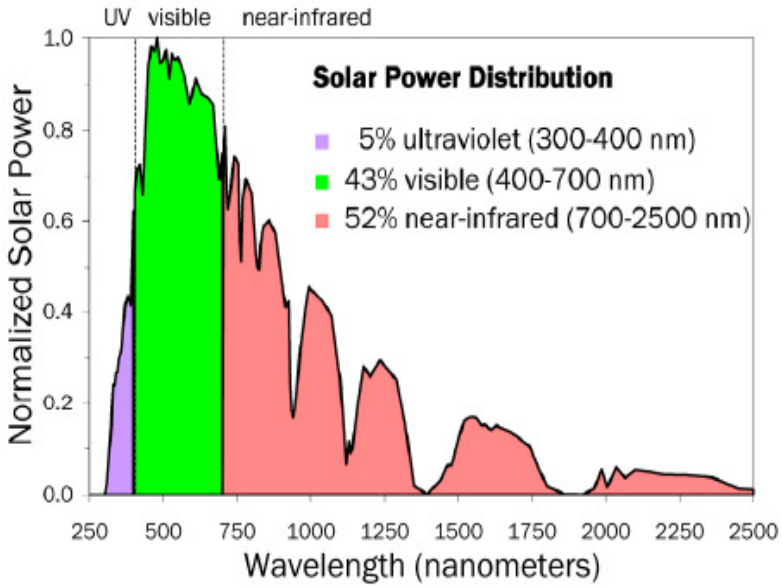

Fig. 1. Spectral solar power distribution.

Much interest has attended roofing materials with high solar reflectance and high thermal emittance, so that interiors stay cool, thereby reducing the demand for air-conditioned buildings [Akbari *et al.* 2005; Jeevanandam *et al.* 2007; Levinson *et al.* 2007; Bendiganavale and Malshe 2008]. Replacing conventional pigments with "cool pigments" that absorb less NIR radiation can provide coatings similar in color to that of conventional roofing materials, but with higher solar reflectance. NIR reflective pigments have been used in the military, construction, plastics and ink industries [Wake 1990]. IR reflective screens useful in green houses, made using a polymer and reflective pigments, allow only visible light transmission but reflect NIR light. NIR reflective pigments can also be useful for camouflage applications [Gupta *et al.* 2001].

Inorganic NIR pigments are mainly metal oxides and are primarily employed in two major applications namely visual camouflage and reduced heat build-up applications. Most of the literature on NIR reflective pigments exists as patents [Modly 1999; Sliwinski *et al.* 2002; Swiler 2002; Swiler *et al.* 2003], which indicate their vast potential application. Complex inorganic pigments based on mixed metal oxides (eg., chromium green, cobalt blue, cadmium stannate, lead chromate, cadmium yellow and chrome titanate yellow), which have been used in camouflage, absorb visible light but reflect the NIR portion of incident radiation [Akbari *et al.* 2005; Levinson *et al.* 2005; Jeevanandam *et al.* 2007]. However, many of these pigments are toxic and there is a need to develop novel colored, NIR-reflecting inorganic pigments that are less hazardous to the environment. Recently, the industrial utilization of lanthanides has increased rapidly because of their low toxicity; consequently, a large number of rare earth based NIR reflective pigments have been proposed as alternatives to traditional pigments [Levinson *et al.*2005; [b]Sreeram *et al.* 2008]. In this work, a series of NIR reflective colored pigments of formula $Y_{6-x}M_xMoO_{12+\delta}$ (where M = Si^{4+} or Pr^{4+} and x ranges from 0 to 1.0) were synthesized and applied to asbestos cement roofing material so as to evaluate their use as "cool pigments".

2.2. Experimental Section

2.2.1. Materials and Methodology

The precursor oxides of Pr_6O_{11} (99.9%), Y_2O_3 (99.9%), SiO_2 (99.9%) and MoO_3 (99.9%) were purchased from Sigma Aldrich and used without further purification. The required precursor oxides were mixed in a stoichiometric ratio, transferred to an agate mortar and homogenized by wet milling in acetone solvent. Residual acetone was removed by evaporation and the resultant powders were calcined in platinum crucibles in a Nabertherm electric furnace at an optimized temperature (1600°C) and time (12 h) in air atmosphere, followed by auto-cooling inside the furnace. The heating of the furnace was programmed to increase the temperature at 5°C /min. The ensuing pigment powders were ground in an agate mortar and characterized.

Procedure for coating on an asbestos cement sheet: Typical designed pigments $Y_5SiMoO_{12+\delta}$ and $Y_{5.4}Pr_{0.6}MoO_{12+\delta}$ samples were ground and sieved to obtain the particles in the range of 20-30 μm. The sieved pigment particles were then mixed with commercially available cold curing liquid 'Acralyn R' and cold cure binding material 'DPI-RR Cold Cure' (denture base polymer resin) and ultrasonicated (Vibronics, 250 W, India) for 10 min to ensure complete dispersion of the pigment particles in an acrylic-acralyn emulsion. The pigment : binder ratio was maintained as 1:1 by wt.%. A small strip of commercially available asbestos cement sheet (made up with small amounts of asbestos fiber locked in cement slurry) was pre-coated with an inexpensive white pigment (TiO_2) that is highly reflective to NIR light. The viscous paint solution was then coated on the surface of the pre-coated asbestos cement sheet, dried and evaluated its optical properties.

2.2.2. Characterization Techniques

The phase purity of the calcined pigment samples were determined using powder X-ray diffraction in a diffractometer (Philips X'pert Pro) employing Ni-filtered Cu Kα (λ = 0.154060 nm) radiation. Data were collected by step scanning over a 2θ range from 20° to 70° with a step size of 0.08° and 5 s counting time at each step.

Scanning electron micrographs of the samples were taken on a Scanning Electron Microscope (SEM) JEOL JSM–6390 model, with an acceleration voltage of 20 kV.

Thermo-gravimetric (TG) and differential thermal analyses (DTA) were performed in a Pyris Diamond TG/DTA Perkin Elmer make. All the experiments were run in a platinum crucible from 50 to 1000°C with a heating rate of 20°C/min in nitrogen atmosphere.

The particle size distribution of the typical pigment sample was investigated in water medium with calgon as the dispersing agent using the Laser Scattering Particle size Distribution Analyzer (CILAS 930). The samples were ultrasonically homogenized for 180 s during measurement and the signal was evaluated on the basis of Fraunhofer bending.

The thickness of the pigment coating on asbestos cement sheet was measured employing LEICA DMRX Optical Microscope.

The diffuse reflectance of the powdered pigment samples were measured in the wavelength range 380–700 nm using a UV–vis Spectrometer (Shimadzu UV-2450 with an integrating sphere attachment, ISR-2200) using illuminant D_{65}, 10° standard observer and measuring geometry d/8°. The near–infrared reflectance (780–2000 nm) of the powdered pigment samples as well as the pigment coated asbestos cement sheet was measured using a UV–vis–NIR spectrophotometer (Shimadzu, UV–3600 with an integrating sphere attachment, ISR–3100). The diffuse reflectance measurement procedure in both UV-vis and NIR regions was used as follows: a set of powder sample holders filled with barium

sulphate for the visible region and poly-tetrafluoroethylene for the NIR region, was mounted on both the sample and reference sides of the exit port of the integrated sphere to set the baseline measurement. The sample holder was then filled with powder pigment and its reflectance measured; in the case of pigment coated asbestos cement sheet, the coated samples were placed in the sample side of the exit port of the integrating sphere by replacing the standard powder sample holder and their reflectance was measured. The CIE 1976 color parameters L^*, a^*, and b^* were determined by coupling an analytical software (UVPC Color Analysis Personal Spectroscopy Software V3, Shimadzu) for color measurements to the Shimadzu UV–2450 spectrophotometer. The CIE 1976 colorimetric method was used to analyze the color coordinates of the designed pigments, as recommended by Commission Internationale de I'Eclairage (CIE). In this method, L^* is the lightness axis [black (0) to white (100)], a^* is the green (−ve) to red (+ve), and b^* is the blue (−ve) to yellow (+ve) axis (Fig. 2). The parameter C^* (chroma) represents saturation of the color and $h°$ represents the hue angle, which denotes whether the color appears red, orange, yellow, green, blue or purple (or some mixture of neighboring pairs in this list). The chroma is defined as:

$$C^* = [(a^*)^2 + (b^*)^2]^{1/2} \qquad (1)$$

The hue angle, h^o is expressed in degrees and ranges from 0^o to 360^o and is calculated using the formula:

$$h^o = \tan^{-1}(b^*/a^*) \qquad (2)$$

For each colorimetric parameter of a sample, measurements were made in triplicate and an average value was chosen as the result. Typically, for a given sample, the standard deviation of the measured colorimetric parameters was <0.10 and the relative standard deviation was ≤1%, indicating that the measurement error can be ignored.

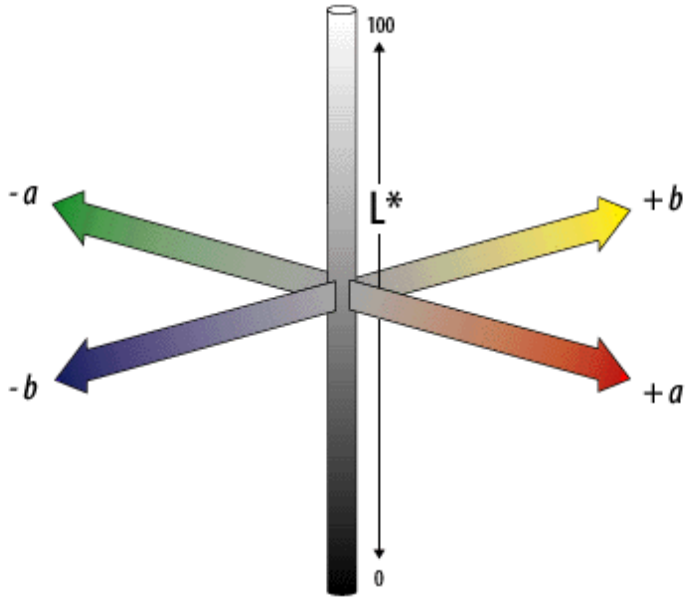

Fig. 2. CIE1976 Lab Color coordinates scale.

2.3. Results and Discussion

2.3.1. Powder X-ray diffraction analysis

Fig. 3 displays the summary of the XRD patterns of Y_6MoO_{12} powder sample calcined at different temperatures ranging from 600°C to 1600°C. The samples calcined at 600°C and 800°C exhibit poor crystallinity, and are also accompanied with precursor oxides (Y_2O_3 and MoO_3) as impurity phases. The XRD pattern of Y_6MoO_{12} compound calcined at 1000°C can be indexed to hexagonal phase (JCPDF 24-1129), while samples calcined at and above 1400°C can be very well indexed to face centered cubic (FCC) phase (JCPDF 30–1456). On the other hand, the XRD pattern of the sample calcined at 1200°C exhibits the mixture of hexagonal and cubic phases of Y_6MoO_{12}. These results are in good agreement with the earlier reports that Y_6MoO_{12} compound was found to be hexagonal at low temperatures, while forming a new face centered cubic phase calcined above 1400°C [Fournier *et al.* 1970]. Thus it can be concluded from the above study that a calcination temperature of 1600°C is necessary to obtain the phase pure products.

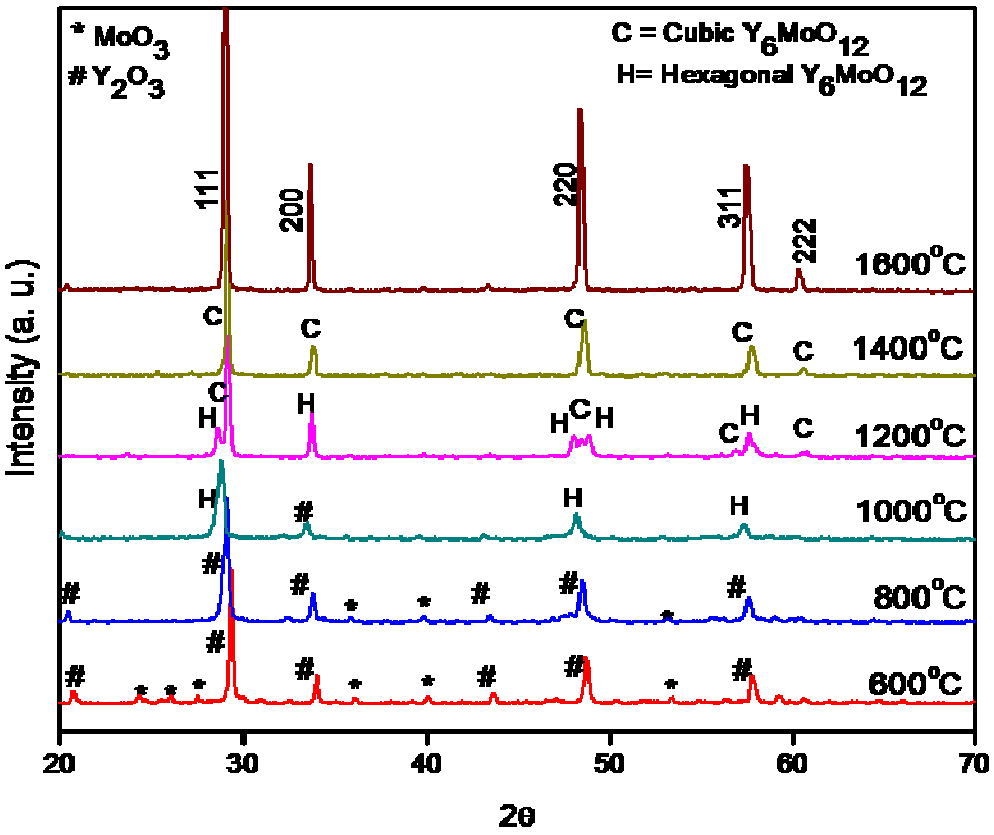

Fig. 3. XRD patterns of Y_6MoO_{12} samples calcined at different temperatures (Time duration: 6 h).

Fig. 4 shows the XRD patterns of $Y_{6-x}Si_xMoO_{12+\delta}$ (x ranges from 0 to 1.0) with different dopant amounts of silicon. The diffraction pattern of Y_6MoO_{12} can be very well indexed to a cubic structure (JCPDF 30-1456) with a lattice constant of 0.5299 nm. The crystal lattice would be distorted with the substitution of Si^{4+} for Y^{3+} in Y_6MoO_{12}. This is due to the smaller ionic radius of Si^{4+} (0.0260 nm) when compared to that of Y^{3+} (0.1019 nm) [Shannon 1976]. Further it can be noted from the XRD patterns that the doping of Si^{4+} for Y^{3+} in Y_6MoO_{12} results in the formation of an additional phase of triclinic α-$Y_2Si_2O_7$ (JCPDF 38-223; Becerro and Escudero 2004).

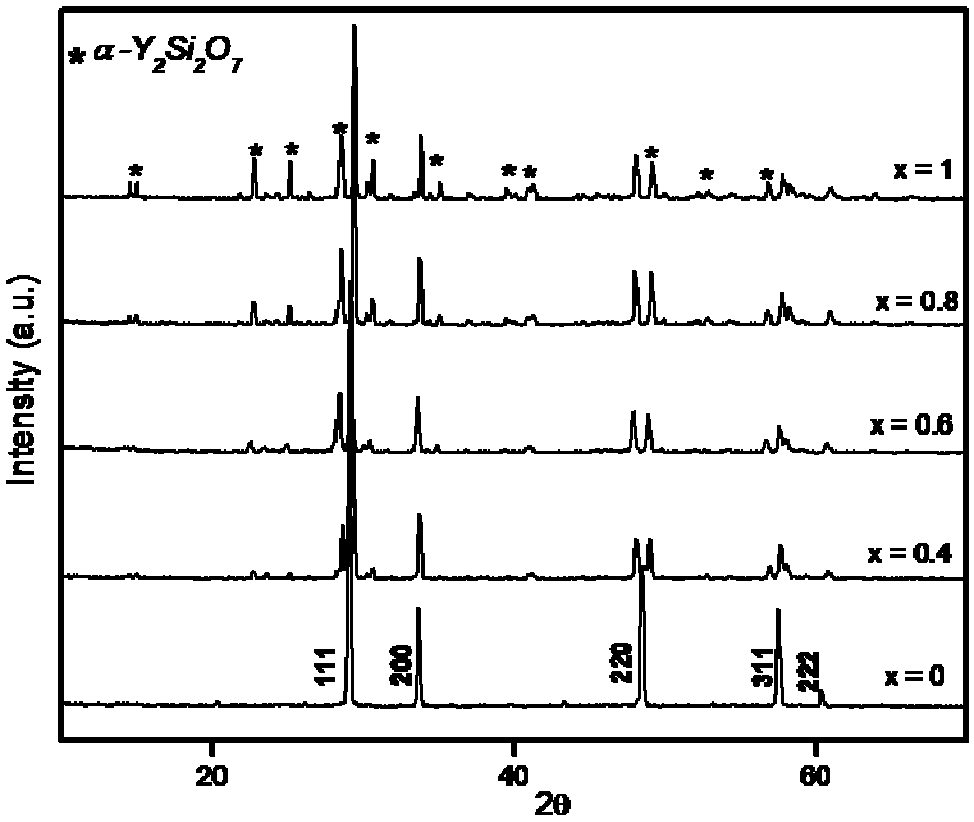

Fig. 4. XRD patterns of $Y_{6-x}Si_xMoO_{12+\delta}$ (x ranges from 0 to 1) samples (Calcination temperature: 1600°C; Time duration 6 h).

On the other hand, the doping of Pr^{4+} (0.096 nm) for Y^{3+} in Y_6MoO_{12} did not alter the phase significantly as can be noted from the XRD patterns given in Fig. 5. The cell parameter value for composition up to doping of 4.3 mol% of Pr^{4+} matches very well with the high temperature cubic form of Y_6MoO_{12}, which implies that the cubic form can be stabilized at room temperature by doping with Pr^{4+} up to 4.3 mol%. Above 4.3 mol%, the lattice constant increases slightly with increase in Pr^{4+} concentration and reaches 0.5332 nm at 12.8 mol%. This increase of lattice constant is resulted from the contribution of substitution of Pr^{4+} for Y^{3+} and introduction of extrinsic vacancies by praseodymium doping, which will expand the lattice [Wang and Fang 2002].

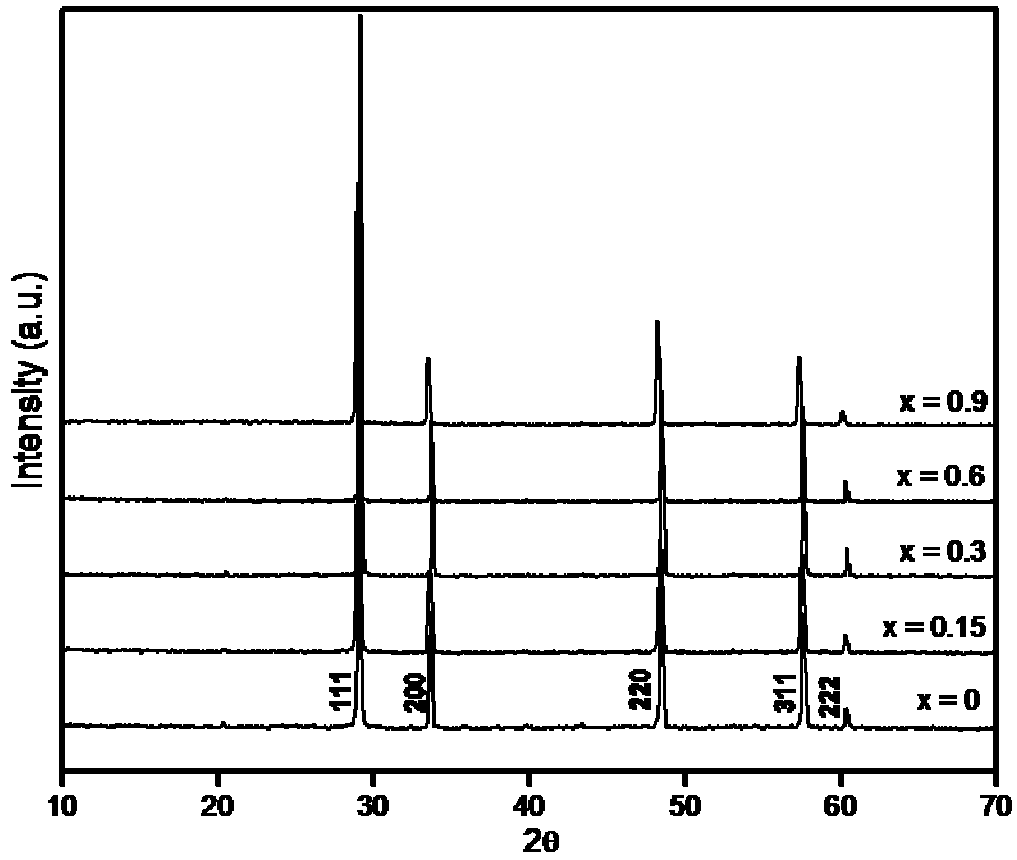

Fig. 5. XRD patterns of $Y_{6-x}Pr_xMoO_{12+\delta}$ (x ranges from 0 to 0.9) samples (Calcination temperature: 1600°C; Time duration 6 h).

2.3.2. Particle size and morphological analysis

Particle size analysis of the typical pigments Y_6MoO_{12}, $Y_5SiMoO_{12+\delta}$ and $Y_{5.4}Pr_{0.6}MoO_{12+\delta}$ reveal a mean diameter of 3.44 μm (size of 90% particles < 6.40 μm, 50% particles < 3.37 μm and 10% particles < 0.14 μm), 8.82 μm (size of 90% particles < 20.91 μm, 50% particles < 6.69 μm and 10% particles < 1.31 μm) and 4.61 μm (size of 90% particles < 8.50 μm, 50% particles < 4.32 μm and 10% particles < 0.96 μm), respectively. The homogeneous nature of the pigments can be understood from the SEM images (Fig. 6), the average grain size being less than 10 μm, which is again in good agreement with the particle size analysis.

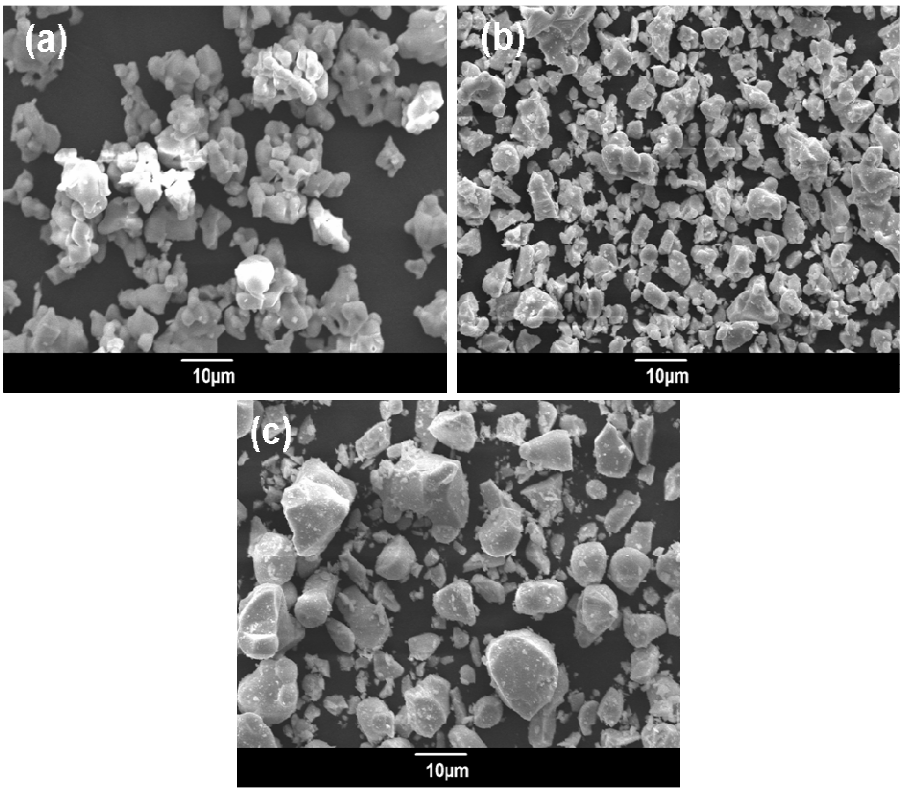

Fig. 6. The SEM micrographs of (a) Y_6MoO_{12} (b) $Y_5SiMoO_{12+\delta}$ and (c) $Y_{5.1}Pr_{0.9}MoO_{12+\delta}$ pigment powders.

2.3.3. Effect of silicon doping on the optical properties of Y_6MoO_{12} pigments

The UV–vis diffuse reflectance and absorption spectra of the $Y_{6-x}Si_xMoO_{12+\delta}$ (x ranges from 0 to 1) pigment samples are shown in Figs. 7 and 8. A strong absorption noted below 485 nm in the UV–vis reflectance spectrum of silicon free Y_6MoO_{12} sample is due to the O_{2p}–Mo_{4d} charge-transfer transition of Mo^{6+} [Chevire *et al.* 2006; Chevire *et al.* 2009; Vishnu *et al.* 2010]. This absorption in the blue region is responsible for the yellow hue of Y_6MoO_{12}, since blue is a complimentary color to yellow. The band gap of the Y_6MoO_{12} pigment is found to be 2.60 eV, which has been calculated by a straight forward extrapolation method from the corresponding absorption spectrum [George *et al.* 2008]. It is evident from the reflectance spectra of these pigments that the progressive doping of Si^{4+} for Y^{3+} in Y_6MoO_{12} gently changes the absorption edge from 484 to 510 nm. The

introduction of Si^{4+} into the Y_6MoO_{12} lattice results in the formation of an additional phase of α–$Y_2Si_2O_7$ which tends to increase the apparent concentration of Mo^{6+} ions in the lattice. These results in a red shift of the charge transfer band and intensify the yellow hue of Y_6MoO_{12} pigments (Fig. 9). Thus the band gap of the Si^{4+} free pigment sample decreases from 2.60 eV to 2.45 eV, with the increase of silicon concentration (from 5.7 to 14.3 mol%). However, one can conclude that the increase of yellow hue of the pigment sample is really not due to the formation of the impurity phase of α–$Y_2Si_2O_7$.

Fig. 10 depicts the NIR reflectance spectra of the $Y_{6-x}Si_xMoO_{12+\delta}$ (x ranges from 0 to 1) pigment samples. The silicon free sample, Y_6MoO_{12} exhibits 92% NIR reflectance at 1100 nm region. Doping of 5.7 mol% Si^{4+} for Y^{3+} in Y_6MoO_{12} increases the NIR reflectance to 98%. On the other hand, further doping of more and more Si^{4+} for Y^{3+} decreases the NIR reflectance to 86%. The high reflectance in the NIR region exhibited by the designed new class of yellow pigments indicates that these pigment formulations can serve as cool pigments.

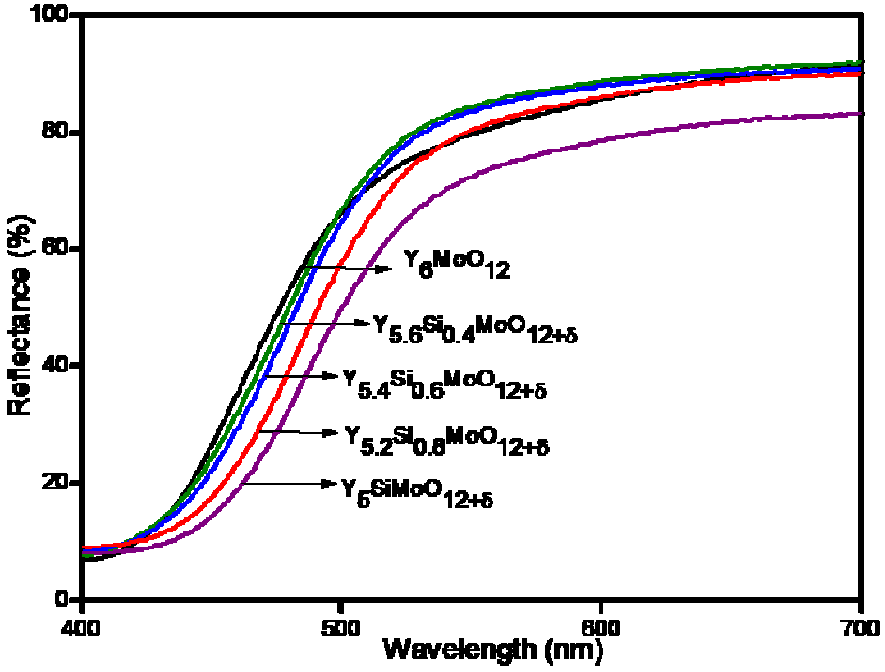

Fig. 7. Reflectance spectra of $Y_{6-x}Si_xMoO_{12+\delta}$ (x ranges from 0 to 1) powders.

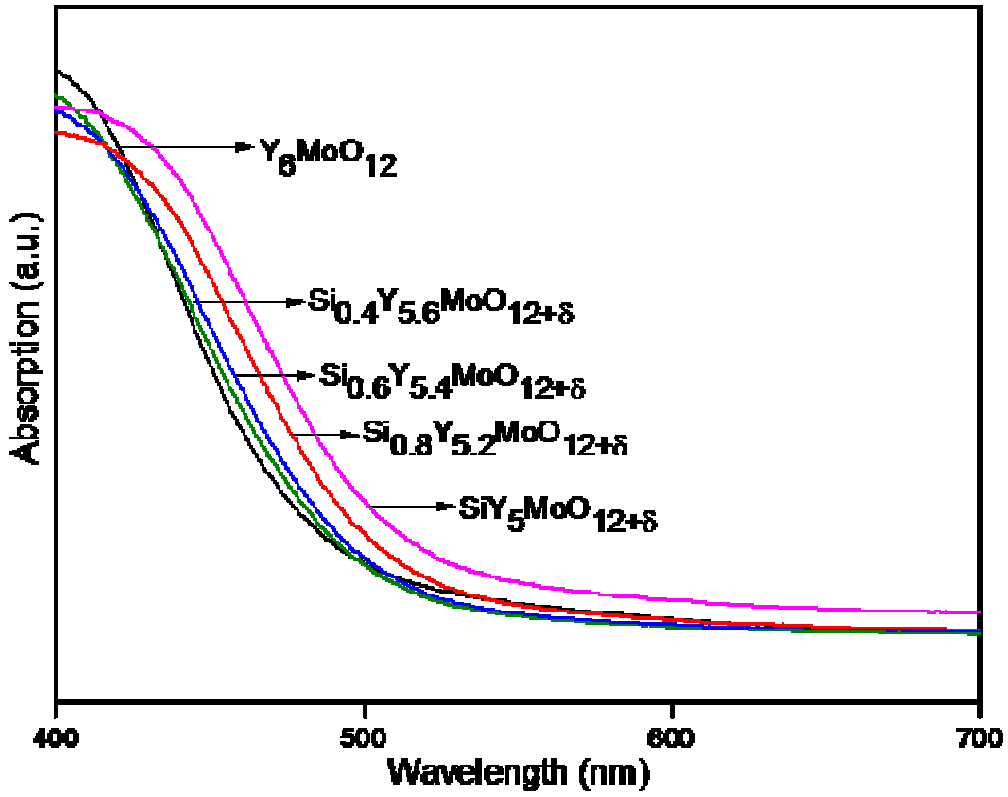

Fig. 8. Absorption spectra of $Y_{6-x}Si_xMoO_{12+\delta}$ (x ranges from 0 to 1) powders.

Fig. 9. Photographs of $Y_{6-x}Si_xMoO_{12+\delta}$ and $Y_{6-x}Pr_xMoO_{12+\delta}$ pigment powders.

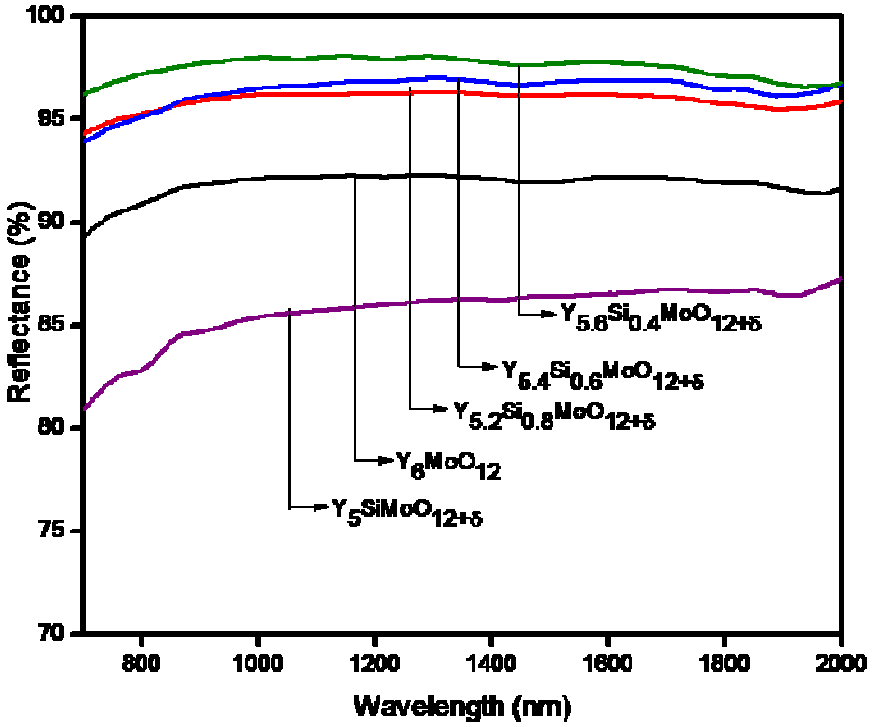

Fig. 10. NIR reflectance spectra of $Y_{6-x}Si_xMoO_{12+\delta}$ powders.

The CIE 1976 color coordinates of the powdered $Y_{6-x}Si_xMoO_{12+\delta}$ (x ranges from 0 to 1) pigment samples are summarized in Table 1. The systematic doping of Si^{4+} (from 5.7 to 14.3 mol%) for Y^{3+} in Y_6MoO_{12} results in an increase in the b^* value from 48.2 to 62.5, which indicates that yellowness of the pigment samples enhances. At the same time, the increase of Si^{4+} substitution leads to the loss of green hue of the pigment that is evident from the lower values of the color coordinate $-a^*$ (a^* changes from –6.3 to –3.5). The presence of silicon cations in the matrix of Y_6MoO_{12} causes an increase in b^* and decreases the $-a^*$ color coordinate values. Hence the color hue expressed by the color coordinates h° decrease from 97.5 to 93.2. The observed hue angle of the designed pigments are found to be in the yellow region of the cylindrical color space (h° = 70-105 for yellow) [Sulcova and Trojan 2008]. Thus the pigments possess yellow hue that are characterized by the improved richness of the yellow color as can be noted from the

increase in C^* values (from 48.6 to 62.6). The coloring mechanism of the present pigments is essentially based on the O_{2p}–Mo_{4d} charge transfer transition which further intensifies upon doping of Si^{4+} for Y^{3+} in Y_6MoO_{12}.

Table 1. The color coordinates (±0.1) of the $Y_{6-x}Si_xMoO_{12+\delta}$(x ranges from 0 to 1) powder pigments and band gap values.

Pigment composition	Color coordinates					Band gap
	L^*	a^*	b^*	C^*	h^o	*(eV)*
Y_6MoO_{12}	89.9	–6.3	48.2	48.6	97.5	2.60
$Y_{5.6}Si_{0.4}MoO_{12+\delta}$	92.9	–7.3	54.3	54.8	97.7	2.54
$Y_{5.4}Si_{0.6}MoO_{12+\delta}$	91.3	–6.9	55.7	56.1	97.1	2.52
$Y_{5.2}Si_{0.8}MoO_{12+\delta}$	89.2	–4.8	60.2	60.3	94.6	2.47
$Y_5SiMoO_{12+\delta}$	87.3	–3.5	62.5	62.6	93.2	2.45

$C^* = [(a^*)^2 + (b^*)^2]^{1/2}$; $h^o = \tan^{-1}(b^*/a^*)$

2.3.4. Effect of praseodymium doping on the optical properties of Y_6MoO_{12} pigments

Figs. 11 and 12 display the UV–vis diffuse reflectance and absorption spectra of the $Y_{6-x}Pr_xMoO_{12+\delta}$ (x ranges from 0 to 1) powdered pigment samples. The doping of 2.1 mol% Pr^{4+} for Y^{3+} in the host lattice of Y_6MoO_{12} introduces an additional energy level due to the $4f^1$ electrons between the O^{2-} valence and Mo^{6+} conduction bands. As a result, the absorption edge is red shifted significantly (from 484 nm to 624 nm) and the band gap of the pigment decreases from 2.60 to 1.99 eV. Therefore, the color of the pigment changes from yellow to brick-red. Further, more and more substitution of Pr^{4+} (from 4.3 to 12.9 mol%) for Y^{3+} in the host lattice gently red shifts the absorption edge and changes the band gap from 1.99 to 1.90 eV. Consequently the pigment samples changes the color from brick-red to dark-brown (Fig. 9).

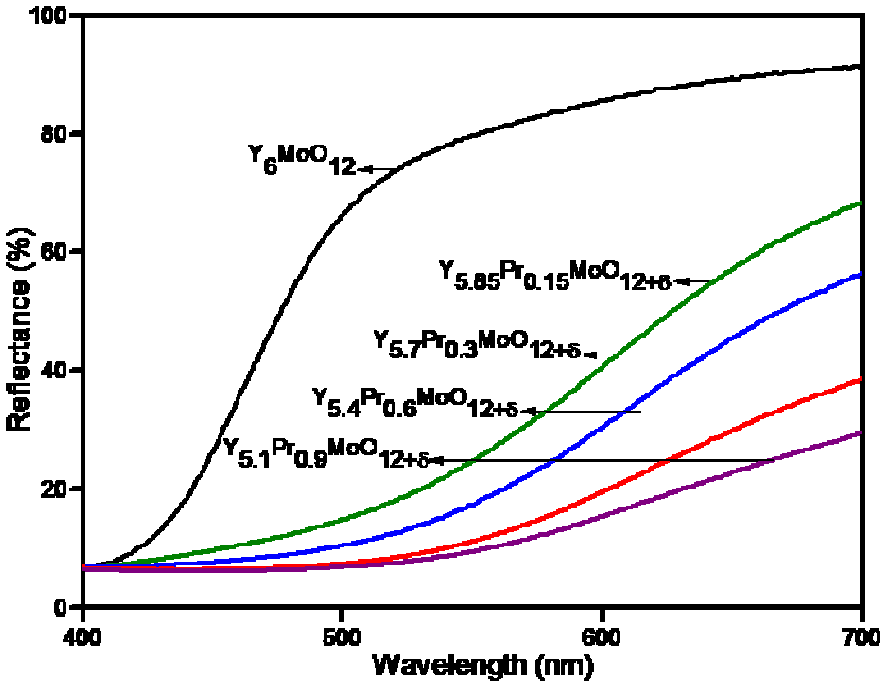

Fig. 11. Reflectance spectra of $Y_{6-x}Pr_xMoO_{12+\delta}$ (x ranges from 0 to 0.9) powders.

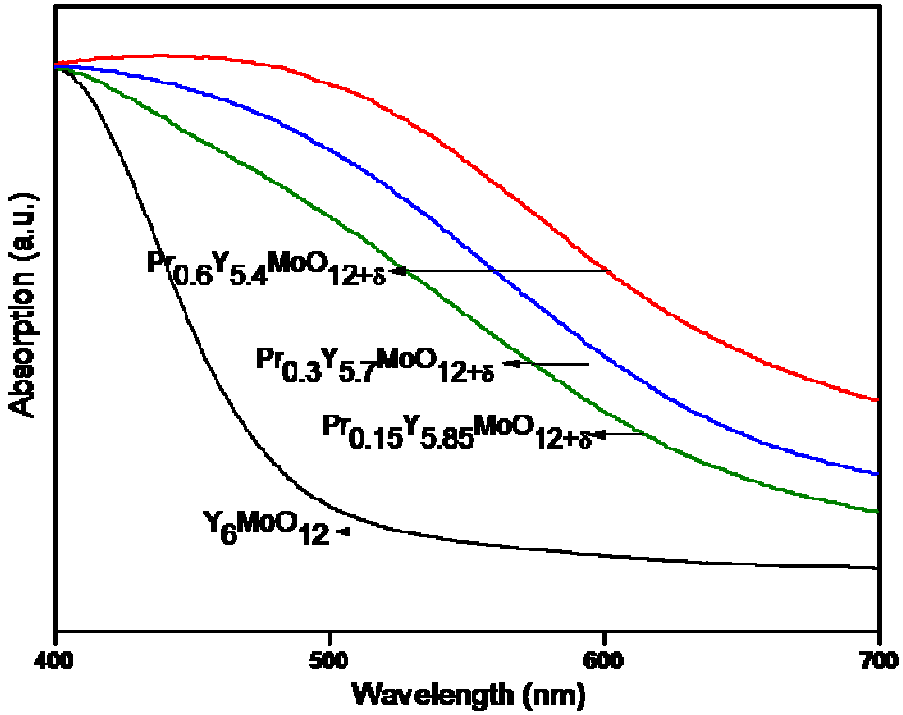

Fig. 12. Absorbance spectra of $Y_{6-x}Pr_xMoO_{12+\delta}$ (x ranges from 0 to 0.9) powders.

It can be seen from the NIR reflectance spectra (700–2000 nm) of the praseodymium doped Y_6MoO_{12} powdered pigment samples shown in Fig. 13 that the NIR reflectance decreases (from 92 to 74%) with the increase in concentration of Pr^{4+} from 2.1 to 12.9 mol%. However the high NIR reflectance values clearly highlight the potential for the utility of these pigment samples as cool pigments. The NIR reflectance of the typical powdered brick-red pigment sample, $Y_{5.85}Pr_{0.15}MoO_{12+\delta}$ is found to be higher (88% at 1100 nm) than that of $Ce_{25}Pr_{0.8}FeO_y$ red and $Ce_{25}Pr_{0.8}MoO_y$ orange-red pigments reported elsewhere (< 70% at 1100 nm) [[b]Sreeram *et al.* 2008].

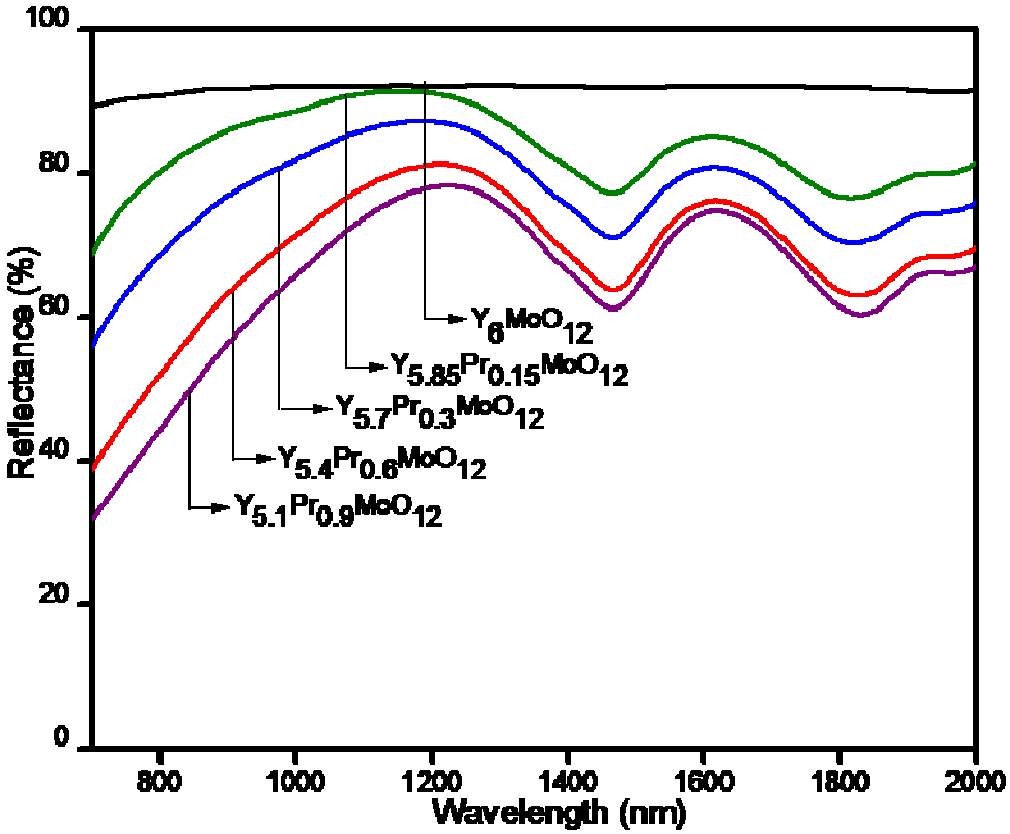

Fig. 13. NIR Reflectance spectra of $Y_{6-x}Pr_xMoO_{12+\delta}$ powders.

From the color coordinates of the Pr^{4+} doped Y_6MoO_{12} powdered pigment samples depicted in Table 2, it is clear that the progressive doping of Pr^{4+} (from 2.1 mol% to 12.9

mol%) for Y^{3+} in Y_6MoO_{12} dramatically decreases the b^* from 48.2 to 15.7. This can be clearly seen from the loss of the yellow hue of the pigment samples with doping of higher concentration of Pr^{4+}. The extent of redness that is expressed by the higher value of color coordinate a^* (from – 6.3 to 20.9) increases up to the content of praseodymium 4.3 mol% ($x = 0.3$). As a result the color changes drastically from yellow to brick–red. Further, more and more doping of Pr^{4+} for Y^{3+} (upto 12.9 mol%) decreases the color coordinate a^* value from 20.9 to 15.2. Thus the color of the pigment gently changes from brick-red to dark-brown (Fig. 9). The pigments have brown hue that are characterized by the lesser richness of color represented by the chroma (C^*) values. The progressive substitution of Pr^{4+} for Y^{3+} in Y_6MoO_{12} significantly decreases the hue angle ($h°$) from 97.5 to 46.0. The hue angle values reveal that the Pr^{4+} doped pigments lie in the brick-red to dark-brown region of the cylindrical color space ($h°$ = 0–35 for red and 35–70 for orange) [Sulcova and Trojan 2008]. The preceding trends in color coordinate values could be due to the introduction of a $4f^1$ energy level of praseodymium between the O^{2-} valence and Mo^{6+} conduction bands with the systematic doping of Pr^{4+} ions for yttrium in Y_6MoO_{12}.

Table 2. The color coordinates (±0.1) of the $Y_{6-x}Pr_xMoO_{12+\delta}$ (x ranges from 0 to 0.9) powder pigments and band gap values.

Pigment composition	Color coordinates					Band gap
	L^*	a^*	b^*	C^*	h^o	(eV)
Y_6MoO_{12}	89.8	–6.3	48.2	48.6	97.5	2.60
$Y_{5.85}Pr_{0.15}MoO_{12+\delta}$	59.5	19.7	36.6	47.0	61.7	1.99
$Y_{5.7}Pr_{0.3}MoO_{12+\delta}$	51.9	20.9	30.9	41.6	55.9	1.95
$Y_{5.4}Pr_{0.6}MoO_{12+\delta}$	42.9	18.7	20.6	37.3	47.7	1.92
$Y_{5.4}Pr_{0.9}MoO_{12+\delta}$	39.3	15.2	15.7	21.9	46.0	1.90

2.3.5. NIR reflectance of the pigments coated on a roofing material (asbestos)

Recently there has been a lot of interest in building roofing materials (like concrete tile, metal, clay tiles, wood and asbestos cement sheets) with high solar reflectance and high thermal emittance such that the interiors stay cool in the sun, reducing demand for cooling power in conditioned buildings and increasing occupant comfort in unconditioned buildings [Smith *et al.* 2003; Levinson *et al.* 2007; Libbra *et al.* 2011; Uemoto *et al.* 2010]. The reflectance in the near-infrared (NIR) spectrum (700–1100 nm) can be maximized by coloring the top coat with inorganic pigments that weakly absorb and strongly backscatter (optional) NIR radiation. Multiple layers of coatings can be applied to increase reflectance; however, each additional coating increases cost. A two-step, two-layer process has proven more cost-effective. In the present study, the pigment which exhibits best chromatic properties has been chosen to coat on the asbestos cement roofing sheet. The photograph of the coated asbestos cement sheet is given in Fig. 14. The NIR reflectance spectrum of the $Y_5SiMoO_{12+\delta}$ and $Y_{5.4}Pr_{0.6}MoO_{12+\delta}$ samples coated with varying thickness over a base coat of TiO_2 on asbestos cement sheet is shown in Figs. 15 and 16, respectively. It is evident from the diffuse reflectance spectrum that the NIR reflectance of the bare asbestos cement roofing sheet shows a low NIR reflectance of 35% (at 1100 nm). The coating of the present pigments has greatly enhanced the NIR reflectance of the asbestos cement sheet. Further it can also be noted that the NIR reflectance increases with increase in thickness of the coatings of the respective pigments (NIR reflectance 71% at 90 μm and 83% at 250 μm for yellow sample; NIR reflectance 66% at 95 μm and 78% at 260 μm for red sample).

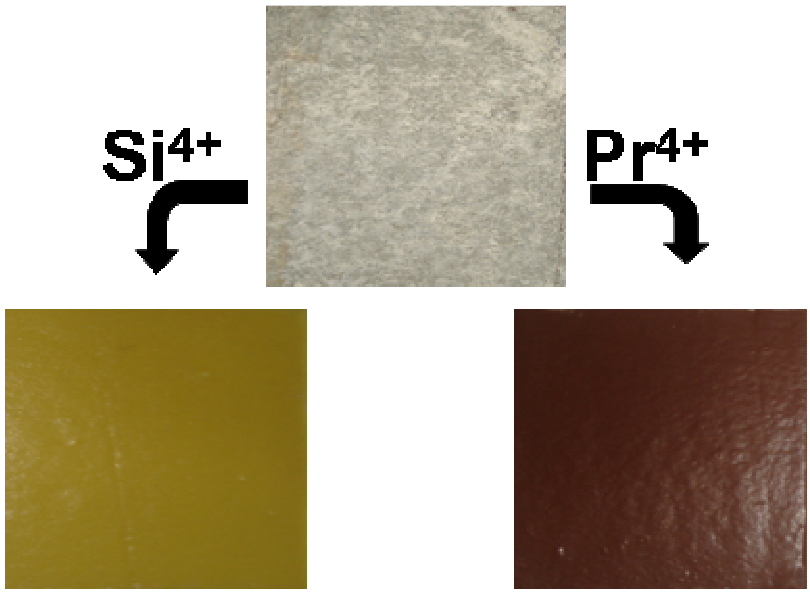

Fig. 14. Photographs of $Y_5Si_1MoO_{12+\delta}$ and $Y_{5.4}Pr_{0.6}MoO_{12+\delta}$ pigments coated on asbestos sheet.

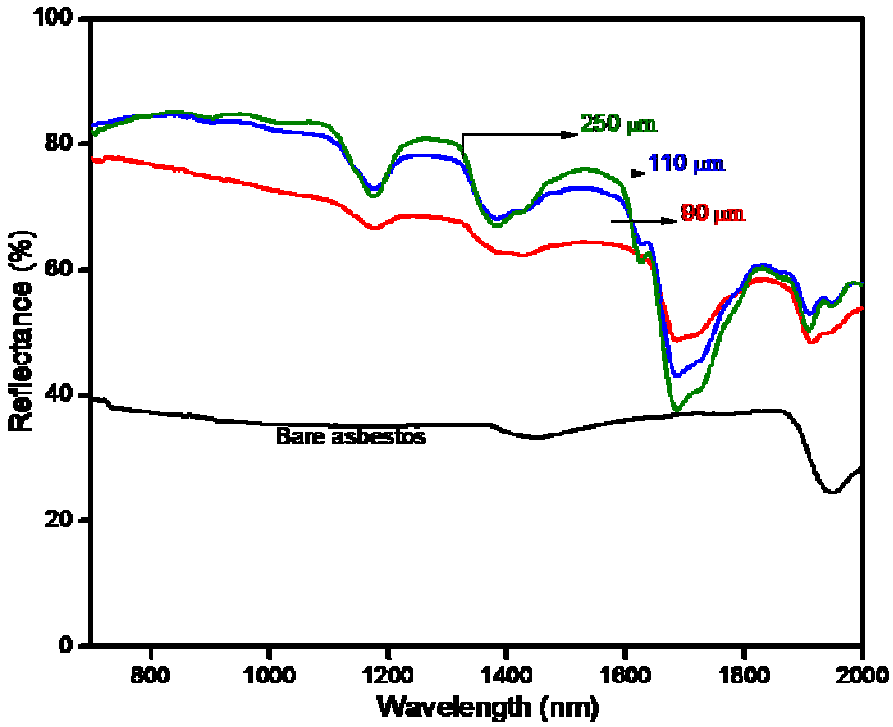

Fig. 15. NIR Reflectance spectra of $Y_5SiMoO_{12+\delta}$ pigment coated on asbestos with different thickness.

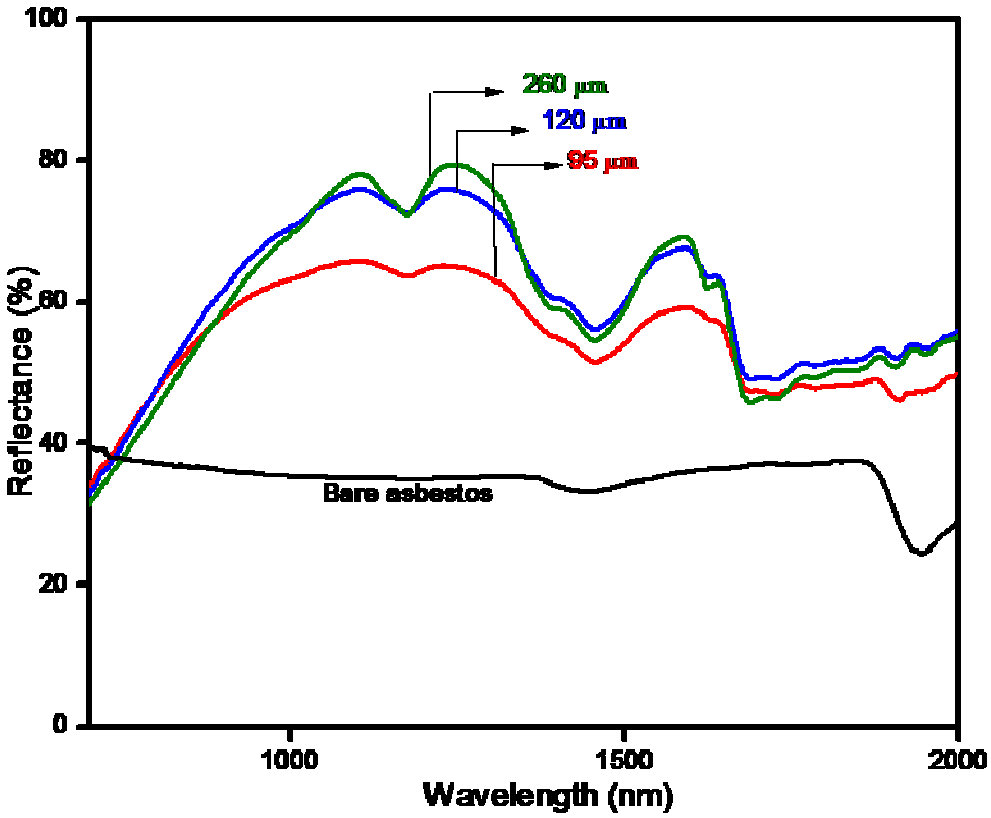

Fig. 16. NIR Reflectance spectra of $Y_{5.4}Pr_{0.6}MoO_{12+\delta}$ pigment coated on asbestos with different thickness.

The data on the color coordinates and NIR reflectance at different thickness of coatings on the asbestos cement roofing material is given in Table 3. As can be noted from the color coordinate data that the b^* value increases (from 49.3 to 54.6) when the thickness of the yellow pigment coating has been almost doubled (110–250 µm). However, the $-a^*$ values which represents the green component of the pigment decreases (from −6.6 to −4.9) with increasing thickness from 110 to 250 µm. On the other hand, in the case of the red pigment coating the variation of thickness from 120 to 260 µm does not have much influence on the color coordinates.

Table 3. Effect of coating on the color coordinates (±0.1) of the (a) $Y_5SiMoO_{12+\delta}$ and (b) $Y_{5.4}Pr_{0.6}MoO_{12+\delta}$ coated pigments with different thickness and NIR reflectance (%) values at 1100 nm.

$Y_5SiMoO_{12+\delta}$					$Y_{5.4}Pr_{0.6}MoO_{12+\delta}$				
Thickness (μm)	*L**	*a**	*b**	NIR (R%) 1100 nm	Thickness (μm)	*L**	*a**	*b**	NIR (R%) 1100 nm
90	84.4	–6.6	49.4	71.1	95	47.0	17.9	19.9	65.8
110	84.4	–6.6	49.3	80.9	120	39.7	15.8	16.3	75.6
250	84.6	–4.9	54.6	82.8	260	38.8	15.7	16.2	78.0

2.3.6. Thermal and chemical stability studies of the pigments

Thermal analysis was performed for Y_6MoO_{12} pigments and the results are given in Fig. 17. The precursor mixture of the oxides (Y_2O_3, and MoO_3) in the mol ratio 3:1 was homogenized in an agate mortar. MoO_3 dissolves in Y_2O_3 during the heat treatment of the starting mixtures resulting in the formation of a solid solution of Y_6MoO_{12}. It is clear from the TG analysis of the solid solution Y_6MoO_{12}, that there is no loss in weight. However, the DTA analysis shows that there is some phase transformation in the temperature range of 400–1000°C. This fact is in agreement with the results shown in XRD patterns in Fig. 3.

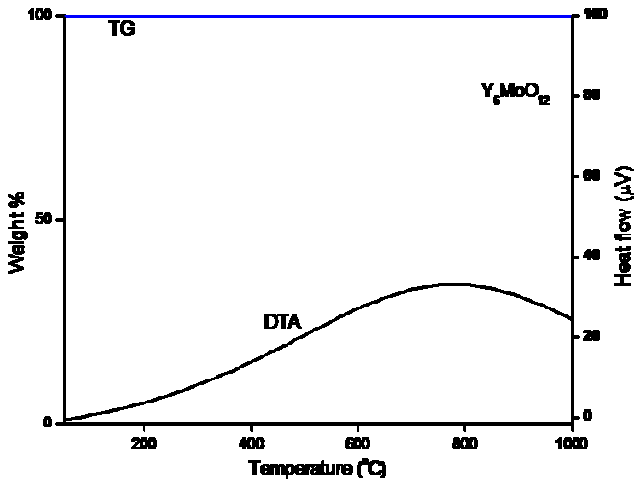

Fig. 17. The TG/DTA of powdered Y_6MoO_{12} pigment.

The acid/alkali and water resistance of the typical pigments $Y_{5.4}Si_{0.6}MoO_{12+\delta}$, and $Y_{5.4}Pr_{0.6}MoO_{12+\delta}$ was investigated with 10% HCl/H_2SO_4/HNO_3/NaOH and H_2O. A pre-weighed amount of the pigment was treated with acid/alkali and soaked for half an hour with constant stirring using a magnetic stirrer. The pigment powder was then filtered, washed with water, dried and weighed. Negligible weight loss of pigment was noticed for all the acids, alkali and water tested. The color coordinates of the pigments were measured after acid/alkali and water treatment and the total color difference, ΔE_{ab} of the pigments are found to be negligible as evident from the data reported in Table 4. The industrially acceptable limits of ΔE_{ab} are as follows: when $\Delta E_{ab} \leq 1$ units indicate that the color change is almost indistinguishable from the original color, whereas, $\Delta E_{ab} \leq 5$ units are considered to be very good. Thus the above studies highlight that the pigments are chemically and thermally stable.

Table 4. The color coordinates (±0.1) of the (a) $Y_{5.4}Si_{0.6}MoO_{12+\delta}$ and (b) $Y_{5.4}Pr_{0.6}MoO_{12+\delta}$ powder pigments after chemical resistance tests.

	$Y_{5.4}Si_{0.6}MoO_{12+\delta}$				$Y_{5.4}Pr_{0.6}MoO_{12+\delta}$			
10% Acid/Alkali	L^*	a^*	b^*	$^a\Delta E_{ab}$	L^*	a^*	b^*	ΔE_{ab}
H_2O	90.7	–6.8	54.7	0.7	41.9	17.9	19.5	0.8
NaOH	90.2	–6.9	54.1	1.5	41.0	17.6	19.7	1.5
HNO_3	90.3	–6.8	54.6	1.1	41.1	17.9	19.8	1.4
H_2SO_4	90.6	–6.9	54.8	0.8	41.9	17.8	20.9	1.1

$^a\Delta E_{ab} = [(\Delta L^*)^2+(\Delta a^*)^2+(\Delta b^*)^2]^{1/2}$

2.4. Conclusions

- A series of NIR reflective inorganic pigments of formula $Y_{6-x}M_xMoO_{12+\delta}$ (x ranges from 0 to 1.0) displaying a wide range of colors from light-yellow to dark-yellow and brick-red to dark-brown have been successfully synthesized by simple calcination route in air atmosphere.
- The X-ray diffraction pattern of Y_6MoO_{12} can be indexed to a cubic structure with a lattice constant of 0.5299 nm. On the other hand, the powder X-ray diffraction analyses of silica doped Y_6MoO_{12} compounds indicate the existence of cubic phase along with an additional phase of α-$Y_2Si_2O_7$.
- The doping of Pr^{4+} for Y^{3+} in Y_6MoO_{12} did not alter the cubic phase significantly.
- The absorption edge of the pigment samples gently shifted to higher wavelengths (485 to 510 nm) upon replacing Si^{4+} for Y^{3+} in Y_6MoO_{12}. In contrast, the absorption edge was drastically changed from 485 to 654 nm in the presence of Pr^{4+}.
- Most importantly, the pigments exhibited high NIR reflectance (75 to 85%) when coated on asbestos cement sheet, thus rendering them excellent candidates for use as "Cool Pigments".
- The designed pigments do not possess any toxic-metal ions and hence these can be considered as environmentally benign inorganic pigments.

The synthesis and characterization of environmentally benign non-toxic inorganic pigments based on CeO_2–TiO_2–Pr_6O_{11} solid solutions: Surface coating studies

Summary

New inorganic pigments of general formula $Ce_{1-(x+y)}Ti_xPr_yO_2$ (x ranges from 0.05 to 0.195 and y ranges from 0.005 to 0.15) based on CeO_2–TiO_2–Pr_6O_{11} solid solutions have been synthesized by solid-state route with a goal of preparing environmentally secure red colorants. Characterizations using XRD, UV–vis spectroscopy and CIE 1976 color coordinate assessment reveal the formation of pigments displaying colors ranging from brick-red to dark-brown. The coloring mechanism is based on the introduction of additional electronic level of energy in the cerianite forbidden band from the unpaired 4f electron of lanthanide ion. The typical designed pigment samples ($Ce_{0.8}Ti_{0.15}Pr_{0.05}O_2$ and $Ce_{0.8}Ti_{0.05}Pr_{0.15}O_2$) have been evaluated for their mass tone/hiding power, tinting strength and weather resistance by coating on an opacity chart. The results demonstrated that the dark-brown ceramic pigment obtained in the present study was found to be an interesting alternative to the existing classical toxic inorganic red pigments for surface coating applications.

Chemistry Letters *35* (2006) 1412-1413

3.1. Introduction

The development of red ceramic pigments with high temperature stability is of great importance to the ceramic industry [Buxbaum and Pfaff 2005; Eppler 1998; Smith 2002]. The classical red pigments used hitherto in the ceramic industry are of two types: iron oxide or cadmium sulfoselenide encapsulated in zircon matrix [$Cd(S_xSe_{1-x})$-$ZrSiO_4$] and lead oxide in tin oxide matrix. However, some of these pigments are toxic and unstable above 900°C [Bondioli *et al*. 1998; Aruna *et al*. 2001; Maso *et al*. 2003]. These materials can be easily replaced by rare earth metal oxides, which generally have a low toxicity rating [Haley 1965; Arvela 1979]. Recently, many rare earth based red pigments have been proposed by several researchers [[a]Sulcova *et al*. 1998; Garcia *et al*. 2001; Sulcova and Trojan 2003; Swiler *et al*. 2003; Bondioli *et al*. 2005; [a]Sreeram *et al*. 2008]. Although these pigments are non-toxic and show promising color hue, it is necessary to heat the starting materials in a flow of toxic and inflammable gases for a long time (20-60 h) to synthesize them [Jansen *et al*. 2000]. Thus serious need arises to search for environmentally friendly and economically viable materials for the replacement of toxic inorganic red pigments.

CeO_2 is a fluorite-structured oxide that can form extensive solid solutions with a variety of alien cations while retaining the fluorite crystal structure. In cerianite doped red pigments, the coloring mechanism is based on the shift of the charge transfer band of the semiconductor CeO_2 to higher wavelengths, by introducing an additional electronic level through doping of a chromophore metal ion. CeO_2 crystallizes in the fluorite structure, where FCC packed Ce^{4+} ions are surrounded by eight oxygen, occupying alternate centers of tetrahedral cavities in the FCC lattice [Trovarelli 1999; Garcia *et al*. 2001]. The 4f valence shell of Ce^{4+}([Xe]) in cerianite is empty, and that of O^{2-} ([He]$2s^2 2p^6$) is full: adjacent Ce^{4+} ions are virtually in contact in the fluorite lattice and, as a result, 4f orbitals

overlap in a cationic conduction band; similarly, overlap of 2p orbitals of oxygen ions gives to an anionic valence band. The band gap between the anionic band and the cationic band is 2.76 eV [Garcia *et al*. 2001]. The CeO_2-Pr_6O_{11} system has been studied as a ceramic pigment by various authors using different synthesis methods: solid-state reactions [Maso *et al.* 2003; [a]Sulcova and Trojan 1998], co-precipitation [Bondioli *et al.* 2000], flux method [Bondioli *et al.* 2000], combustion [Aruna *et al.* 2001] and hydrothermal [Shuk and Greenblatt 1999]. Nevertheless, little is known of its surface coating applications. However, some of the synthesis methods employed for the above pigments uses toxic gases and mineral acids for dissolving the starting materials. Further the obtained optical properties are not satisfactory for commercial use. Accordingly, the major objective of the present investigation is to develop environmentally secure inorganic red pigments with high temperature stability to replace the toxic ceramic pigments, currently used in the pigment industry. In the present study, a series of new colorants having the general formula $Ce_{1-x-y}Ti_xPr_yO_2$ (x ranges from 0.05 to 0.195 and y ranges from 0.005 to 0.15) were synthesized by solid-state reaction of the respective oxides and characterized by various spectroscopic techniques. The typical designed pigment samples have also been evaluated for their surface coating applications.

3.2. Experimental Section

3.2.1. Materials and Methodology

A series of new pigments having the general formula $Ce_{1-(x+y)}Ti_x\,Pr_yO_2$ (x ranges from 0.05 to 0.195 and y ranges from 0.005 to 0.15) based on CeO_2–TiO_2–Pr_6O_{11} solid solutions have been synthesized by ceramic method. The precursors employed for the traditional ceramic pigment synthesis route are the corresponding oxides: TiO_2 (99.9%), CeO_2 (99.9%) and Pr_6O_{11} (99.9%) supplied by M/s. Sigma Aldrich. In this method, the reactants were stoichiometrically mixed and homogenized by wet milling with acetone in an agate mortar for 30 min. The homogeneous mixture was then calcined in platinum crucibles in a

Nabertherm electric furnace at a temperature of 1200°C for 3 h in air atmosphere. The heating of the furnace was programmed to increase the temperature initially at 10°C/min up to 900°C and afterwards the heating rate was decreased to 5°C/min up to 1200°C. In order to ensure the completion of the reaction, the calcination process was repeated thrice. To refine and homogenize the particle size after calcinations, the resulting products were ground in an agate mortar and utilized for the determination of their optical properties.

3.2.2. Methodology adopted for coloration of plastic materials

Poly (methyl methacrylate) (PMMA; S.D. Fine Chemicals, India) was utilized as a binder phase for fabricating the pigmented compact. The typical pigment sample, $Ce_{0.8}Ti_{0.05}Pr_{0.15}O_2$ (10%) was ultrasonicated (Vibronics, 250 W, India) in an alcohol/ water (1:4) mixture for 10 min to ensure the complete dispersion of the pigment particles. A viscous solution consists of PMMA (90 wt.%) was made using a conventional electrical coil heater. The pigment dispersion was then added to the PMMA viscous solution by vigorous stirring and converted into a thick paste. The paste after 2 h of curing, compressed uniaxially into a form of cylindrical discs using a hydraulic press (Lawrence & Maya, India) at a pressure of 25 MPa. Both sides of the pigmented polymer were lapped using a fine grade emery sheet for obtaining a polished surface. The intensity of the color of plastics will depend on the concentration of the pigment.

3.2.3. Characterization Techniques

The instrumental techniques employed for the characterization of various pigments designed in the present study are the same as that described in the previous chapter 2.

3.3. Results and Discussion

3.3.1. Powder X-ray diffraction analysis

The XRD patterns of the typical pigment sample $Ce_{0.8}Ti_{0.05}Pr_{0.15}O_2$ calcined at different temperatures ranging from 1000°C to 1300°C for 9 h are shown in Fig.1. The samples

calcined at 1000°C to 1100°C exhibit poor crystallization, accompanying with precursor oxide, rutile TiO_2 (PDF No. 21-1276; Baidya *et al.* 2006) phase. On the other hand, the sample calcined at and above 1200°C can be very well indexed to a cubic fluorite phase of CeO_2 (JCPDS No. 34-394; Baidya *et al.* 2006). Thus it is clear from the above study that a calcination temperature of 1200°C is necessary to obtain the desired products.

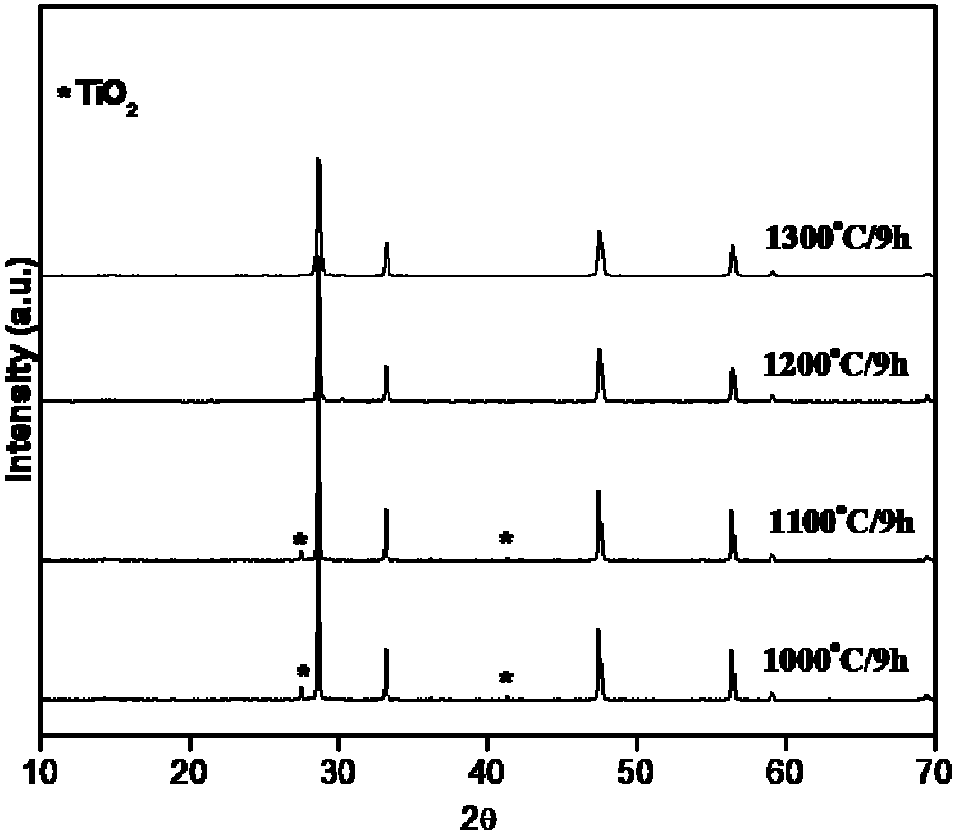

Fig. 1. XRD patterns of $Ce_{0.8}Ti_{0.05}Pr_{0.15}O_2$ samples calcined at different temperatures.

Fig. 2 depicts the XRD patterns of the pigments $Ce_{1-(x+y)}Ti_xPr_yO_2$ (x ranges from 0.05 to 0.195 and y ranges from 0.005 to 0.15) calcined at an optimized time (9 h) and temperature (1200°C). All the XRD patterns shows the characteristic reflections of the cubic fluorite structure of CeO_2 [Baidya *et al.* 2006] and also in good agreement with the JCPDS No. 34-394. The intense and sharp peaks found in the diffraction patterns reveal the crystalline nature of the phase.

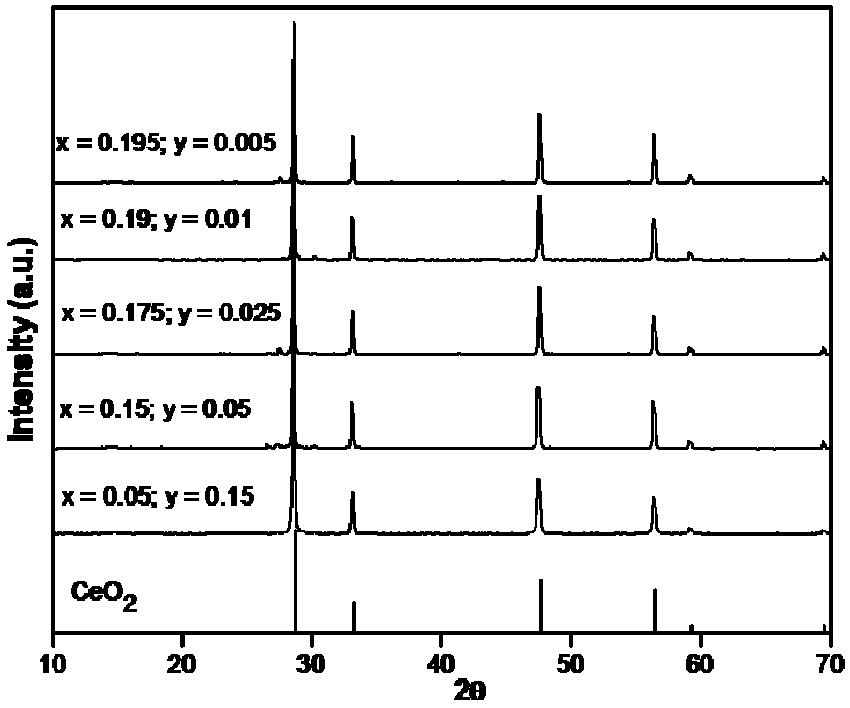

Fig. 2. XRD patterns of $Ce_{1-(x+y)}Ti_x Pr_y O_2$ (x ranges from 0.05 to 0.195 and y ranges from 0.005 to 0.15) samples (Calcination temperature: 1200°C; Time duration 9 h).

The crystallite size is calculated from Debye-Scherrer formula, $D = 0.9 \lambda / \beta \cos \theta$, where D is the particle size, λ is the wave length of X-ray used, β and θ are the half width of X-ray diffraction lines and half diffraction angle of 2θ. The crystallite size of the pigments was found to be 7–19 nm. Doping of small amounts of praseodymium and titanium in cerium oxide retains the fluorite structure except minor variations in the lattice parameters (Table 1). As the ionic radii of Ce^{4+} and Pr^{4+} in eightfold coordination are 0.097 and 0.096 nm [Shannon 1976], respectively, only minor variations would be expected. The incorporation of 15% of praseodymium into CeO_2 lattice decreases the unit cell parameter to 0.5405 nm. On the other hand, doping of Ti^{4+} (19.5%) having a smaller ionic radii (0.074 nm) decreases relatively more the lattice parameter value to 0.5397 nm. The decrease in lattice parameter confirms $Ce_{1-(x+y)}Ti_xPr_yO_2$ solid-solution formation.

3.3.2. Particle size and morphological analysis

Particle size analysis of the typical pigment $Ce_{0.8}Ti_{0.05}Pr_{0.15}O_2$ reveals a mean diameter of 7.63 μm (size of 90% particles < 60.19, 50% particles < 17.91 μm and 10% particles < 4.46 μm). The homogeneous and crystalline nature of the sample has also been noticed from the SEM photograph of the $Ce_{0.8}Ti_{0.05}Pr_{0.15}O_2$ pigment given in Fig. 3. From the SEM photograph, it is clear that there is an even grain distribution; the average grain size is less than 5 μm.

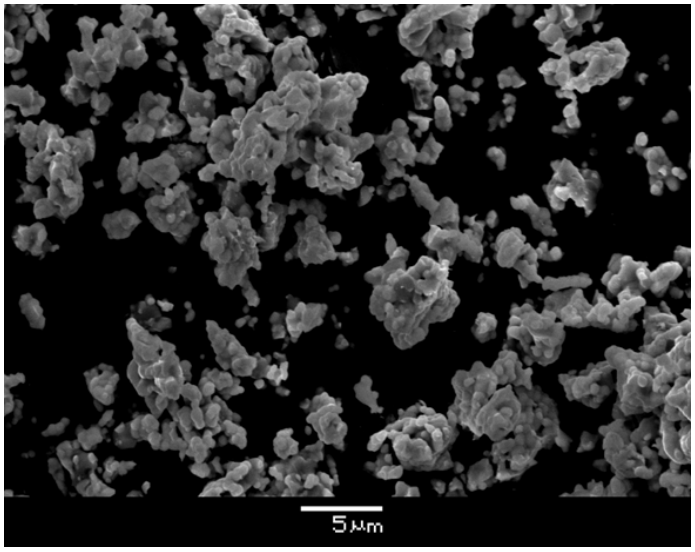

Fig. 3. The SEM micrograph of $Ce_{0.8}Ti_{0.05}Pr_{0.15}O_2$ pigment powder.

3.3.3. The optical properties of $Ce_{1-(x+y)}Ti_xPr_yO_2$ pigments

Figs. 4 and 5 displays the diffuse reflectance and absorption spectra of the corresponding $Ce_{1-(x+y)}Ti_xPr_yO_2$ pigment samples. The CeO_2 band gap (2.76 eV) falls in the indigo region of visible wavelengths, and a complementary light yellow color is observed. The reflectance spectra of $Ce_{1-(x+y)}Ti_xPr_yO_2$ pigment samples show greater absorptions in the visible region with an increasing number of chromophore ions (Pr^{4+}) because the gap between the valence and conduction bands narrows. This causes color of the pigment to vary from brick-red to dark-brown (Fig. 6). According to the band structure model

proposed for CeO_2 and $Pr_6O_{11,}$ the electronic spectra arise due to the electron transfer from the ligand orbitals to the localized $4f^1$ level of the Pr^{4+} cation [Koelling *et al.* 1983]. It is evident from the absorption spectra of these pigments depicted in Fig. 5 that the position of the absorption edge is critically dependent on the praseodymium content and it is red-shifted with increasing Pr^{4+} concentration. The slope of the electronic spectra decreases with increasing praseodymium concentration. This evaluation is consistent with the observed charge transfer spectra of tetravalent lanthanide ions in oxides [Maso *et al* .2003; Hoefdraad 1975] and confirms the substitution of Pr^{4+} for Ce^{4+} in the fluorite ceria crystal. The coloring mechanism is based on the shift of the charge transfer band of semiconductor CeO_2 to higher wavelengths, introducing an additional electronic level by doping of Pr^{4+}. This causes the color of the pigment vary from brick-red to dark-brown and reduces the band gap to ~ 1.86 eV (Table 1).

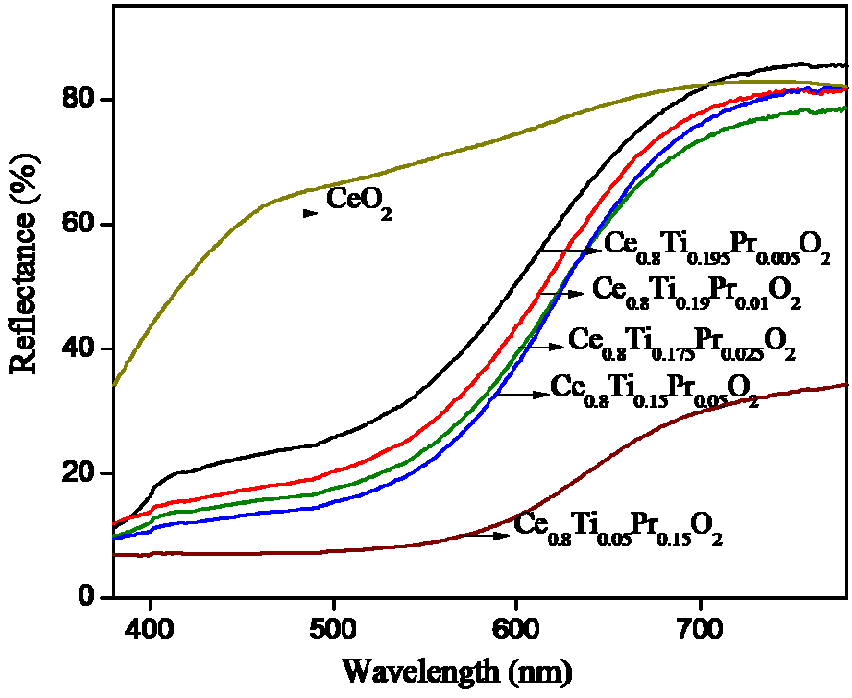

Fig. 4. The reflectance spectra of the $Ce_{1-(x+y)}Ti_xPr_yO_2$ (x ranges from 0.05 to 0.195 and y ranges from 0.005 to 0.15) pigments.

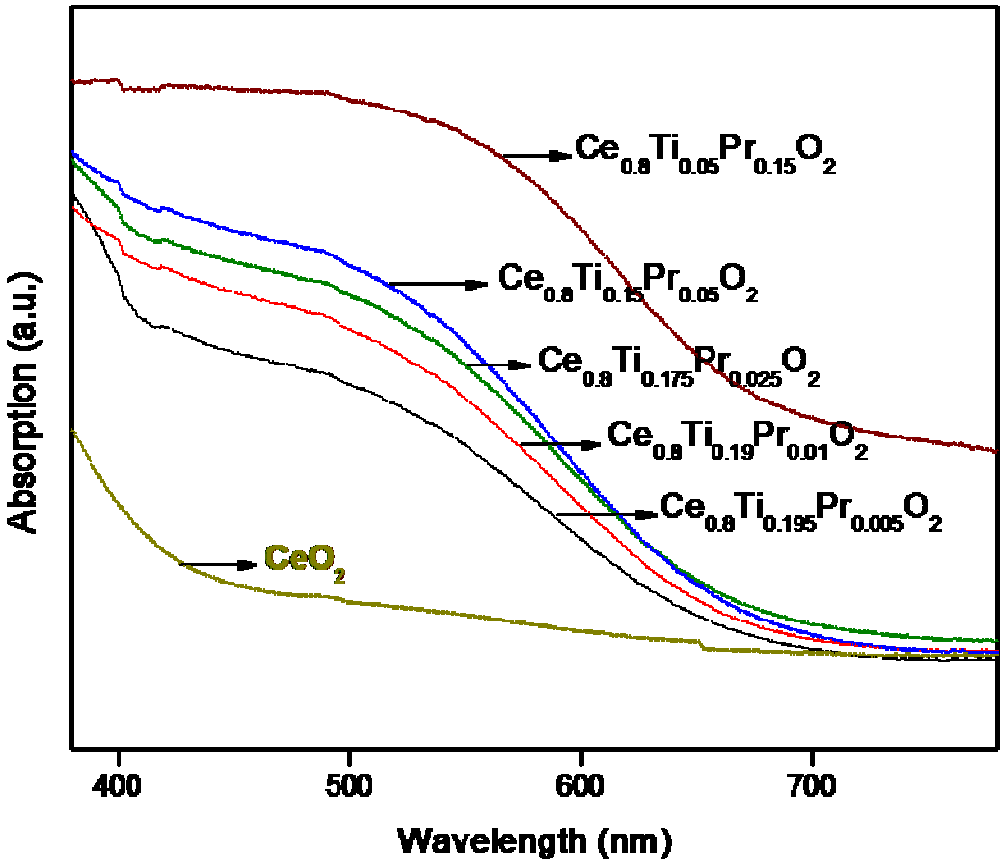

Fig. 5. The absorption spectra of the $Ce_{1-(x+y)}Ti_xPr_yO_2$ (x ranges from 0.05 to 0.195 and y ranges from 0.005 to 0.15) pigments.

Fig. 6. Photographs of the $Ce_{1-(x+y)}Ti_xPr_yO_2$ pigment powders.

The $L^*a^*b^*$ values of the $Ce_{1-(x+y)}Ti_xPr_yO_2$ (x ranges from 0.05 to 0.195 and y ranges from 0.005 to 0.15) pigments synthesized at the optimized temperature of 1200°C for 9 h are summarized in Table 1. It is evident from Table 1 that the substitution of small amounts (0.5 to 5 mol%) of Pr^{4+} for Ce^{4+} in CeO_2 increases the a^* value. However, it does not have significant influence on both b^* and C^* values. Further, more and more addition of Pr^{4+} ions (15 mol%) decreases both the a^* and b^* values drastically and hence the color of the pigment gently changes from brick-red to dark-brown. The progressive addition of titanium to the CeO_2–Pr_6O_{11} solid solution significantly increases the lightness (L^*) of the pigment retaining the color coordinates corresponding to the red hue. The hue angles of the currently synthesized pigments are found to be in the orange-red region of the cylindrical color space (h° = 0–35 for red and 35–70 for orange) [Sulcova and Trojan 2008].

Table 1. The color coordinates (±0.1) of the $Ce_{1-(x+y)}Ti_xPr_yO_2$ (x ranges from 0.05 to 0.195 and y ranges from 0.005 to 0.15) powder pigments, cell parameter and band gap values.

Composition	Color coordinates					a /nm	Energy (eV)
	L^*	a^*	b^*	C^*	h^o		
CeO_2	77.7	1.3	9.9	9.9	82.4	0.5411	2.76
$Ce_{0.8}Ti_{0.195}Pr_{0.005}O_2$	61.8	15.3	17.7	23.4	49.0	0.5397	1.90
$Ce_{0.8}Ti_{0.19}Pr_{0.01}O_2$	56.8	17.2	18.0	24.9	46.3	0.5402	1.89
$Ce_{0.8}Ti_{0.175}Pr_{0.025}O_2$	53.1	17.9	17.0	24.7	43.6	0.5401	1.89
$Ce_{0.8}Ti_{0.15}Pr_{0.05}O_2$	51.3	18.8	17.4	25.6	42.8	0.5405	1.88
$Ce_{0.8}Ti_{0.05}Pr_{0.15}O_2$	34.5	10.7	7.4	13.1	34.6	0.5405	1.86

$C^* = [(a^*)^2 + (b^*)^2]^{1/2}$; $h^o = \tan^{-1}(b^*/a^*)$

It is clear from the color coordinate values summarized in Table 1 that the present values are significantly higher than recently reported praseodymium-doped ceria powders (5% praseodymium-doped CeO_2: L^* = 51; a^* = 12; b^* = 9.5), synthesized by microwave-

assisted hydrothermal route [Bondioli *et al.* 2005]. It is also clear from this study that the solid solutions of these pigments can be prepared at lower calcination temperatures by the addition of titanium as compared to the previously reported CeO_2–Pr_6O_{11} solid solutions [Maso *et al.* 2003] which were calcined at higher temperatures (1400–1500°C).

3.3.4. Thermal and chemical stability studies

Thermo gravimetric (TG) and differential thermal analyses (DTA) of the typical pigment sample $Ce_{0.8}Ti_{0.05}Pr_{0.15}O_2$ were carried out in the temperature range of 50–1000°C with a heating rate of 20°C /min in nitrogen atmosphere and the results are given in Fig. 7. It is clear from the TG/ DTA analysis of the solid solution $Ce_{0.8}Ti_{0.05}Pr_{0.15}O_2$, that there is no weight loss and phase transformation in the temperature range investigated.

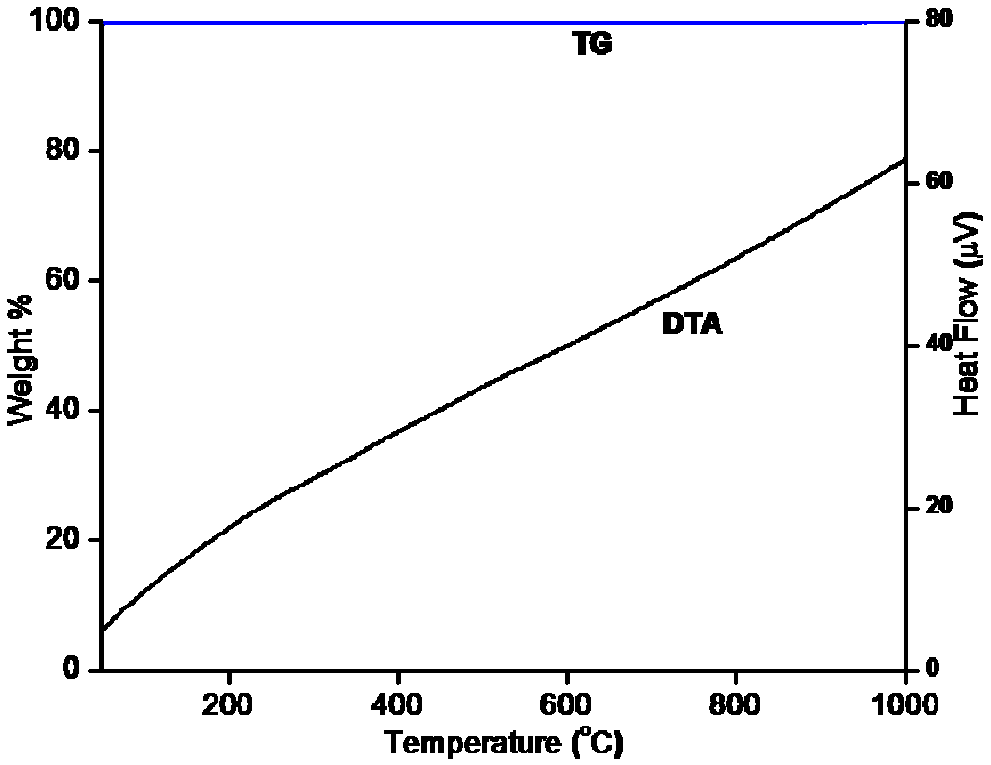

Fig. 7. TG/DTA of powdered $Ce_{0.8}Ti_{0.05}Pr_{0.15}O_2$ pigment.

The typical pigment $Ce_{0.8}Ti_{0.05}Pr_{0.15}O_2$ was tested for its chemical resistance in 10% HCl, H_2SO_4, HNO_3 and NaOH. A pre-weighed amount of the pigment was treated with acid/alkali and soaked for half an hour with constant stirring using a magnetic stirrer. The pigment powder was then filtered, washed with water, dried and weighed. Negligible weight loss of pigment was noticed for all the acids and alkali tested. The color coordinates of the pigments were measured after acid/alkali treatment and the total color difference, ΔE_{ab} of the pigments are found to be negligible, as evident from the data reported in Table 2. The above studies highlight that the pigments are chemically and thermally stable.

Table 2. The color coordinates (±0.1) of the $Ce_{0.8}Ti_{0.05}Pr_{0.15}O_2$ powder pigments after acid/alkali resistance tests.

10% Acid/Alkali	Color coordinates			[a] ΔE_{ab}
	L^*	a^*	b^*	
HCl	34.3	10.6	7.5	0.29
HNO_3	35.3	9.9	7.1	1.18
H_2SO_4	34.6	10.1	7.5	0.62
NaOH	34.0	10.3	7.6	0.65

[a] $\Delta E_{ab} = [(\Delta L^*)^2+(\Delta a^*)^2+(\Delta b^*)^2]^{1/2}$

3.3.5. Development of paint formulation and evaluation of mass tone/hiding power and tinting strength

The typical pigment samples $Ce_{0.8}Ti_{0.05}Pr_{0.15}O_2$ and $Ce_{0.8}Ti_{0.15}Pr_{0.05}O_2$ were ground, sieved to obtain the particles in the range of 25-45 μm and analyzed for their mass tone/hiding power and tinting strength. For this, a standard commercial paint composition consisting of a long oil alkyd as a binder, oleic acid as a plasticizer and aluminium stearate as a rheological agent was used. A paint formulation, consisting of 20 g (~ 27 wt.%) pigment,

50 g (~ 68 wt.%) resin, 3 g (~ 4 wt.%) plasticizer and 0.5 g (~ 0.7 wt.%) rheological agent, were mixed along with mineral turpentine in a ball mill for 60 min [Aby *et al.* 2007; [a]Sreeram *et al.* 2008]. For tinting strength measurements, the pigment was replaced by a mixture of 15 g (~ 20 wt.%) TiO_2 and 5 g (~ 7 wt.%) pigment. The paint formulation thus developed was used for coating.

The hiding power and tinting strength was evaluated by coating on an opacity chart at a thickness of 150 µm (Figs. 8 and 9). The CIELAB 1976 method of determination of L^*, a^* and b^* was employed to determine the hiding power and tinting strength of the colorants by comparison of values when coated on a board with a checkered, white and black background and the results are summarized in Tables 3 and 4. The color difference has been quantified on the CIELAB based color difference (ΔE_{ab}), which is calculated using the equation (1) [CIE 1986; CIE 2004; Ohno 2000].

$$\Delta E_{ab} = [(\Delta L^*)^2+(\Delta a^*)^2+(\Delta b^*)^2]^{1/2} \quad (1)$$

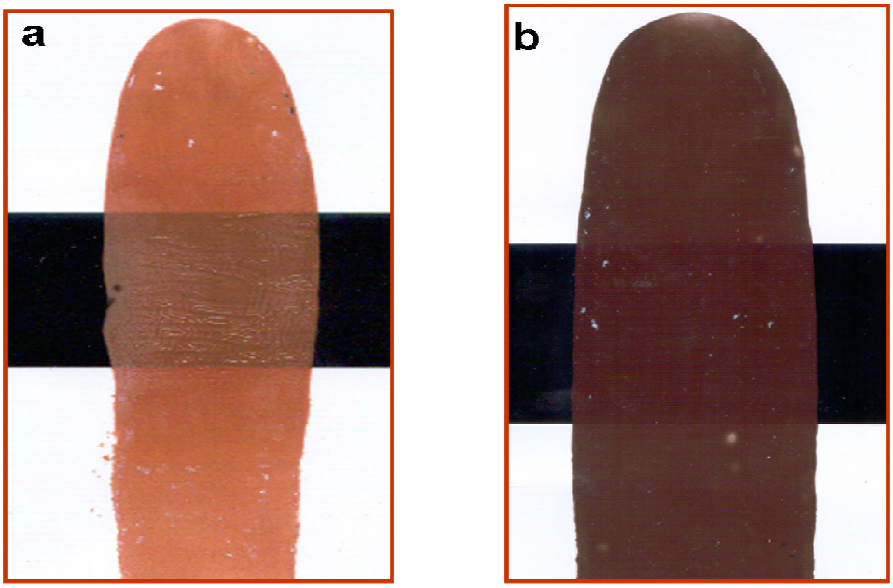

Fig. 8. Photographs of the hiding power of (a) $Ce_{0.8}Ti_{0.15}Pr_{0.05}O_2$ and (b) $Ce_{0.8}Ti_{0.05}Pr_{0.15}O_2$ pigments.

For mass tone, the color difference between the black and white region was found to be ΔE_{ab} = 10.8 for $Ce_{0.8}Ti_{0.15}Pr_{0.05}O_2$ and 3.3 in the case of $Ce_{0.8}Ti_{0.05}Pr_{0.15}O_2$. A lower value of ΔE_{ab} (3.3) for mass tone on the black versus the white regions in the case of $Ce_{0.8}Ti_{0.05}Pr_{0.15}O_2$ sample indicates the ability of the dark-brown colorant to cover black and white regions uniformly well. On the other hand, poor covering power was noted in the case of brick-red sample. However, the color difference between tinted and untinted colorants is high, indicating the poor ability of the colorant to transfer its color completely to TiO_2.

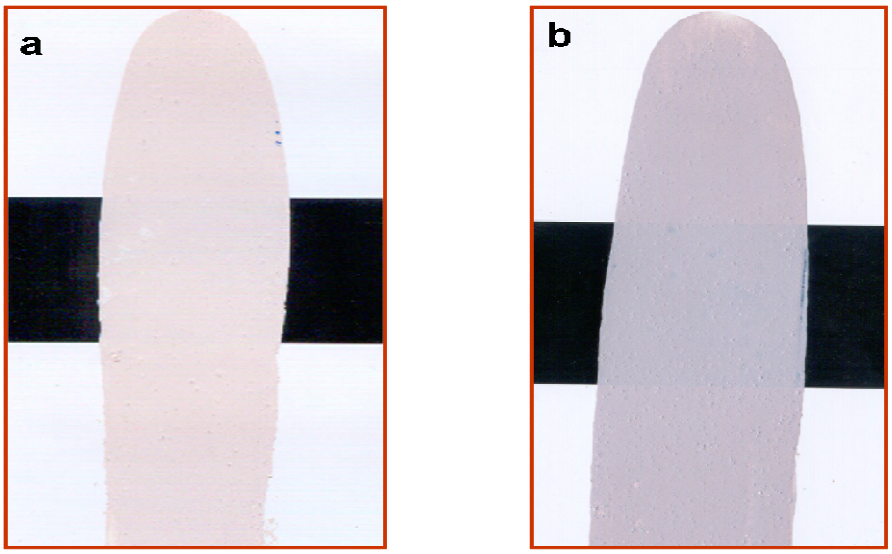

Fig. 9. Photographs of the tinting strength of (a) $Ce_{0.8}Ti_{0.15}Pr_{0.05}O_2$ and (b) $Ce_{0.8}Ti_{0.05}Pr_{0.15}O_2$ pigments.

Table 3. The color coordinates (±0.1) of the powder pigments after hiding power analysis on a white and black surface.

	$Ce_{0.8}Ti_{0.15}Pr_{0.05}O_2$				$Ce_{0.8}Ti_{0.05}Pr_{0.15}O_2$			
Surface	*L**	*a**	*b**	[a]ΔE_{ab}	*L**	*a**	*b**	ΔE_{ab}
Powder	49.3	24.0	23.6	-	31.9	11.9	7.3	-
Black	44.1	17.4	17.3	10.5	24.7	11.5	7.2	7.2
White	51.6	24.2	21.1	3.4	27.9	12.1	7.7	4.0

Table 4. The color coordinates (±0.1) of the powder pigments after tinting strength analysis on a white and black surface.

	$Ce_{0.8}Ti_{0.15}Pr_{0.05}O_2$				$Ce_{0.8}Ti_{0.05}Pr_{0.15}O_2$			
Surface	*L**	*a**	*b**	[a] ΔE_{ab}	*L**	*a**	*b**	ΔE_{ab}
Powder	49.3	24.0	23.6	-	31.9	11.9	7.3	-
Black	85.6	5.7	4.8	44.8	73.8	3.4	-0.5	43.3
White	85.7	4.7	4.8	45.3	74.6	4.5	0.2	43.9

[a] $\Delta E_{ab} = [(\Delta L*)^2+(\Delta a*)^2+(\Delta b*)^2]^{1/2}$

3.3.6. Weather resistance studies

The typical paint formulation consisting of $Ce_{0\cdot8}Ti_{0.05}Pr_{0.15}O_2$, was coated on a board with a checkered, white and black background and evaluated for its weather resistance by exposing to natural sunlight (12 h exposure, 45° angle facing the sun, 30 days). The CIELAB 1976 method of determination of *L*, a** and *b** was employed to determine the weather resistance of the colorants by comparison of values when coated on a board with a checkered, white and black background against unexposed sample and the results are depicted in Table 6. The color coordinates were measured in the interval of five days. The negligible values of ΔE_{ab} reveal that the pigments posses good weather stability.

Table 6. The color coordinates (±0.1) of the white/black surface coated with $Ce_{0\cdot8}Ti_{0.05}Pr_{0.15}O_2$ pigment after exposed to sunlight.

Time duration	White surface				Black surface			
	Color coordinates			ΔE_{ab}	Color coordinates			ΔE_{ab}
	*L**	*a**	*b**		*L**	*a**	*b**	
Unexposed sample	27.9	12.1	7.7	–	24.7	11.5	7.2	–
Day 5	27.8	12.1	7.8	0.12	24.7	11.2	7.2	0.38
Day 10	27.8	12.2	7.7	0.21	24.7	11.3	7.2	0.18
Day 15	27.8	12.2	7.7	0.21	24.8	11.1	7.1	0.42
Day 20	27.9	11.8	7.7	0.27	24.8	11.2	7.2	0.33
Day 25	27.7	11.9	7.4	0.38	24.9	11.4	7.3	0.14
Day 30	27.9	11.8	7.7	0.26	24.9	11.2	7.2	0.27

3.3.7. Oil absorption study

The typical pigment $Ce_{0.8}Ti_{0.05}Pr_{0.15}O_2$ has been evaluated for its oil absorption and found to be 15.95g. This means that 15.95g of linseed oil is required for making paint with 100g of the sample. The oil absorption value of this pigment is in the acceptable range considering the inorganic nature of the pigment.

3.3.8. Applications in coloring of plastics

The coloring performance of the typically synthesized pigments $Ce_{0.8}Ti_{0.05}Pr_{0.15}O_2$ was tested for its coloring application in a substrate material like PMMA. Typically, 10 wt.% pigment sample was dispersed in PMMA and compressed to a cylindrical disc (Fig. 10). The color coordinates of the test pieces were measured at different locations and an average value is depicted in Table 7. The *L*a*b** values obtained were more or less the same indicating the uniform distribution of pigment particles in the polymer matrix.

Fig. 10. Photograph of (a) $Ce_{0.8}Ti_{0.05}Pr_{0.15}O_2$ (10%) + PMMA.

Table 7. The color coordinates (±0.1) of the $Ce_{0.8}Ti_{0.05}Pr_{0.15}O_2$ powder pigment after applied on polymer.

Composition	Color coordinates		
	*L**	*a**	*b**
$Ce_{0.8}Ti_{0.05}Pr_{0.15}O_2$	34.5	10.7	7.4
$Ce_{0.8}Ti_{0.05}Pr_{0.15}O_2$ (10%)+PMMA	34.1	11.9	6.3

3.4. Conclusions

- Novel environmentally benign inorganic pigments displaying colors ranging from brick-red to dark-brown based on CeO_2–TiO_2–Pr_6O_{11} solid solutions have been successfully designed and evaluated their surface coating applications.
- The coloring mechanism is based on the shift of the charge transfer band of CeO_2 to higher wavelengths, introducing an additional electronic level by doping praseodymium ions.
- The synthesized powder pigment samples are found to be thermally and chemically stable.
- Most importantly, the color coordinates of the present pigment samples are superior to that of the commercially available Zinc-Iron-Chromite red pigments marketed by M/s Kawamura Chemicals, Japan.
- The hiding power of the dark-brown pigment was found to be good and it could effectively cover both white and black surfaces, highlighting its excellent surface coating applications. Further, this particular pigment also demonstrates its weather resistance capability.
- The designed pigments are also found to be useful for coloration of plastic materials.
- However, the techno-economic feasibility of the designed pigments, especially dark-brown pigment needs to be established for further industrial utility.

Chapter 4

The synthesis and characterization of alkaline-earth metal doped $Pr_2Mo_2O_9$ pigments: Applications in coloring of plastics

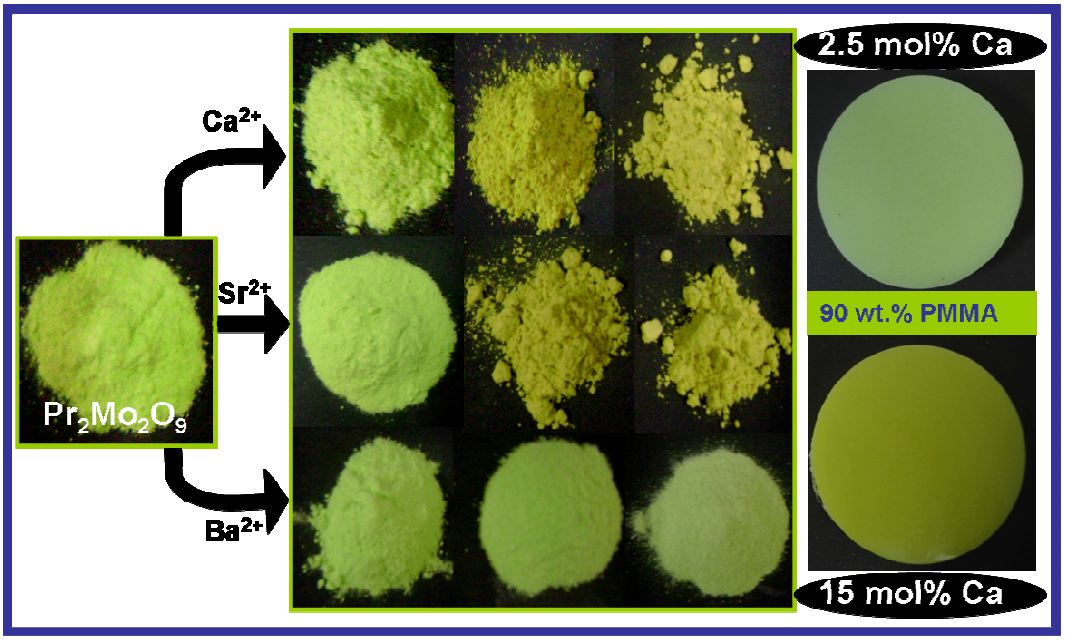

Summary

A new class of inorganic pigments based on praseodymium molybdate having the general formula $Pr_{2-x}A_xMo_2O_{9-\delta}$ (where A = Ca^{2+}, Sr^{2+} and Ba^{2+} and x ranges from 0 to 1.0), displaying colors ranging from green to greenish-yellow were synthesized by traditional solid-state route, as alternatives to lead, cadmium and chromium based colorants. The products were characterized by X-ray powder diffraction, UV–vis diffuse reflectance spectroscopy and CIE-$L^*a^*b^*$ 1976 color scales. The coloring mechanism is based on the strong absorptions of the pigments in the blue and red regions due to electronic transitions between $4f^2 \rightarrow 4f^15d^1$ states of Pr^{3+}. The designed pigments consist of non-toxic elements and are further found to be thermally and chemically stable. The greenish-yellow pigments were found to be interesting alternatives to existing toxic pigments for coloration of plastics.

Chemistry Letters *34* (2005) 1702-1703;

Journal of Solid State Chemistry *181* (2008) 487-492

4.1. Introduction

There is a strong incentive to design new colorants based on inorganic materials to substitute for industrial pigments that are based on heavy elements hazardous to health and the environment [Smith 2002]. Green and yellow are particularly important colors in the pigment industry with high performance in their thermal and chemical stability and the consumption of the green and yellow exceeds that of any other colored pigments. There are various important yellow pigment families: tin vanadium yellow (11-22-4 DCMA, dry color manufacturers association), praseodymium zircon (14-43-4 DCMA) and zirconium vanadium yellow (1-01-4 DCMA), cadmium yellow and lead antimonite. Among them, praseodymium yellow ($ZrSiO_4$:Pr) has been known as one of the environmentally benign inorganic colorants, which can be applied to paints, inks, plastics, rubbers, ceramics, enamels and glasses because of its thermal stability [Hill and Lehman 2000; Del Nero *et al.* 2004]. However, this pigment requires high temperature calcinations (>1573 K) for the preparation, which tends to induce particle growth of the pigment. Hence, it is difficult to apply the praseodymium yellow to paints and inks in which fine dispersion of the pigment is essential. Other yellow pigments commonly used such as $Pb_2Sb_2O_7$, $PbCrO_4$, CdS are now being expelled from the market because of their toxicity.

Recently, many rare earth-based inorganic yellow pigments have been proposed by several researchers [Huguenin *et al.* 1996; Jansen *et al.* 2000; Sreeram *et al.* 2007]. Although these pigments are non-toxic, it is necessary to heat the starting materials in a flow of toxic and inflammable ammonia gas for a long time (20–60 h) to synthesize them [Jansen *et al.* 2000]. Further, their chromatic properties are not very attractive. Therefore, research needs to be performed in developing novel green and yellow inorganic pigments with various advantages over traditional pigment formulations.

Thus the present chapter is focused on the development of novel class of green and yellow pigments based on alkaline-earth metal doped $Pr_2Mo_2O_9$ system from an

environmental point of view. The new pigments of the formula $Pr_{2-x}A_xMo_2O_{9-\delta}$ (A= Ca^{2+}, Sr^{2+} and Ba^{2+}) have been synthesized by solid-state reaction of the respective oxides and characterized for their structure and optical properties. The thermal and chemical stabilities of the pigments and their application for coloring plastics have also been investigated.

4.2. Experimental Section

4.2.1. Materials and Methodology

Several compositions based on $Pr_{2-x}A_xMo_2O_{9-\delta}$ (A= Ca^{2+}, Sr^{2+} and Ba^{2+} and x ranges from 0 to 1.0) were prepared by corresponding oxides: Pr_6O_{11} (99.9%), $CaCO_3$ (99%), $SrCO_3$ (99%), $BaCO_3$ (99%) and $(NH_4)_6Mo_7O_{24}.4H_2O$ (99.9%), supplied by Sigma Aldrich. In this method, the reactants were mixed and homogenized by wet milling with acetone media in an agate mortar for 30 min. The homogeneous mixture was calcined in platinum crucibles in an electric furnace at optimized temperatures (1000°C for $Pr_2Mo_2O_9$, 1050°C for Ca^{2+}-doped system, 1000°C for Sr^{2+}-doped system and 950°C for Ba^{2+}-doped system) and time (9 h) in air atmosphere. The heating of the furnace was programmed to increase the temperature at 5°C/min. The final pigment powders were subsequently ground in an agate mortar with the aim of refining and homogenizing the particle size.

4.2.2. Methodology adopted for coloration of plastic materials

The typical pigment samples, $Pr_{1.9}Ca_{0.1}Mo_2O_{9-\delta}$ (10%) and $Pr_{1.4}Ca_{0.6}Mo_2O_{9-\delta}$ (10%) was studied for their application in coloring of plastics and the procedure used for coloring is same as that described in chapter 3.

4.2.3. Characterization Techniques

The instrumental techniques employed for the characterization of various pigments designed in the present study are the same as that described in the previous chapter 2.

4.3. Results and Discussion

4.3.1. Powder X-ray diffraction analysis

The XRD patterns of alkaline-earth metal free $Pr_2Mo_2O_9$ pigment sample calcined at various temperatures (900°C to 1000°C) for 9 h are depicted in Fig. 1. The sample calcined at 900°C exhibits poor crystallization. On the other hand, the sample calcined at 1000°C shows the characteristic reflections of the cubic structure of $Pr_2Mo_2O_9$ with a lattice constant of 0.7068 nm, which is in good agreement with the earlier report [Yamazaki *et al.* 2002]. The diffraction pattern of $Pr_2Mo_2O_9$ shown in the figure resembles to that of $La_2Mo_2O_9$ with a cubic structure [Lacorre *et al.* 2000; Subasri *et al.* 2004; Tealdi *et al.* 2004; Marrero-Lopez *et al.* 2007]. Thus it can be concluded from the above study that a minimum of 1000°C calcination temperature is essential to obtain the phase pure product of $Pr_2Mo_2O_9$.

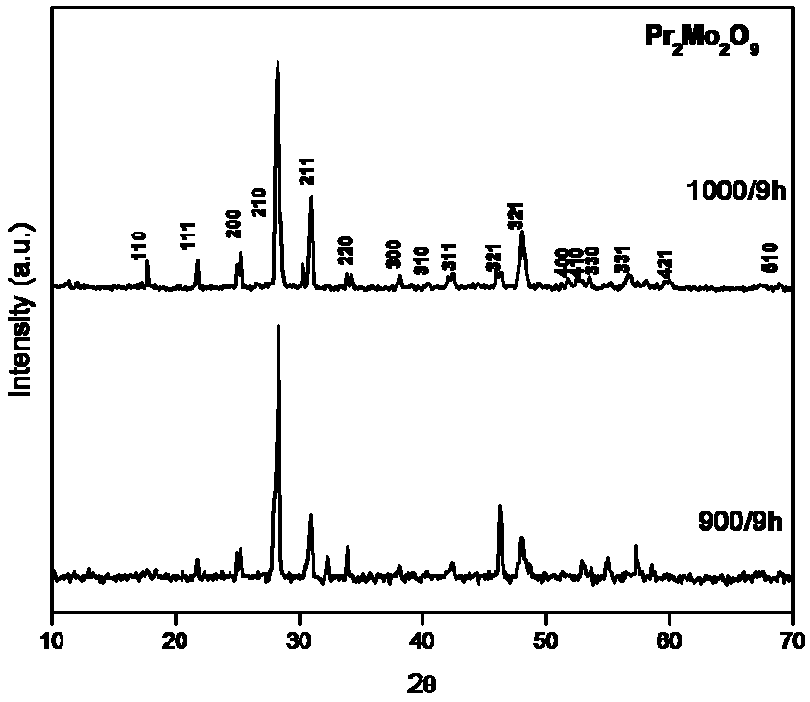

Fig. 1. XRD patterns of $Pr_2Mo_2O_9$ samples calcined at different temperatures.

Fig. 2 shows the powder X-ray diffraction patterns for $Pr_{2-x}Ca_xMo_2O_{9-\delta}$ with different doping content of Ca, where x = 0, 0.10 and 0.20, respectively. The XRD pattern of the pure $Pr_2Mo_2O_9$ sample can be indexed very well as a cubic structure of *P*213 with a lattice constant of 0.7068 nm. Since Ca^{2+} (ionic radius: 0.099 nm) is slightly smaller in size than Pr^{3+} (0.112 nm) and in addition, the substitution of a lower valence ion in the Pr^{3+} sites leads to creation of O^{2-} vacancies, the cell volume lowers with increasing Ca^{2+} content up to 10% as can be seen from Fig. 3 [Subasri *et al.* 2004]. With increase of Ca^{2+}-dopant content, the lattice constant decrease first, reaches to a minimum of 0.7058 nm at 10% Ca^{2+} doping content and increases to a value, which is even greater than the lattice constant of Ca^{2+} free specimen. This variation rule of lattice constant is resulted from the contribution of substitution of Ca^{2+} for Pr^{3+} and introduction of extrinsic vacancies by Ca^{2+} doping, the former of which will shrink the lattice while the latter of which will expand the lattice [Wang *et al.* 2002].

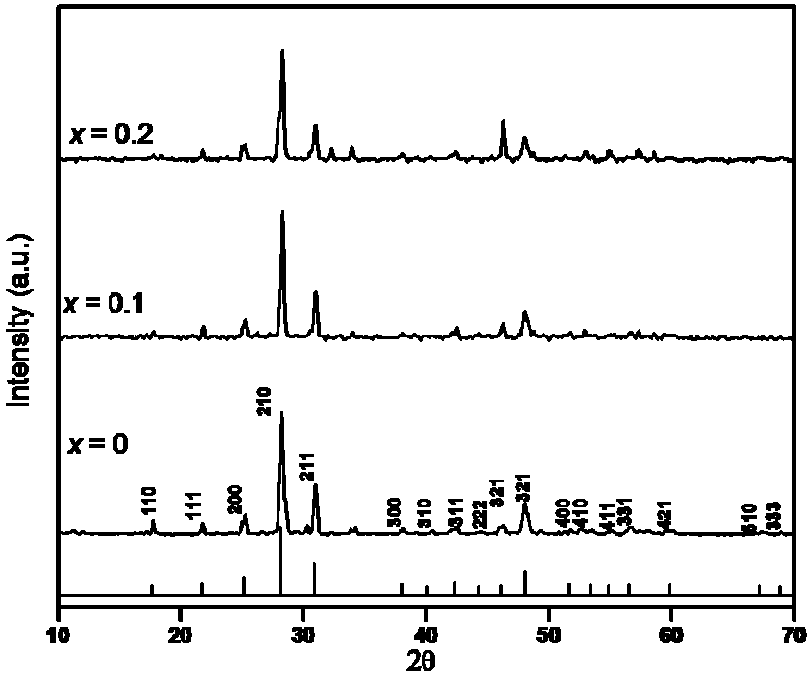

Fig. 2. XRD patterns of the $Pr_{2-x}Ca_xMo_2O_{9-\delta}$ (x= 0, 0.1 and 0.2) samples (Calcination temperature: 1050°C; Time duration 9 h).

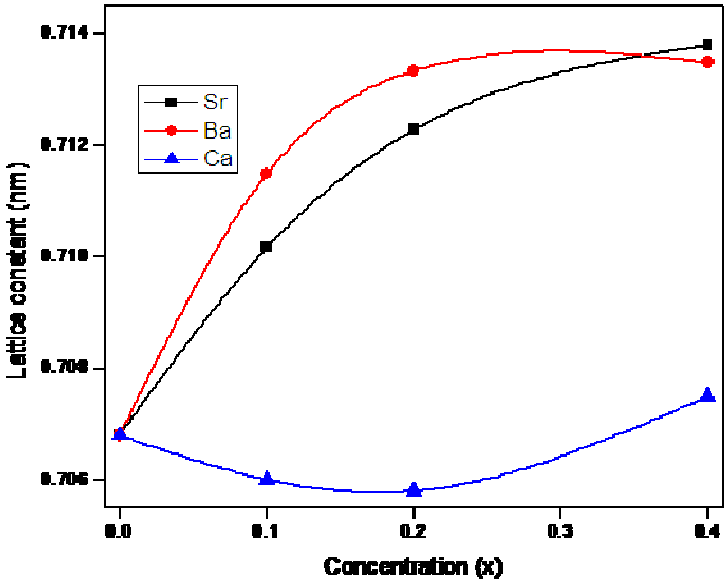

Fig. 3. Lattice constants of the $Pr_{2-x}A_xMo_2O_{9-\delta}$ (A = Ca^{2+}, Sr^{2+} and Ba^{2+}) pigment samples.

With the increase of Ca^{2+}-doping in $Pr_{2-x}Ca_xMo_2O_{9-\delta}$ (x = 0.4–1.0) beyond 10%, structural transformation from cubic to monoclinic fergusonite-type (JCPDS No. 22-1180) has been noticed from the XRD patterns of the pigment samples given in Fig. 4 [Tkachenko and Fedorov 2003]. Further, some minor peaks appeared in the XRD patterns when the Ca^{2+} concentration is greater than 10% can be indexed to $CaMoO_4$ with tetragonal phase as reported elsewhere [Subasri *et al.* 2004; Marrero-Lopez *et al.* 2007].

The XRD patterns of Sr^{2+} and Ba^{2+}-doped into $Pr_2Mo_2O_9$ samples are summarized in Figs. 5 and 6. With the increase of Sr^{2+} or Ba^{2+}-dopant concentration in $Pr_{2-x}A_xMo_2O_{9-\delta}$ (A= Sr^{2+} or Ba^{2+}; x > 0.1) beyond 2.5%, structural transformation from cubic to monoclinic fergusonite-type (JCPDS No. 22-1180) has been observed from the XRD patterns of the pigment samples [Tkachenko and Fedorov 2003]. It is also evident that there are some additional diffraction peaks (indicated with stars) for the compositions with x > 0.1 for Sr^{2+} and Ba^{2+}-doped systems. The extra peaks above the solubility limit are attributed to the presence of a secondary phase ($SrMoO_4$: JCPDF No. 8-482; or $BaMoO_4$: JCPDF No. 29-193) with tetragonal phase as noted earlier by many investigators [Subasri

et al. 2004; Marrero-Lopez *et al.* 2007]. The variation of lattice constant with the dopant concentration is presented in Fig. 3. For Sr^{2+} and Ba^{2+} substitution in $Pr_2Mo_2O_9$, the cell parameter increases with the dopant content in agreement with the large ionic radii of these cations (Sr^{2+} = 0.131 nm and Ba^{2+} = 0.147 nm) compared to Pr^{3+}. Since Sr^{2+} and Ba^{2+} are also aliovalent dopant ions like Ca^{2+}, substitution by these ions in Pr^{3+} sites also leads to formation of oxygen vacancies. As both Sr^{2+} and Ba^{2+} are larger than Pr^{3+}, they partially occupy the space created by the neighboring oxygen vacancies and can still stabilize the structure. Similar trends in cell parameter values have been reported elsewhere for the substitution of alkaline-earth metals into $La_2Mo_2O_9$ [Gao *et al.* 2008; Yan *et al.* 2010].

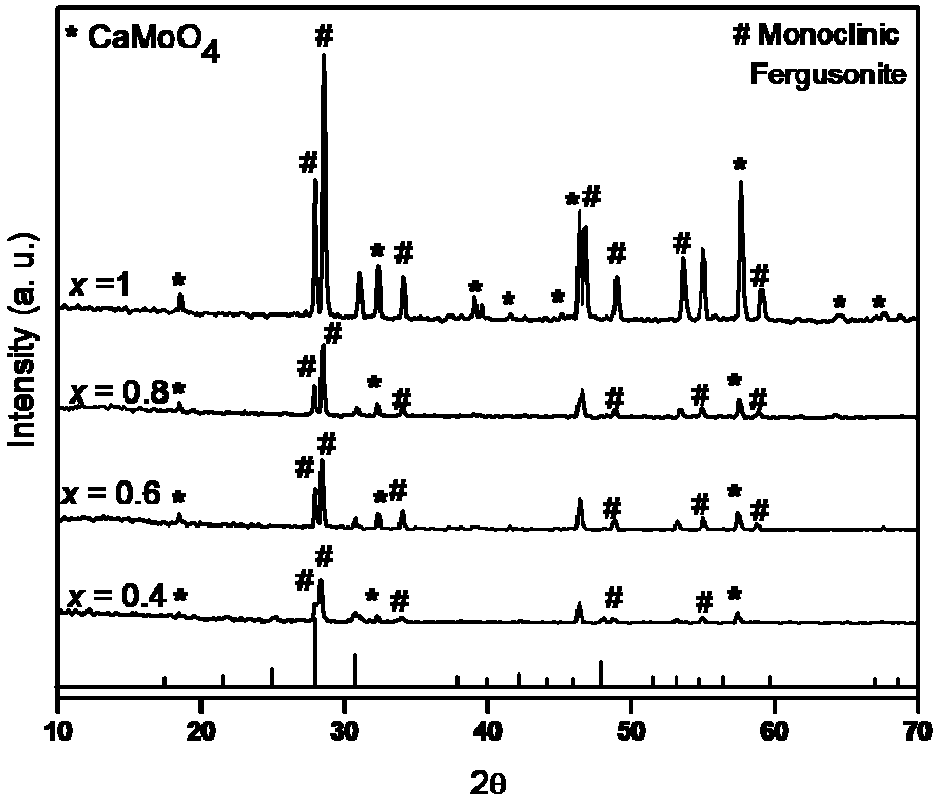

Fig. 4. XRD patterns of the $Pr_{2-x}Ca_xMo_2O_{9-\delta}$ (x = 0.4 to 1.0) samples (Calcination temperature: 1050°C; Time duration 9 h).

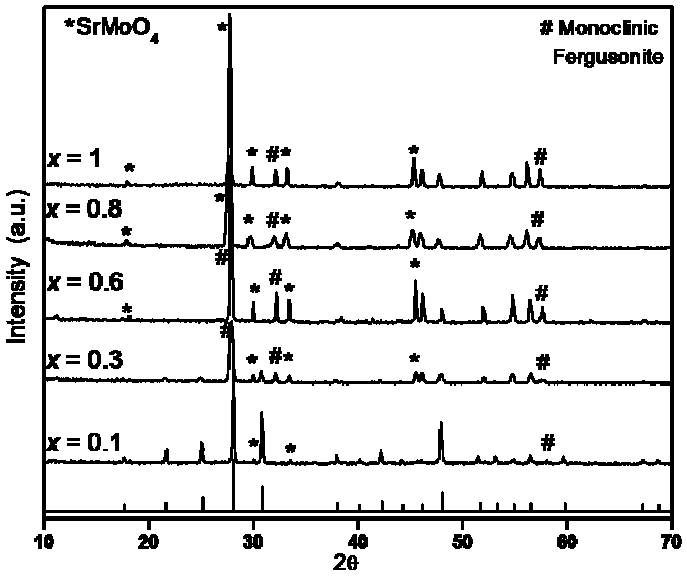

Fig. 5. XRD patterns of the $Pr_{2-x}Sr_xMo_2O_{9-\delta}$ (x = 0 to 1.0) samples (Calcination temperature: 1000°C; Time duration 9 h).

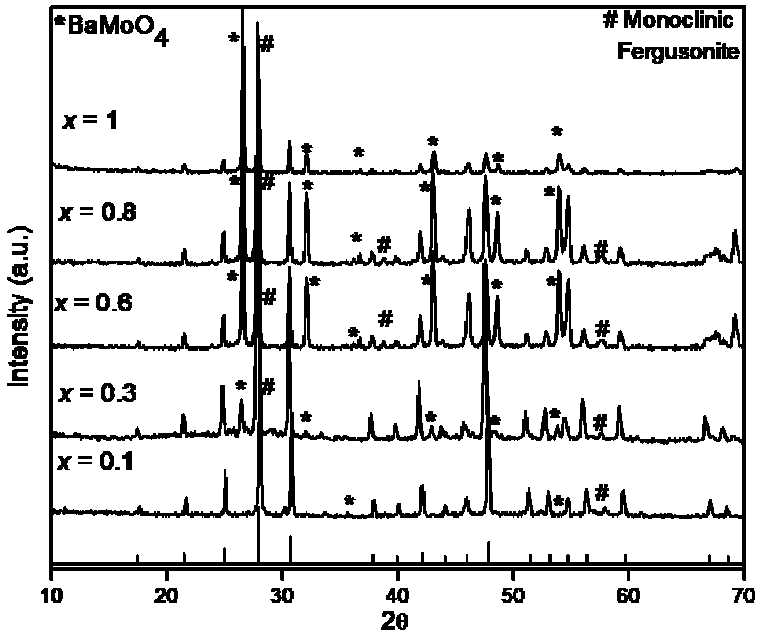

Fig. 6. XRD patterns of the $Pr_{2-x}Ba_xMo_2O_{9-\delta}$ (x = 0 to 1.0) samples (Calcination temperature: 950°C; Time duration 9 h).

4.3.2. Particle size and morphological analysis

Particle size analysis of the typical pigments, $Pr_{1.4}Ca_{0.6}Mo_2O_{9-\delta}$, $Pr_{1.4}Sr_{0.6}Mo_2O_{9-\delta}$ and $Pr_{1.4}Ba_{0.6}Mo_2O_{9-\delta}$ reveal a mean diameter of 28.46 μm (size of 90% particles < 54.56 μm,

50% particles < 22.43 μm and 10% particles < 0.37 μm), 27.63 μm (size of 90% particles < 61.34 μm, 50% particles < 20.50 μm and 10% particles < 7.12 μm) and 29.41 μm (size of 90% particles < 63.78 μm, 50% particles < 19.19 μm and 10% particles < 11.32 μm), respectively. The homogeneous nature of the synthesized pigment samples can be understood from the SEM images (Fig. 7) and the average grain size being less than 20 μm.

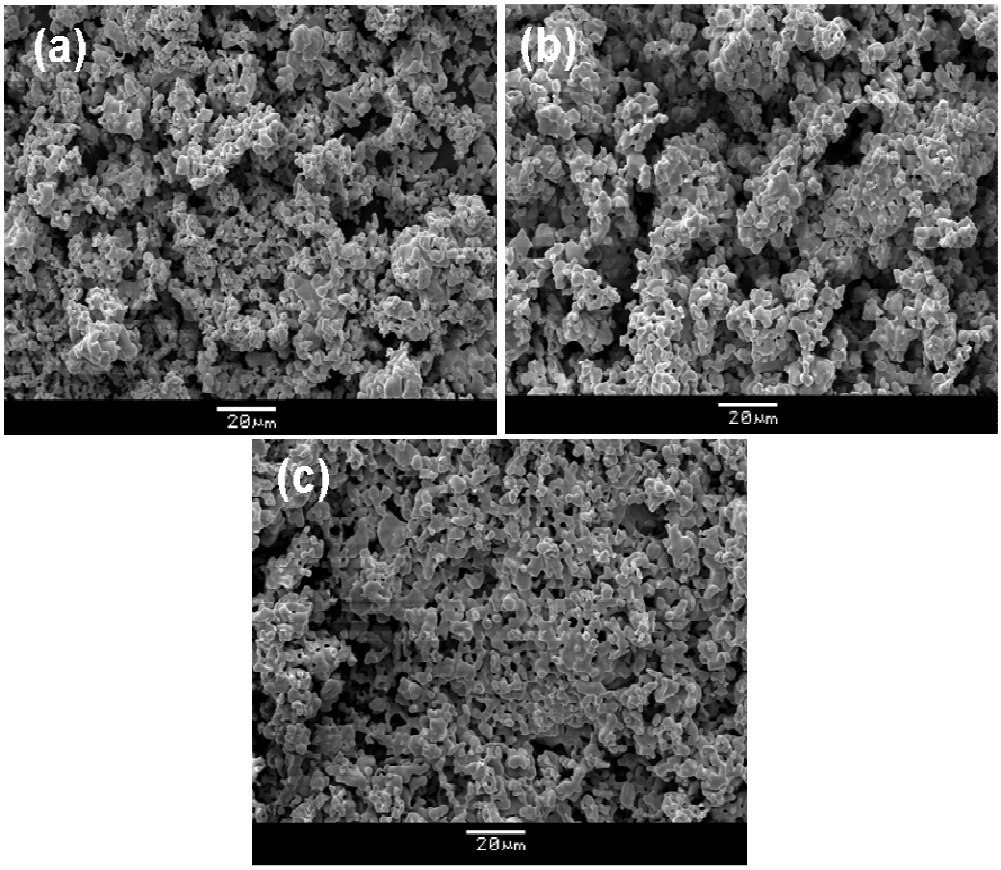

Fig. 7. The SEM micrographs of (a) $Pr_{1.4}Ca_{0.6}Mo_2O_{9-\delta}$; (b) $Pr_{1.4}Sr_{0.6}Mo_2O_{9-\delta}$; (c) $Pr_{1.4}Ba_{0.6}Mo_2O_{9-\delta}$ pigment powders.

4.3.3. The optical properties of $Pr_2Mo_2O_9$ pigment

The absorption spectrum of $Pr_2Mo_2O_9$ compound is shown in Fig 8. Several bands in the visible region have been observed, which can be assigned to the electronic transitions between $4f^2 \rightarrow 4f^1 5d^1$ states of Pr^{3+}. The bands in the region 440–490 (blue) and 590–625

nm (red), can be assigned based on the energy levels $^3H_4 \rightarrow {}^3P_2$, $^3H_4 \rightarrow {}^3P_1$, $^3H_4 \rightarrow {}^3P_0$ (upper) and $^3H_4 \rightarrow {}^1D_2$ and $^3H_6 \rightarrow {}^3P_0$ (lower), respectively [Sivakumar and Varadaraju 2005; Logvinovich *et al.* 2010]. Weak absorptions in the blue region and strong absorptions in the red region can be noted from the absorption spectrum of the alkaline-earth metal free $Pr_2Mo_2O_9$. Thus, the pigment exhibits green color, since red is complementary color to green (Fig. 15).

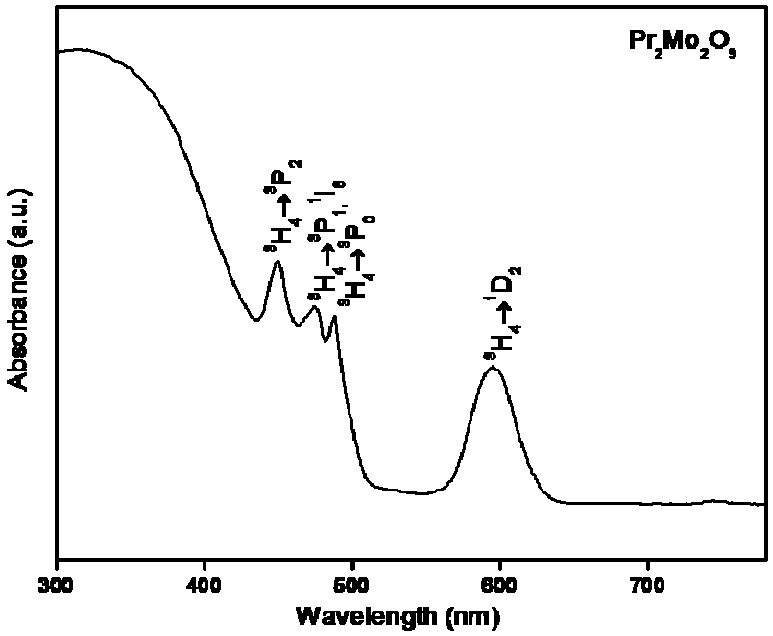

Fig. 8. Absorption spectra of $Pr_2Mo_2O_9$ pigment.

4.3.4. The optical properties of alkaline-earth metal doped $Pr_2Mo_2O_9$ pigments

The effect of alkaline-earth metal ions (Ca^{2+}, Sr^{2+} and Ba^{2+}) doping on the optical properties of $Pr_2Mo_2O_9$ based pigments was analyzed from the diffuse reflectance and absorption spectra and the results are displayed in Figs. 9 to 14, respectively. With the progressive doping of Ca^{2+} or Sr^{2+} into the matrix of $Pr_2Mo_2O_9$, strong absorptions in the blue region can be noticed with simultaneous weakening of the absorptions in the red region. The doping of Ca^{2+} or Sr^{2+} for Pr^{3+} in $Pr_2Mo_2O_9$ creates oxygen vacancies, which in turn may impart strong optical absorptions at a wavelength below 500 nm. Thus, the color of the pigment gently changes from green to greenish-yellow with increasing Ca^{2+} or

Sr^{2+} concentration, since blue is complementary color to yellow (Fig. 15). The systematic doping of Ca^{2+} for Pr^{3+} in $Pr_2Mo_2O_9$ matrix decreases the band gap of the resultant pigments significantly from 2.44 eV to 2.24 eV. However, in the case of Sr^{2+}-doped systems, the band gap of the pigments gently changes from 2.44 eV to 2.35 eV as compared to Ca^{2+}-doped systems.

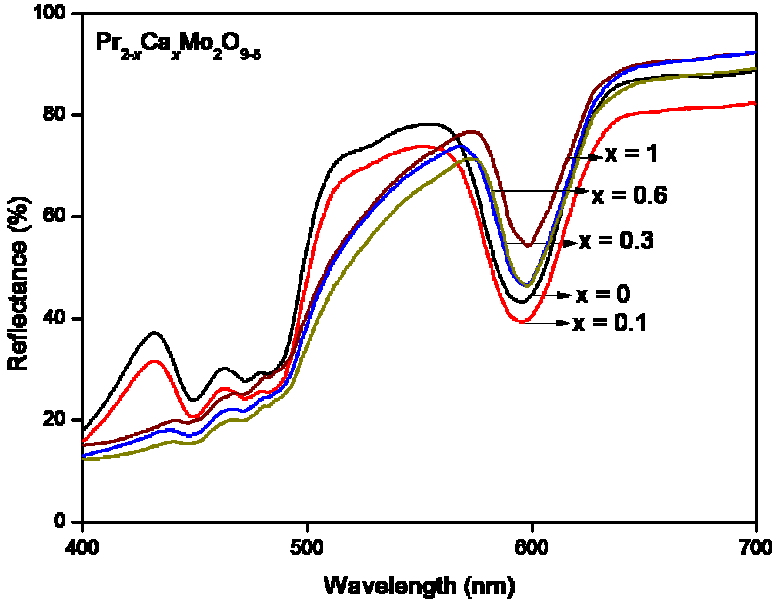

Fig. 9. Reflectance spectra of the $Pr_{2-x}Ca_xMo_2O_{9-\delta}$ (x = 0 to 1.0) samples.

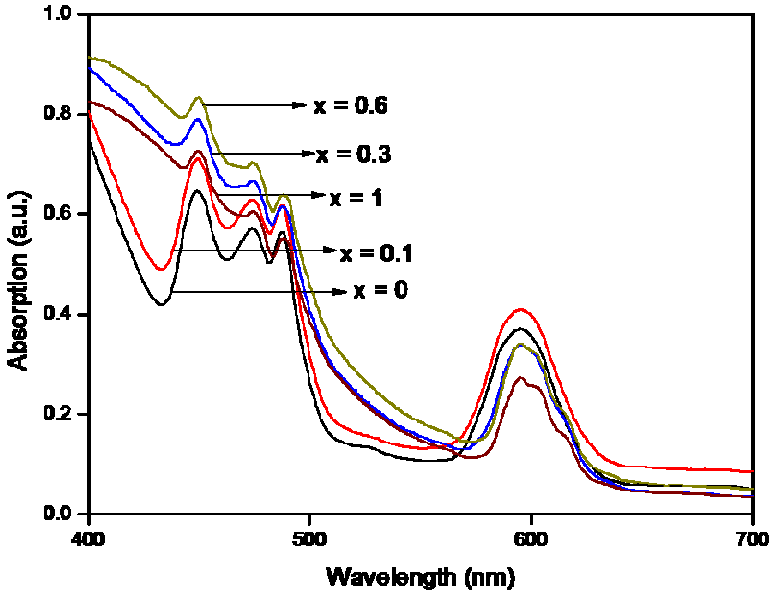

Fig. 10. Absorption spectra of the $Pr_{2-x}Ca_xMo_2O_{9-\delta}$ (x = 0 to 1.0) samples.

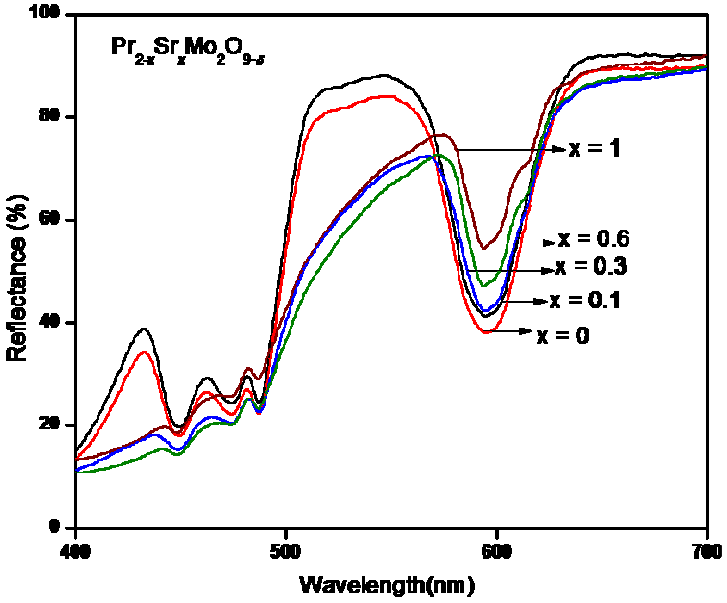

Fig. 11. Reflectance spectra of the $Pr_{2-x}Sr_xMo_2O_{9-\delta}$ (x = 0 to 1.0) samples.

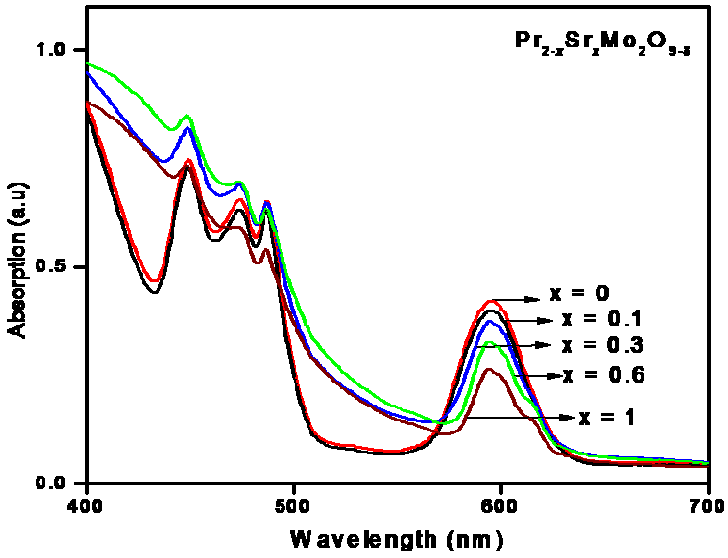

Fig.12. Absorption spectra of the $Pr_{2-x}Sr_xMo_2O_{9-\delta}$ (x = 0 to 1.0) samples.

It is evident from the UV–vis diffuse reflectance spectra of the Ba^{2+}-doped $Pr_2Mo_2O_9$ pigment samples shown in Fig.14 that the increase of dopant concentration results in the simultaneous weakening of absorptions in both blue and red regions, which is contrary to Ca^{2+} or Sr^{2+}-doped systems. Thus minor variations in the band gap of the resultant pigment samples is noticed (2.44 eV to 2.40 eV) and consequently, no significant change in the color of the Ba^{2+}-doped pigment samples has been observed.

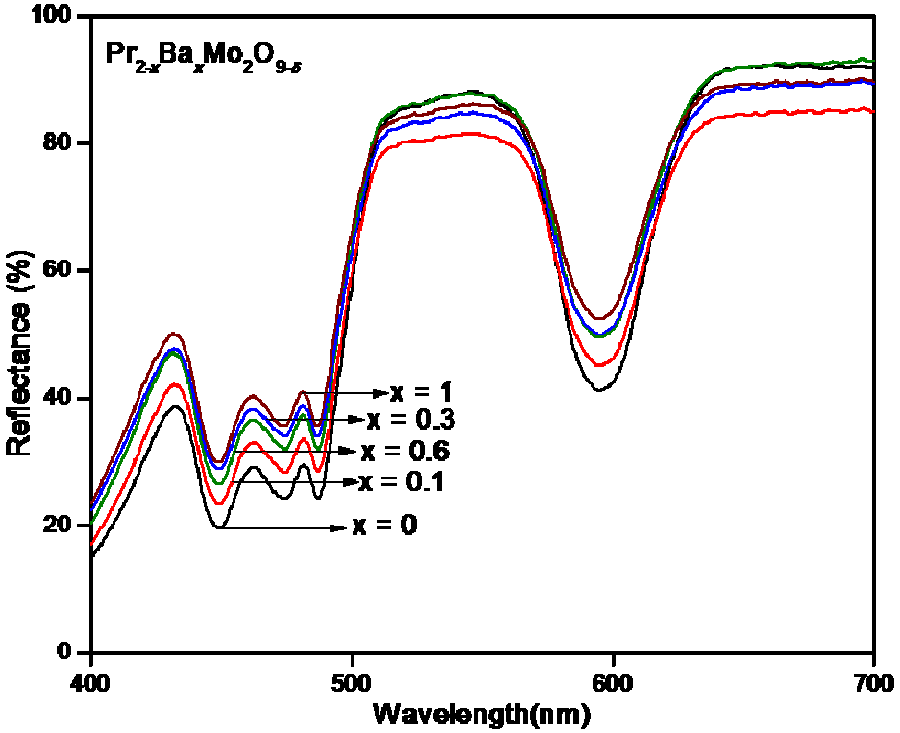

Fig. 13. Reflectance spectra of the $Pr_{2-x}Ba_xMo_2O_{9-\delta}$ (x = 0 to 1.0) samples.

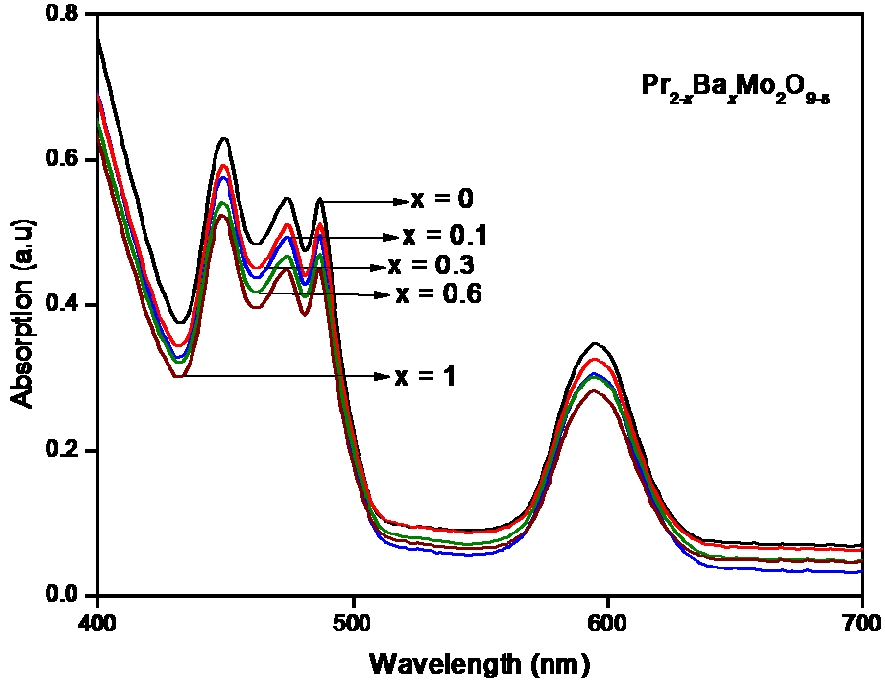

Fig. 14. Absorption spectra of the $Pr_{2-x}Ba_xMo_2O_{9-\delta}$ (x = 0 to 1.0) samples.

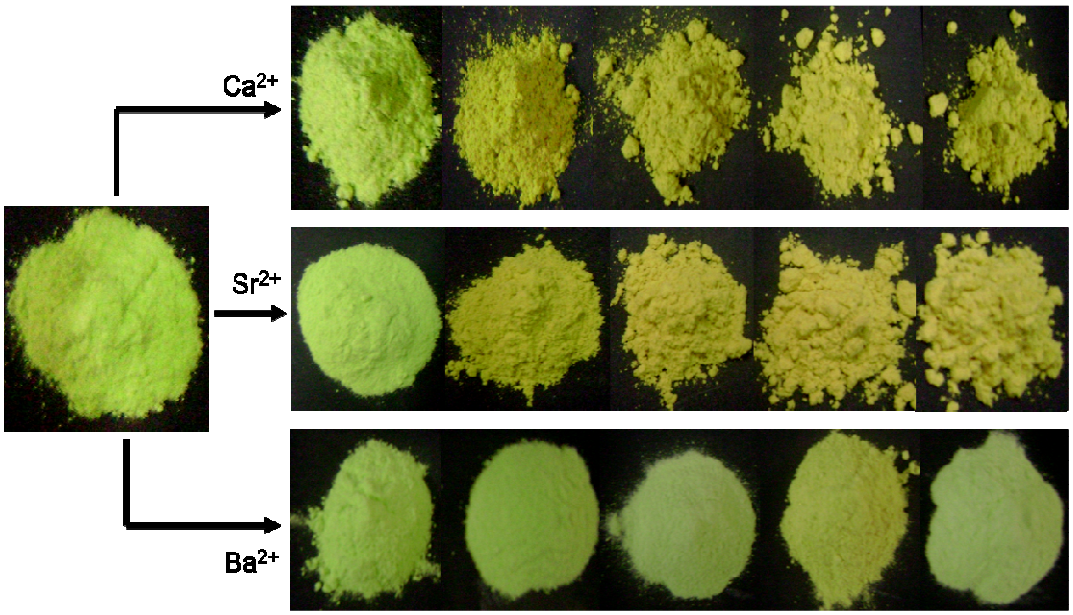

Fig. 15. Photograph of the $Pr_{2-x}A_xMo_2O_{9-\delta}$ (x = 0 to 1.0) pigment powders.

The CIE 1976 color coordinates of the alkaline-earth metal doped $Pr_2Mo_2O_9$ pigments are summarized in Table 1. The increase of b^* and C^* values and decrease of $-a^*$ with the increase of dopant concentration of Ca^{2+} or Sr^{2+} from x = 0 to 0.6 in $Pr_{2-x}A_xMo_2O_{9-\delta}$, clearly indicates that color of the pigment gently changes from green to greenish-yellow. Further, at higher Ca^{2+} or Sr^{2+} concentrations, the yellow hue of the pigment decreases may be due to the formation of dominant phase of $CaMoO_4$ or $SrMoO_4$. In the case of Ba^{2+}-doped pigments, the b^* value which represents the yellowness of the pigment decreases with increasing the dopant concentration. This may be due to the formation of more stable $BaMoO_4$ phase even at smaller dopant amounts of Ba^{2+} as compared to Ca^{2+} or Sr^{2+}. On the other hand, the change in the $-a^*$ value, which represents the green hue of the pigment is not significant. Thus the green color of the $Pr_2Mo_2O_9$ resultant pigment has not been affected with the doping of Ba^{2+}. The observed hue angle of the designed pigments are found to be in the greenish-yellow region of the cylindrical color space ($h°$ = 70–105 for yellow, $h°$ = 105–140 for green). The color coordinates of the typical Ca^{2+}-doped

pigment, $Pr_{1.4}Ca_{0.6}Mo_2O_{9-\delta}$ (L^* = 81.53, a^* = −9.01, b^* = 59.95), especially yellow hue was found to be higher than that of the commercially available pigment (L^* = 89.93, a^* = −3.49, b^* = 43.34) Zircon Yellow (Zircon 1561: (Zr, Pr)SiO_4 of M/s Kawamura Chemicals, Japan).

Table 1. The color coordinates (±0.1) of the $Pr_{2-x}A_xMo_2O_{9-\delta}$ (x ranges from 0 to 1.0) powder pigments and band gap values.

$Pr_{2-x}M_xMo_2O_{9-\delta}$ (M= Ca^{2+}, Sr^{2+}, Ba^{2+})		Color coordinates			C^*	h^o	*Band gap*
		L^*	a^*	b^*			*(eV)*
	x = 0	87.8	−21.6	37.3	43.1	107.6	2.44
Ca^{2+}	x = 0.1	87.5	−22.8	39.6	45.6	118.4	2.43
	x = 0.3	86.3	−15.6	56.4	56.4	96.6	2.28
	x = 0.6	81.5	−9.0	59.9	60.6	99.8	2.24
	x = 0.8	79.2	−6.7	52.0	52.3	98.2	2.25
	x = 1	83.3	−7.6	54.2	54.8	98.7	2.23
Sr^{2+}	x = 0.1	84.2	−23.5	45.5	51.2	117.3	2.43
	x = 0.3	80.8	−11.7	51.9	53.2	102.7	2.39
	x = 0.6	83.1	−7.6	54.7	55.2	97.9	2.35
	x = 0.8	82.6	−7.0	52.4	52.9	97.6	2.36
	x = 1	83.9	−7.1	49.9	50.4	98.1	2.38
Ba^{2+}	x = 0.1	84.1	−25.5	46.1	52.7	119.0	2.43
	x = 0.3	85.8	−22.7	42.6	48.3	118.1	2.43
	x = 0.6	89.4	−21.6	40.5	45.9	118.1	2.42
	x = 0.8	83.7	−12.5	43.5	45.3	106.1	2.40
	x = 1	85.1	−19.6	36.0	41.0	118.6	2.44

$C^* = [(a^*)^2 + (b^*)^2]^{1/2}$; $h^o = \tan^{-1}(b^*/a^*)$

4.3.5. Thermal and chemical stability studies of the pigments

The thermal analysis (TG/DTA) of the typical pigment powder $Pr_2Mo_2O_9$ has been investigated and the results are given in Fig. 16. It is clear from the TG/DTA analysis of

the solid solution $Pr_2Mo_2O_9$, that there is no loss in weight and no phase transformation in the temperature range of 50–1000°C. This fact is in agreement with the results shown in XRD patterns in Fig. 1.

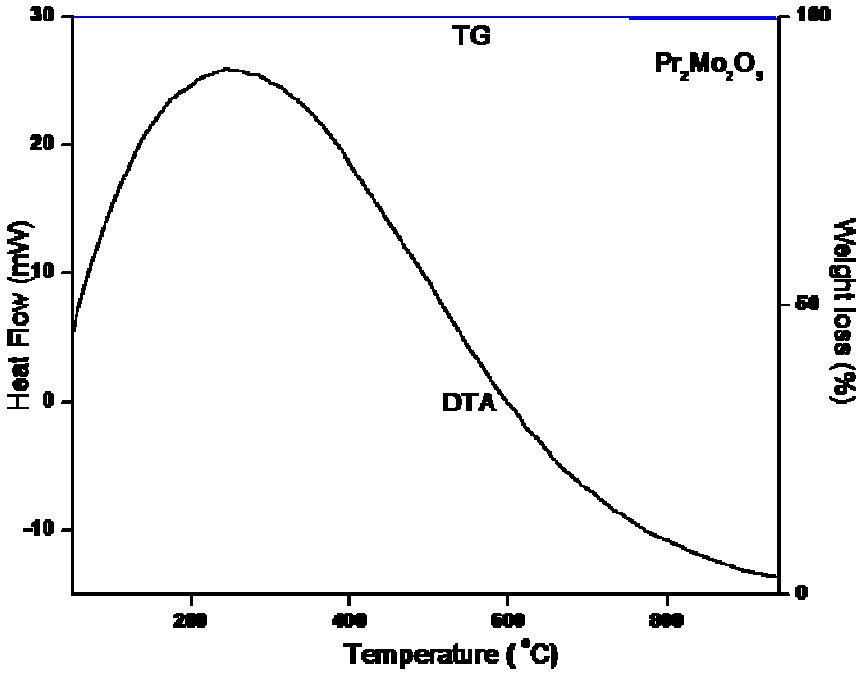

Fig. 16. TG/DTA of powdered $Pr_2Mo_2O_9$ pigment.

The acid/alkali and water resistance of the typical pigment powders $Pr_{1.4}Ca_{0.6}Mo_2O_{9-\delta}$ and $Pr_{1.4}Sr_{0.6}Mo_2O_{9-\delta}$ were investigated with 5% of $HCl/H_2SO_4/HNO_3/NaOH$ and H_2O. A pre-weighed amount of the pigment powder was treated with acid/alkali and soaked for half an hour with constant stirring using a magnetic stirrer. The pigment powder was then filtered, washed with water, dried and weighed. Negligible weight loss of pigment was noticed for all the acids, alkali and water tested. The color coordinates of the pigments were measured after acid/alkali and water treatment and the total color difference, ΔE_{ab} of the pigments are found to be negligible as evident from the data reported in Table 2. The above studies highlight that the pigment powders are chemically and thermally stable.

Table 2. The color coordinates (±0.1) of the $Pr_{1.4}A_{0.6}Mo_2O_{9-\delta}$ (A= Sr and Ba) powder pigments after acid/alkali resistance tests.

	$Pr_{1.4}Ca_{0.6}Mo_2O_{9-\delta}$				$Pr_{1.4}Sr_{0.6}Mo_2O_{9-\delta}$			
Acid/ Alkali	*L**	*a**	*b**	[a] ΔE_{ab}	*L**	*a**	*b**	ΔE_{ab}
H_2O	81.2	–8.9	59.5	0.5	83.5	–7.8	54.9	0.5
NaOH	80.9	–10.1	58.9	1.6	84.2	–6.8	54.3	1.3
HCl	81.9	–9.4	58.8	1.2	84.1	–7.2	53.8	1.4
HNO_3	81.8	–9.6	58.7	1.4	82.6	–7.7	55.6	1.0
H_2SO_4	82.6	–9.9	59.7	1.3	84.2	–6.9	54.4	1.2

[a] $\Delta E_{ab} = [(\Delta L^*)^2+(\Delta a^*)^2+(\Delta b^*)^2]^{1/2}$

4.3.6. Applications in coloring of plastics

The coloring performance of the typically synthesized pigments ($Pr_{1.9}Ca_{0.1}Mo_2O_{9-\delta}$ and $Pr_{1.4}Ca_{0.6}Mo_2O_{9-\delta}$) was tested for its coloring application in a substrate material like PMMA. Typically, 10wt.% pigment sample was dispersed in PMMA and compressed to a cylindrical disc (Fig. 17). The color coordinates of the test pieces were measured at different locations and an average value is depicted in Table 3. The *L*a*b** values obtained were more or less the same indicating the uniform distribution of pigment particles in the polymer matrix. The TG analysis of the pigmented polymer sample indicates that the colored polymer is thermally stable up to 236^{o}C (Fig. 18).

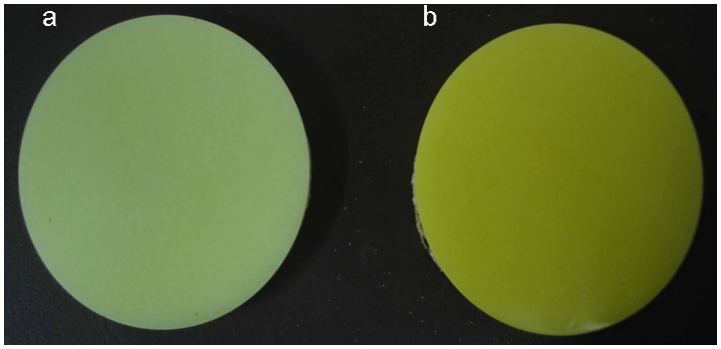

Fig. 17. Photograph of (a) $Pr_{1.9}Ca_{0.1}Mo_2O_{9-\delta}$(10%) + PMMA and (b) $Pr_{1.4}Ca_{0.6}Mo_2O_{9-\delta}$(10%) + PMMA.

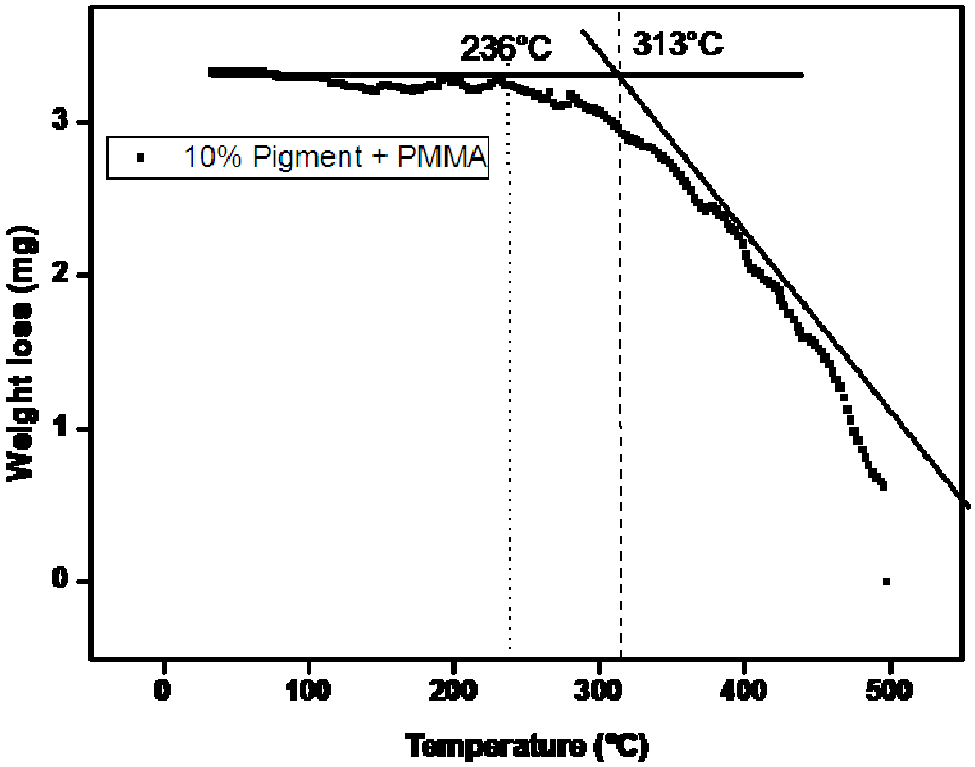

Fig. 18. TG of 10% $Pr_{1.9}Ca_{0.1}Mo_2O_{9-\delta}$+ PMMA.

Table 3. The color coordinates (±0.1) of the $Pr_{1.6}Ca_{0.4}Mo_2O_{9-\delta}$ powder pigments after applied on polymer.

Composition	Color coordinates		
	*L**	*a**	*b**
$Pr_{1.9}Ca_{0.1}Mo_2O_{9-\delta}$	87.5	–22.8	39.6
x = 0.1 (10%)+PMMA	79.08	–13.9	35.5
$Pr_{1.6}Ca_{0.4}Mo_2O_{9-\delta}$	81.5	–9.0	59.9
x= 0.6 (10%)+PMMA	75.0	–5.52	61.05

4.4. Conclusions

- The effect of alkaline-earth metal ions doping on the optical properties of $Pr_2Mo_2O_9$ based pigment powder was systematically investigated.
- The results demonstrated that the progressive doping of Ca^{2+} for Pr^{3+} in $Pr_2Mo_2O_9$ matrix, having smaller ionic radii than Pr^{3+}; impart strong optical absorptions in the blue region with simultaneous weakening of the absorptions in the red region. Thus, the color of the pigment powder changes from green to greenish-yellow with increasing Ca^{2+} concentration, since blue is a complementary color to yellow.
- On the other hand, the doping of Sr^{2+} for Pr^{3+}, having an ionic radii moderately higher than Pr^{3+}, impart weak absorptions in the blue region as compared to Ca^{2+} system, with simultaneous decreasing of absorptions in the red region. Consequently, the color of the pigment powder gently changes from green to greenish-yellow.
- However, contrary to the above observations, the doping of Ba^{2+} for Pr^{3+}, having higher ionic radii than Pr^{3+}, no significant changes in the absorption bands in both blue and red regions are noted and hence no change in the color of the $Pr_2Mo_2O_9$ pigment powder.
- The newly developed pigment powders are found to be thermally and chemically stable and also do not contain toxic metals. Thus, the present pigment powders may find potential alternative to the classical toxic yellow inorganic pigments for coloring plastics.

References

Aby, C. P.; Sreeram, K. J.; Nair, B. U.; Ramasami, T. "Doped oxides of cerium as inorganic colorants", *Color. Technol.,* 123, **2007**, 374.

Akbari, H.; Levinson, R.; Miller, W.; Berdahl, P. "Cool colored roofs to save energy and improve air quality", Santorini, Greece, *Proc. International Conf. on Passive and Low Energy Cooling for the Built Environment*, **2005**, p.89.

Ardit, M.; Dondi, M.; Cruciani, G.; Matteucci, F. "Ti–Ca–Al-doped $YCrO_3$ pigments: XRD and UV–vis investigation", *Mater. Res. Bull.,* 44, **2009**, 666.

Arvela, P. "Toxicity of rare earths", *Progress in Pharmacology,* 2, **1979**, 69.

Aruna, S. T.; Ghosh, S.; Patil, K. C. "Combustion synthesis and properties of $Ce_{1-x}Pr_xO_{2-\delta}$ red ceramic pigments", *Int. J. Inorg. Mater.,* 3, **2001**, 387.

Baidya, T.; Gayen, A.; Hegde, M. S.; Ravishankar, N.; Dupont, L. "Enhanced reducibility of $Ce_{1-x}Ti_xO_2$ compared to that of CeO_2 and higher redox catalytic activity of $Ce_{1-x-y}Ti_xPt_yO_{2-\delta}$ compared to that of $Ce_{1-x}Pt_xO_{2-\delta}$", *J. Phys. Chem. B,* 110, **2006**, 5262.

Badenes, J. A.; Vicent, J. B.; Llusar, M.; Tena, M. A.; Monros, G. "The nature of Pr-$ZrSiO_4$ yellow ceramic pigment", *J. Mater. Sci*., 37, **2002**, 1413.

Barnett, J. R.; Miller, S.; Pearce, E. "Colour and art: A brief history of pigments", *Opt. Laser Technol.,* 38, **2006**, 445.

Becerro, A. I.; Escudero. "Revision of the crystallographic data of polymorphic $Y_2Si_2O_7$ and Y_2SiO_5 compounds", *Phase transitions*, 77, **2004**, 1093.

Bendiganavale, A. K.; Malshe, V. C. "Infrared Reflective Inorganic Pigments", *Recent Patents in Chem. Eng.,* 1, **2008**, 67.

Berke, H. "The invention of blue and purple pigments in ancient times", *Chem. Soc. Rev*., 36, **2006**, 15.

Biswas, S. K.; Dhak, D.; Pathak, A.; Pramanik, P. "Chemical synthesis of environment-friendly nanosized yellow titanate pigments", *Mater. Res. Bull.,*43, **2008**, 665.

Bittler, K.; Ostertag, W. "Developments in the Field of Inorganic Pigments", *Angew. Chem. Int. Ed. Engl.*, 19, **1980**, 190.

Blonski, R. P. "Stable heavy metal free zircon pigments for use in plastics and paints and method for coloring thereof", *U.S. Patent No.* 5,316,570, **1994**.

Bondioli, F.; Ferrari, A. M.; Leonelli, C.; Manfredini, T. "Synthesis of Fe_2O_3/silica red inorganic inclusion pigments for ceramic applications", *Mater. Res. Bull.,* 33, **1998**, 723.

Bondioli, F.; Corradi, A. B; Manfredini, T.; Leonelli, C.; Bertoncello, R. "Nonconventional Synthesis of Praseodymium-Doped Ceria by Flux Method*", Chem. Mater.,* 12, **2000**, 324.

Bondioli, F.; Ferrari, A. M.; Leonelli, C.; Siligardi, C.; Hart, N. A.; Evans, N. G. "The application of microwaves in the synthesis of $Ce_{0.9}Pr_{0.1}O_2$ nanostructured powders", *J. Mater. Chem*., 11, **2001**, 2620.

Bondioli, F.; Ferrari, A. M.; Lusvarghi, L.; Manfredini, T.; Nannarone, S.; Pasquali, L.; Selvaggi, G. "Synthesis and characterization of praseodymium-doped ceria powders by a microwave-assisted hydrothermal (MH) route", *J. Mater. Chem.,* 15, **2005**, 1061.

Busnot, S.; Macaudiere, P. "Composition based on samarium sesquisulfide, preparation and method and use as coloring pigment", *U.S. Patent No.* 6,641,735, **2002**.

Buxbaum, G.; Pfaff, G. "Industrial Inorganic Pigments", 3rd Edition, Wiley-VCH, Weinheim, **2005**.

CIE (Commission Internationale de l'Eclairage). Colorimetry – Technical Report. CIE Pub. No. 15, Second Edition (Vienna: CIE Central Bureau CIE, **1986**).

CIE (Commission Internationale de l'Eclairage). Colorimetry – Technical Report. CIE, Third Edition (Vienna: CIE Central Bureau CIE, **2004**).

Chevire, F.; Munoz, F.; Baker, C. F.; Tessier, F.; Larcher, O.; Boujday, S.; Colbeau-Justin, C.; Marchand, R. "UV absorption properties of ceria-modified compositions within the fluorite-type solid solution CeO_2–Y_6WO_{12}", *J. Solid State Chem.,* 179, **2006**, 3184.

Chevire, F.; Clabau, F.; Larcher, O.; Orhan, E.; Tessier, F.; Marchand, R. "Tunability of the optical properties in the $Y_6(W,Mo)(O,N)_{12}$ system", *Solid State Sci.*, 11, **2009**, 533.

Chopin, T.; Dupuis, D. "Rare earth metal sulfide pigment compositions", *U.S. Patent No.* 5,401,309; **1995**.

Chopin, T.; Macaudiere, P. "Inorganic rare earth pigments/colorants and synthesis/applications thereof", *U.S. Patent No.* 6,284,033; **2001**.

Cornell, R. M.; Schwertmann, U. "The Iron Oxides; Structure, Properties, Reactions, Occurrence and Uses", VCH, **1996**.

Del Nero, G.; Cappelletti, G.; Ardizzone, S.; Fermo, P.; Gilardoni, S. "Yellow Pr-zircon pigments: The role of praseodymium and of the mineralizer", *J. Eur. Ceram. Soc.,* 24, **2004**, 3603.

Dohnalova, Z.; Sulcova, P.; Trojan, M. "Synthesis and characterization of $LnFeO_3$ Pigments", *J. Therm. Anal. Calorim.,* 91, **2008**, 559.

Eppler, R. A. Ullmann's encyclopedia of industry, Vol. A5. Weinheim, Germany: VCH; **1998.**

Fournier, J. P.; Fournier, J.; Kohlmuller, R. "Etude des systemes La_2O_3-MoO_3, Y_2O_3-MoO_3, et des phases Ln_6MoO_{12}", *Bull. Soc. Chim. Fr.,* 12, **1970**, 4277.

Furukawa, S.; Masui, T.; Imanaka, N. "Synthesis of new environment-friendly yellow pigments", *J. Alloys Compd.,* 418, **2006**, 255.

Furukawa, S.; Masui, T.; Imanaka, N. "New environment-friendly yellow pigments based on CeO_2–ZrO_2 solid solutions", *J. Alloys Compd.,* 451, **2008**, 640.

Garcia, A.; Llusar, M.; Calbo, J.; Tena, M. A.; Monros, G. "Low-toxicity red ceramic pigments for porcelainised stoneware from lanthanide-cerianite solid solutions", *Green Chem.,* 3, **2001**, 238.

Gao, X.; He, T.; Shen, Y. "Structures, electrical and thermal expansion properties of Sr-doped $La_2Mo_2O_9$ oxide-ion conductors", *J. Alloys Compd.,* 464, **2008**, 461.

Garrote, E. U.; Martínez, F. .; Landa-Cánovas, A. R.; Otero-Díaz, L. C. "New inorganic pigments in the Ca–Nd–S system: Stabilization of γ phase", *J. Alloys Compd.,* 418, **2006**, 86.

Gauthier, G.; Jobic, S.; Evain, M.; Koo, H-J.; Whangbo, M-H.; Fouassier, C.; Brec, R. "Syntheses, Structures, and Optical Properties of Yellow Ce_2SiS_5, $Ce_6Si_4S_{17}$, and $Ce_4Si_3S_{12}$ Materials", *Chem. Mater.,* 15, **2003***,* 828.

George, H. C.; Ming-Ling, L.; Li-Dong, C.; Fu-Qiang, H.; Daniel, E.B.; Daniel, M. W.; John, R. I.; Mark, C. H.; Richard, P. V.; James, A. I. "Syntheses, crystal structures, and physical properties of $La_5Cu_6O_4S_7$ and $La_5Cu_{6.33}O_4S_7$", *Inorg. Chem.,* 47, **2008**, 4368.

Gupta, K. K.; Nishkam, A.; Kasturiya, N. "Camouflage in the non-visible region", *J. Ind. Tex.,* 31, **2001**, 27.

Haley, T. J. “Pharmacology and toxicity of the rare earth elements”, *J. Phar. Sci.,* 54, **1965**, 663.

Hill, K; Lehman, R. “Effects of selected processing variables on color formation in Praseodymium doped Zircon pigments”, *J. Am. Ceram. Soc,* 83, **2000**, 2177.

Hoefdraad, H. E. “Charge-transfer spectra of tetravalent lanthanide ions in oxides”, *J. Inorg. Nucl. Chem.*, 37, **1975**, 1917.

Huguenin, D.; Pettini, F.; Seguelong, T. “Yellow/orange pigments comprising zirconium oxide and cerium, praseodymium and/or terbium values”, *U.S. Patent* 5,560,772, **1996**.

Imanaka, N.; Masui, T.; Itaya, M. “Synthesis of an Environmentally Friendly and Nontoxic New Pigment Based on Rare Earth Phosphate”, *Chem. Lett.,* 32, **2003**, 400.

Jansen, M.; Letschert, H. P. “Inorganic yellow-red pigments without toxic metals”, *Nature*, 404, **2000**, 980.

Jansen, M.; Letschert, H. P. “Oxonitrides of the formula $LNTAON_2$ with enhanced brightness and a process for their use”, *U.S. Patent No*. 5,693,102; **1997**.

Jeevanandam, P.; Mulukutla, R. S.; Phillips, M.; Chaudhuri, S.; Erickson, L. E.; Klabunde, K. J. “Near Infrared Reflectance Properties of Metal Oxide Nanoparticles”, *J. Phys.Chem. C,* 111, **2007**, 1912.

Jorgensen, C. K.; Rittershaus, E. “Powder-Diagram and Spectroscopic Studies of Mixed Oxides of Lanthanides and Quadrivalents Metals,” *K. Dan. Vidensk. Selsk., Mat.-Fys. Medd.*, 35, **1967**, 1.

Kar, J. K.; Stevens, R.; Bowen, C. R. “Novel terbium-zircon yellow pigment”, *J. Mater. Sci.*, 39, **2004**, 5755.

Kar, J. K.; Stevens, R.; Bowen, C. R. "Effect of cerium oxide on colour hue of praseodymium-zircon yellow pigment", *Adv. Appl. Ceram.,* 106, **2007**, 175.

Koelling, D. D.; Boring, A. M.; Wood, J. H. "The electronic structure of CeO_2 and PrO_2", *Solid State Commun.,* 47, **1983**, 227.

Kumari, L. S.; George, G.; Rao, P. P.; Reddy, M. L. P. "The synthesis and characterization of environmentally benign praseodymium-doped $TiCeO_4$ pigments", *Dyes Pigm.,* 77, **2008**, 427.

Kumari, L. S.; Rao, P. P.; Koshy, P. "Red Pigments Based on CeO_2–MO_2–Pr_6O_{11} (M = Zr and Sn): Solid Solutions for the Coloration of Plastics", *J. Am. Ceram. Soc*., 93, **2010**, 1402.

Lacorre, P.; Goutenoire, F.; Bohnke, O.; Retoux, R.; Laligant, Y. "Designing fast oxide-ion conductors based on $La_2Mo_2O_9$", *Nature*, 404, **2000**, 856.

Levinson, R.; Berdahl, P.; Akbari, H. "Solar spectral optical properties of pigments–Part II: Survey of common colorants", *Sol. Energy Mater. Sol. Cells*, 89, **2005**, 351.

Levinson, R.; Berdahl, P.; Akbari, H.; Miller, W.; Joedicke, I.; Reilly, J.; Suzuki, Y.; Vondran, M. "Methods of creating solar-reflective nonwhite surfaces and their application to residential roofing materials", *Sol. Energy Mater. Sol. Cells,* 91, **2007**, 304.

Libbra, A.; Tarozzi, L.; Muscio, A.; Corticelli, M. A. "Spectral response data for development of cool coloured tile coverings", *Opt. Laser Technol.*, 43, **2011**, 394.

Linke, E. A. E.; Zwart, C. H.; Smout, A. D. "Doped zirconium mixed silicate pigment, method for the preparation thereof and products containing such pigment or a thus prepared pigment", *U.S. Patent No.* 5,275,649; **1994**.

Logvinovich, D.; Arakcheeva, A.; Pattison, P.; Eliseeva, S.; Tomes, P.; Marozau, I.; Chapuis, G. "Crystal Structure and Optical and Magnetic Properties of $Pr_2(MoO_4)_3$", *Inorg. Chem.,* 49, **2010**, 1587.

Marc, D.; Fernando, L.; Paulo, D. S. "Pigments inorganiques jaunes a base de sels de lanthanides et compositions pigmentees", *European patent No*. EP0542343;**1993**.

Martos, M.; Julian-Lopez, B.; Cordoncillo, E.; Escribano, P. "Structural and spectroscopic study of a novel erbium titanate pink pigment prepared by sol-gel methodology", *J. Phys. Chem. B,* 112, **2008**, 2319.

Martos, M.; Julian-Lopez, B.; Cordoncillo, E.; Escribano, P. "Structural and Spectroscopic Study of a New Pink Chromium-Free $Er_2(Ti,Zr)_2O_7$ Ceramic Pigment", *J. Am. Ceram. Soc*., 92, **2009**, 2987.

Marrero-Lopez, D.; Perez-Coll, D.; Ruiz-Morales, J. C.; Canales-Vazquez, J.; Martın-Sedeno, M. C.; Nunez, P. "Synthesis and transport properties in $La_{2-x}A_xMo_2O_{9-\delta}$ (A=Ca^{2+}, Sr^{2+}, Ba^{2+}, K^+) series", *Electrochim. Acta.*, 52, **2007**, 5219.

Maso, N.; Beltran, H.; Munoz, R.; Julian, B.; Carda, J. B.; Escribano, P.; Cordoncillo, E. "Optimization of praseodymium-doped cerium pigment synthesis temperature", *J. Am. Ceram. Soc.,* 86, **2003**, 425.

Masui, T.; Tategaki, H.; Furukawa, S.; Imanaka, N. "Synthesis and characterization of new environmetally friendly pigments based on cerium phosphate", *J. Ceram. Soc. Jpn.*, 112, **2004**, 646.

Masui, T.; Furukawa, S.; Imanaka, N. "Preparation and Characterization of Amorphous $Ce_{1-x}Zr_xW_2O_8$ Fine Particles for Environmental-friendly Yellow Pigments", *Chem. Lett*., 34, **2005**, 1322.

Masui, T.; Furukawa, S.; Imanaka, N. "Synthesis and Characterization of CeO_2–ZrO_2–Bi_2O_3 Solid Solutions for Environment-friendly Yellow Pigments", *Chem. Lett.,* 35, **2006**, 1032.

Melo, D. M. A.; Melo, M. A .F.; Martinelli, A. E.; Silva, Z. R.; Cunha, J. D.; Lima, A. C. "Synthesis and characterization of lanthanum- and yttrium-doped Fe_2O_3 pigments", *Cerâmica,* 53, **2007**, 79.

Modly, Z. M. "High infrared reflecting brown rutile pigment composition", *U. S. Patent* 5,006,175; **1999**.

Nunes, M. G. B.; Cavalcante, L. S.; Santos, V.; Sczancoski, J. C.; Santos, M. R. M. C.; Santos-Júnior, L. S.; Longo, E. "Sol–gel synthesis and characterization of $Fe_2O_3 \cdot CeO_2$ doped with Pr ceramic pigments", *J. Sol-Gel Sci. Technol.,* 47, **2008**, 38.

Ohno, Yoshi. "CIE Fundamentals for Color Measurements", Paper for IS&T NIP16 Conference, Vancouver, Canada, **2000**, Oct. 16.

Seabright, C. A. "Yellow ceramic pigments", *U.S. Patent No.* 2,992,123; **1961**.

Shannon, R. D. "Revised effective ionic radii and systematic studies of interatomic distances in halides and chalcogenides", *Acta Crystallogr., Sec. A,* 32, **1976**, 751.

Shuk, P; Greenblatt, M. "Hydrothermal synthesis and properties of mixed conductors based on $Ce_{1-x}Pr_xO_{2-\delta}$ solid solutions", *Solid State Ionics,* 116, **1999**, 217.

Sivakumar, V.; Varadaraju, U. V. "Environmentally benign novel green pigments: $Pr_{1-x}Ca_xPO_4$ (x = 0–0.4)", *Bull. Mater. Sci.,* 28, **2005**, 299.

Sliwinski, T. R.; Pipoly, R. A.; Blonski, R. P. "Infrared reflective color pigment", *U. S. Patent* 6,174,360, **2002**.

Smith, H. M. "High performance pigments". Weinheim: Wiley-VCH, **2002**.

Smith, G. B.; Gentle, A.; Swift, P.; Earp, A.; Mronga, N. "Coloured paints based on coated flakes of metal as the pigment, for enhanced solar reflectance and cooler interiors: description and theory", *Sol. Energy Mater. Sol. Cells,* 79, **2003**, 163.

Smith, A. E.; Mizoguchi, H.; Delaney, K.; Spaldin, N. A.; Sleight, A. W.; Subramanian, M. A. "Mn^{3+} in Trigonal Bipyramidal Coordination: A New Blue Chromophore", *J. Am. Chem. Soc*., 131, **2009**, 17084.

Sorly, S.; Tena, M. A.; Badenes, J. A.; Calbo, J.; Llusar, M.; Monros, G. "Structure and color of $Ni_xA_{1-3x}B_{2x}O_2$ (A=Ti, Sn; B=Sb, Nb) solid solutions", *J. Eur. Ceram. Soc.,* 24, **2004**, 2425.

[a]Sreeram, K. J.; Kumeresan, S., Radhika, R., Sundar, V. J., Muralidharan, C., Nair, B. U., Ramasami, T. "Use of mixed rare earth oxides as environmentally benign pigments", *Dyes Pigm.,* 76, **2008**, 243.

[b]Sreeram, K. J.; Aby, C. P.; Nair, B. U.; Ramasami, T. "Colored cool colorants based on rare earth metal ions", *Sol. Energy Mater. Sol. Cells*, 92, **2008**, 1462.

Sreeram, K. J.; Radhika, S.; Devi, J. M.; Nair, B. U.; Ramasami, T. "Cerium molybdenum oxides for environmentally benign pigments". *Dyes Pigm.,* 75, **2007**, 687.

[a]Sulcova, P.; Trojan, M.; Solc, Z. "Cerium Dioxide Fluorite Type Pigments", *Dyes Pigm.*, 37, **1998**, 65.

[b]Sulcova, P.; Trojan, M. "Synthesis of $Ce_{1-x}Pr_xO_2$ pigments with other lanthanides", *Dyes Pigm.*, 40, **1998**, 87.

Sulcova, P.; Trojan, M. "The synthesis and analysis of $Ce_{0.95-y}Pr_{0.05}Sm_yO_{2-y/2}$ pigments", *Dyes Pigm.*, 58, **2003**, 59.

Sulcova, P.; Trojan, M. "Thermal analysis of the Bi_2O_3–Y_2O_3–ZrO_2 pigments", *J. Therm. Anal. Calorim.,* 93, **2008**, 795.

Subasri, R.; Matusch, D.; Nafe, H.; Aldinger, F. "Synthesis and characterization of $(La_{1-x}M_x)_2Mo_2O_{9-\delta}$;M=$Ca^{2+}$, Sr^{2+} or Ba^{2+}", *J. Eur. Ceram. Soc.* 24, **2004**, 129.

Swiler, D. R. "Manganese vanadium oxide pigments",*U. S. Patent* 6,485,557; **2002**.

Swiler, D. R.; Detrie, T. J.; Axtell, E.A. "Rare earth transition metal oxide pigments", *U. S. Patent* 6,582,814; **2003**.

Tealdi, C.; Chiodelli, G.; Malavasi, L.; Flor, G. "Effect of alkaline-doping on the properties of $La_2Mo_2O_9$ fast oxygen ion conductor"; *J. Mater. Chem.,*14, **2004**, 3553.

Tkachenko, E. A.; Fedorov, P. P. "Lower rare earth molybdates", *Inorg. Mater.,* 39, **2003**, 25.

Trovarelli, A. "Structural and Oxygen Storage/Release Properties of CeO_2-Based Solid Solutions", *Comments Inorg. Chem.,* 20, **1999**, 263.

Uemoto, K. L.; Sato, N. M. N.; John, V. M. "Estimating thermal performance of cool colored paints*", Energ. Bui.,* 42, **2010**,17.

Vishnu, V. S.; George, G.; Divya, V.; Reddy, M. L. P. "Synthesis and characterization of new environmentally benign tantalum–doped $Ce_{0.8}Zr_{0.2}O_2$ yellow pigments: Applications in coloring of plastics", *Dyes Pigm.,* 82, **2009**, 53.

Vishnu, V. S.; George, G.; Reddy, M. L. P. "Effect of molybdenum and praseodymium dopants on the optical properties of $Sm_2Ce_2O_7$: tuning of band gaps to realize various color hues", *Dyes Pigm.,* 85, **2010**, 117.

Wake, L. V. "The effect of pigments in formulating solar reflecting and infrared emitting coatings for military applications", *J. Oil Colour Chem. As.,* 73, **1990**, 78.

Wang, X. P.; Fang, Q. F. "Effects of Ca doping on the oxygen ion diffusion and phase transition in oxide ion conductor $La_2Mo_2O_9$", *Solid State Ionics,* 146, **2002**, 185.

Wang, Y.; Mori, T.; Ji-Guang, Li.; Ikegami, T. "Low-temperature synthesis of praseodymium-doped ceria nano powders", *J. Am. Ceram. Soc.,* 85, **2002**, 3105.

Yamazaki, T.; Shimazaki, T.; Hashizume, T.; Terayama, K. “Investigation of double oxides in the system of Pr-Mo-O”, *J. Mater. Sci. Lett.,* 21, **2002**, 29.

Yan, B.; Li, M.; Zhang, J.; Chou, K, C. “Structural and electrical properties of $La_{2-x}Ba_xMo_2O_{9-x/2}$ (x = 0–0.18)”, *Mater. Res. Bull*., 45, **2010**, 382.